Final Technical Report

Missouri University of Science and Technology
Modeling and Optimizing Pumped Storage in a Multi-stage Large Scale Electricity Market under Portfolio Evolution
Award DE-EE0008781

Federal Agency	Department of Energy, EERE Water Power Technologies Office
FOA Name and Number	DE-FOA-0001836, Innovative Design Concepts for Standard Modular Hydropower and Pumped-Storage Hydropower
Nature of the Report	Final Report
Award Number	DE-EE0008781
Award Type	Grant
Prime Recipient	Mr. Craig David Missouri University of Science and Technology 300 W. 12th St, 202 Centennial Hall Rolla, MO 65409 research@mst.edu 573-341-4134
Prime Recipient Type	University
Project Title	Modeling and Optimizing Pumped Storage in a Multi-stage Large Scale Electricity Market under Portfolio Evolution
Principal Investigator	Rui Bo, Assistant Professor rbo@mst.edu 573-341-6400
Prime Recipient's DUNS	804883767
Date of The Report	November 29, 2021

Contents

ACKNOWLEDGEMENT:

This material is based upon work supported by the U.S. Department of Energy's Office of Energy Efficiency and Renewable Energy (EERE) under the Water Power Technologies Office (WPTO) Award Number DE-EE0008781.

DISCLAIMER:

Acronyms:

ACF	Auto correlation function
ADP	Approximate dynamic programming
ARIMA	Autoregressive integrated moving average
ARIMAX	Autoregressive integrated moving average with exogenous variable
ARPA-E	Advanced Research Projects Agency–Energy
CCGT	Combined-cycle gas turbine
CO2	Carbon dioxide
DA	Day-ahead
ED	Economic dispatch
FERC	Federal Energy Regulatory Commission
FRAC	Forward Reliability Assessment and Commitment
GE	General Electric
HIPPO	High-Performance Power-Grid Optimization
LAC	Look ahead commitment
LMP	Locational marginal price
MAE	Mean Absolute Error
MIP	Mixed integer programming
MISO	Midcontinent Independent System Operator
PACF	Partial auto correlation function
PNNL	Pacific Northwest National Laboratory
PSH	Pumped storage hydro
PSHU	Pumped storage hydro unit
R&D	Research and development
RAC	Reliability Assessment Commitment
RMSE	Root Mean Square Error
RT	Real-time
SCED	Security-constrained economic dispatch
SCUC	Security-constrained unit commitment
SOC	State of charge
SOPO	Statement of Project Objectives
STD	Standard deviation
UC	Unit commitment
VOW	Value of water

I. Executive Summary

To leverage the fast-ramping capability of resources to provide great value to the grid, electricity system operators such as the Midcontinent Independent System Operator (MISO) continue to evolve their approaches for integrating energy storage resources, including pumped-storage hydro (PSH), into the electricity markets. However, new challenges arise in modeling and optimizing these energy-limited resources across multiple market clearing processes and planning studies with uncertainties and imperfect information. For instance, current market practices of PSH owners specifying pumping/generating hours can result in sub-optimal generation dispatch. Letting grid operators optimize PSH with the consideration of multiple operating modes and energy limitation constraints can potentially bring economic benefits to both the system and the PSH owners. However, in multi-stage clearing process of electricity markets, utilizing the PSH flexibility to deal with realized uncertainties can cause deviation in the multi-stage scheduling processes. The resulting financial risks from the schedule deviation may not be acceptable to PSH owners. In addition, to effectively utilize this energy limited resource, the state of charge (SOC) constraints of PSH needs to be continuously optimized and the marginal cost of deviation need to reflect the expected cost to purchase or sell energy at future times to compensate for deviations.

This project aims to develop a prototype enhanced PSH model and improved price signals in the multi-stage market clearing process with proper consideration of the unique characteristics of PSH, in order to better align underlying PSH capabilities with evolving grid needs, particularly including the needs for more frequent and larger cycling to manage variability and uncertainty from renewables.

The project is carried out in collaboration with industry partners representing all PSH owners in MISO footprint. The project uses realistic tools, models, and data that allow the research team to study, evaluate and quantify opportunities to improve the market design. For example, the prototype PSH models have been developed and implemented in High-Performance Power-Grid Optimization tool (HIPPO[1]) software and tested with MISO Day-ahead cases with realistic data from PSH plant operators.

The project has resulted in the following major accomplishments:

- A prototype deterministic day-ahead (DA) security constrained unit commitment (SCUC) model with PSH optimization has been developed and implemented using HIPPO. It meets MISO's solution quality and performance requirement. Studies on actual MISO system showed 0.04%-0.67% reduction in system total cost and mostly positive with up to 97% increase in PSH profit. The benefits are expected to be higher with more penetration of PSH and renewable generation.
- A "tighter" formulation of the state-of-charge constraints with binary variables has been proposed and implemented to improve the computational performance of the proposed deterministic DA SCUC model. Statistical data based on repeated tests using MISO cases show that the tightened constraints typically have approximately neutral or positive impact (e.g., up to 34% reduction in studied cases) on average computational time.

[1] HIPPO is High-Performance Power-Grid Optimization tool developed by MISO, GE, GUROBI, and PNNL under ARPA-E funding. It is currently used by MISO for R&D prototyping, and MISO will consider implementing some of the HIPPO technology in production system in the future.

- An energy reserve (or MWh reserve) concept has been proposed to deal with the SOC deviation in real-time. Head room and floor room are derived using statistical models. Two methods including the rolling based stochastic approach and the approximate dynamic programming (ADP) approach have been employed to evaluate the value of water of PSHs outside a finite time horizon. Studies show that both approaches can lead to a better utilization of available water with higher profits for PSHs in real-time (RT) markets, than exactly staying with the DA solutions. In addition, no approach consistently outperforms the other, and their performances depend on the quality of RT price forecasts as well as similarities between price patterns in RT and those used for ADP training.
- A rolling window simulation platform has been developed in HIPPO, which closely mimics the look-ahead commitment (LAC) of MISO. It is a valuable tool for investigation of the intra-day clearing process.
- An Autoregressive Integrated Moving Average with Exogenous Variable (ARIMAX)-based deterministic price forecast and a scenario generation-based stochastic price forecast have been developed to predict RT prices. The price forecasts can be used in the developed deterministic and stochastic PSHU models respectively to guide intra-day dispatch. Studies using MISO data show the developed ARIMAX model can capture the trend, the peaks and the turning points of the actual RT-LMP significantly better than the Facebook Prophet model.
- A risk-averse formulation has been developed to address the concern of profit loss in the RT market. Studies demonstrate the effect of the risk management formulation in reducing system total cost and avoiding negative real time profits for the PSHU.
- A planning model with improved realistic characteristics of PSH and the incorporation of market optimization enhancement has been developed. Studies using actual PSH plant parameters and MISO planning models reveal the SOC error from inaccurate PSH input-output curve modeling will accumulate quickly in chronological production cost simulation, and consequently requires periodical adjustment of SOC or the adoption of proposed improved input-output curve modeling.
- A novel disjunctive convex hull model for input-output curve approximation has been developed to improve the computational performance, and studies show an order of magnitude speedup over the common piece-wise linear approximation methods.
- Studies using MISO planning models show using DA storage shadow price as an indicator for future value of water can exploit the flexibility of PSH in RT and reduce RT system total cost (with a monthly average of 0.22% reduction in studied cases).
- A linear program based approximated model is used to approximate the nonconvex unit commitment model to accelerate the solution of stochastic production cost simulation models. Studies using a MISO planning model show the proposed method can produce acceptable accuracy in results (with 0.35% difference in system total cost) and significant solution time improvement (with 71.6% reduction in solution time).

By optimizing PSH operations with consideration of multiple operating modes and energy limitation constraints to mitigate uncertainties, the above project findings will enable greater utilization of PSH flexibility in multi-stage clearing process and facilitate a deeper market penetration of renewable and/or distributed energy resources. *MISO considers incorporating the developed models from this project into production in the future, pending further extensive tests, stakeholder process and prioritization.*

This aforementioned project accomplishments have been achieved through research investigations in the following three areas.

- Area 1: PSH optimization in DA large-scale SCUC with uncertainty;
- Area 2: PSH optimization within the operating day through establishing a near term price forecasting methodology and incorporating that price forecast into LAC and RT dispatch;
- Area 3: PSH optimization in longer-term economic planning study: reflect market optimization in a planning model and explore stochastic optimization.

The research in **Area 1** enables deeper participation of PSHs through offering their characteristics into the DA market, instead of letting them specify a schedule of hourly generation and pumping levels to be submitted to MISO. Also, the proposed withholding of energy (energy reserve or MWh reserve) from energy-limited resources as well as the stochastically determined SOC headroom can mitigate increased uncertainties from a changing portfolio. The research in **Area 2** creates a framework to optimize PSH in intra-day operation (including LAC and RT) and utilizes probabilistic price forecast to incorporate RT uncertainties. It also provides a risk management model that can consider PSH owners' risk aversion preference when deviating RT from DA schedule. The research in **Area 3** demonstrates the value of enhanced market optimizations from Area 1 and Area 2 using long-term planning studies. In addition, the proposed PSH modeling for planning analyses provides both necessary model enhancements and correction to the existing modeling inaccuracy.

The detailed work accomplishments for each of the three research areas are further elaborated as follows.

Area 1 – Day-ahead Market Optimization

First, the team established prototype DA SCUC model with PSH optimization that can meet solution quality and performance requirement. The prototype PSH model has been developed and implemented in HIPPO software and tested with MISO Day-ahead cases. Through discussion with the industry advisors[2] about state-of-charge (SOC) parameter settings, the team updated the mathematical model to better characterize the operation details of the PSHs in the MISO system[3]. The deterministic PSH DA SCUC model has been further enhanced with a "tighter" formulation of the state-of-charge constraints with binary variables. Statistical data collected based on repeated tests using MISO cases show that *the tightened constraints typically have approximately neutral or positive impact on the computational time*.

Second, the team has developed the energy reserve modeling of pumped storage hydro units (PSHUs). A reserve secure constraint of PSH in day-ahead SCUC model is developed to address the potential SOC boundary violation issue in real-time economic dispatch (ED). The team used MISO's historical data to assess energy reserve secure requirements of PSHs in the day-ahead SCUC model. Studies using actual MISO data have shown that *energy reserve secure constraints can improve system security against uncertainties and contingencies, while not necessarily reducing the profits of PSH units*.

[2] DTE Electric, Consumers Energy, and Ameren Missouri

[3] MISO system includes two large-scale PSH plants: 2,172MW Ludington station (jointly owned and operated by DTE Electric and Consumers Energy) and 450MW Taum Sauk station (owned and operated by Ameren Missouri).

Third, the team has developed a stochastic model to calculate the MWh headroom reserve requirement in the day-ahead Forward Reliability Assessment Commitment (FRAC) model, to handle potential SOC discrepancies between day-ahead market clearing and real-time operation. The team introduced new parameters to define scenarios describing DA to RT discrepancy by exploring MISO's historical data, and thereby generated multiple scenarios to cast the stochastic model. Numerical simulations are conducted to verify the effectiveness and impacts of the proposed stochastic SOC headroom. In addition, the team has used both the rolling based stochastic approach and the ADP approach to evaluate the value of water of PSHs outside a finite time horizon. The rolling based stochastic approach relies on the availability and accuracy of explicitly simulated/forecasted uncertain RT prices of future time periods; the ADP learns SOC-price curves based on historical RT price data, and can derive good-enough solutions if RT price patterns are close to the historical RT price data used in ADP training. The learned SOC-price curves could be used in the FRAC and LAC models to optimize the SOC levels at the end of the finite time horizon, without explicitly simulating uncertainties of future time periods. Numerical results on a real-time one-hour look-ahead PSH profit maximization problem show that *both approaches can lead to a better utilization of available water with higher profits for PSHs in RT markets, than exactly staying with the DA solutions, while no approach consistently outperforms the other as their performances depends on the quality of RT price forecasts as well as similarities between price patterns in RT and those used for ADP training*.

Area 2 - Intra-day Market Optimization

First, the team established mathematical formulations to incorporate price forecasts beyond the end of the study window for PSH optimization purpose. After investigating the challenges in PSH optimization within the operating day that result from the rolling short lookahead window, the team has developed LAC rolling window simulation platform in HIPPO, and MISO case studies have shown *high consistency between LAC rolling windows solution and DA solutions*. Then, a single point price forecast is developed and used in the model to provide guidance to the PSH in the series of LAC simulation. The formulation *sets the foundation for the development of a stochastic PSHU model in LAC considering the uncertainty*.

Second, to capture price forecast uncertainty in persistent deviation model of RT dispatch, a probabilistic price forecast method is developed using scenario generation method. Based on the developed deterministic PSHU model, the team developed stochastic PSHU models in LAC. Probabilistic price forecast is used to incorporate RT uncertainties. Based on the discussion with and feedback from the industry advisors, a risk averse formulation is developed to address the concern of the profit loss in the RT market. The team prototyped the proposed stochastic PSHU model and the risk management formulation. The preliminary results on developed case studies show the value of capturing uncertainties in the stochastic PSHU model and the improvement in the system objective (namely, system production cost). The results *demonstrate the effect of the risk management formulation in improving system objective and avoiding negative profits for the PSHU*.

Area 3 - Planning Horizon Optimization

First, the team has proposed an improved PSH model with more realistic input-output curves and detailed water balance constraints for PSH units, and validated the feasibility of interleaving DA

and RT market in planning models. The team also implemented the proposed detailed PSH model and DA/RT interleaved simulation method in PLEXOS. The value of accurate PSH modeling in long-term chronological production cost simulation model is illustrated using a MISO planning system, and the value of DA/RT interleaved simulation in MISO planning is also investigated. The team further enhanced the input-output curve modeling with a hypograph relaxation-based approach. Numerical studies on Ludington PSH station *show the computational advantages of the proposed modeling enhancement*.

Second, the team established a deterministic PSH optimization model for economic planning while reflecting enhanced market optimizations (from Area 1 and Area 2) in a MISO planning system via PLEXOS. A MWh reserve modeling is included and a value-of-water based approach is used for the RT operation of PSH units to exploit the flexibility of storage resources. Through value-of-water based rolling horizon framework, the benefit of withholding energy is demonstrated using MISO planning system. Test results show *the enhanced modeling can enable the flexibility of PSH and reduce the overall system cost in the RT market*.

Third, the team developed a stochastic optimization approach for economic planning studies with a unit commitment approximation strategy to accelerate the solution process. Test results on a MISO planning model *show acceptable accuracy and significant solution time reduction from the proposed approach*. The team further explored a stochastic transmission expansion planning method with the same approximation strategy together with a decomposition framework. In addition, long-term production cost simulation performed on MISO planning cases showed *enhanced PSH optimization can reduce load cost and in some cases increase carbon dioxide (CO2) emission*.

II. Introduction

This project aims to analyze potential approaches to maximize the value of PSH resources for the reliability and efficiency of electricity market planning and operations.

Large system operators such as MISO continue to evolve their approaches for integrating energy storage resources into the markets. Such resources, including PSH resources, present unique characteristics such as fast-ramping capability that can provide great value to the grid. Indeed, conversations with stakeholders have indicated a desire for enhanced optimization of energy storage resources like PSHs. However, modeling and optimizing these energy-limited resources present new challenges. In particular, key research questions include developing the best approaches to optimize across multiple market clearing processes (e.g., from 7-day FRAC to 5-minute RT markets) and deciding what optimization approach is best suited to address uncertainties and imperfect information across the multi-stage clearing processes. Furthermore, the implications for MISO's large-scale optimization software performance must also be investigated to ensure that proposals can be practically implemented.

Under the current rules as well as the proposed rules in response to the FERC Order 841, a PSH unit could offer into MISO market but would need to specify bids for either charging or discharging across the day. MISO's unit commitment software only optimizes for the hours offered as generators (i.e., discharging) in the Day Ahead Reliability Assessment Commitment (RAC) and LAC processes, on the basis of a maximum daily energy constraint. The pumping (or charging) status needs to be self scheduled. That is, participants need to determine which hours to pump and which hours to generate in the offers. Currently, they make this decision through price forecasting,

while also considering efficiency losses in order to determine the maximum daily energy to be offered for generation and the energy to be utilized for pumping. However, price is an outcome of the market clearing and thus not very easy to predict accurately ahead of time. This process can result in sub-optimal scheduling of the resource: the region may not receive the best value, and the participants may not get the best profit from these resources. Thus, optimizing PSHs with consideration of multiple operating modes and energy limitation constraints can potentially bring additional benefit to the market, especially under large renewable penetration.

Furthermore, current market clearing is a multi-stage process. Specifically, MISO market clearing processes include 7-day Forward RAC, Day Ahead Market, 2-day Forward RAC, Intra-day RAC, 3-hour LAC, and 5-minute RT Market. A multi-day optimization horizon may be necessary to best utilize a large PSH with multi-day storage. Typical planning by PSH operators for daily or weekly scheduling seeks to return the SOC at the end of the horizon to be the same as at the beginning of the horizon—this is accomplished implicitly through the maximum daily energy constraints for generation as mentioned above. Explicitly requiring SOCs at the end and beginning of the planning horizon to be the same is called the "SOC target constraint". On the other hand, it is desirable to allow for some deviation between day ahead planned use of the PSH and the actual dispatch in RT markets, since as with all other dispatchable generation resources, deviations of real time generation from day ahead schedule allow recourse to respond to realizations of uncertainties. That is, a significant part of the potential value of PSH is in its ability to quickly ramp to balance for deviations between RT and day ahead schedules; however, current scheduling practice tends to limit deviations from day ahead or longer-term decisions. Thus, representation of energy limited resources in the cascaded scheduling and pricing model needs to be addressed in order to best utilize these resources and to provide fair compensation to them. A key representational issue is the effective marginal cost in one market of deviating from a value scheduled from a previous market. The simplest example of this is the valuation of marginal deviation costs in real-time from the day-ahead scheduled pumping or generation. Intuitively, the marginal cost of deviating should be related to the expected cost to purchase or sell energy at future times to compensate for deviations.

An additional issue is that, in real time, the transition between pumping and generating can happen in a short time window. It can provide flexibility if managed well. However, if it is not properly managed, a large change of output in a short time window may cause system ramping issues because other resources may not be able to pick up the sudden changes in output from PSHs. MISO developed processes outside of the market to coordinate with participants in providing efficient pumping schedules and avoiding negative impacts from the transition. However, it would be valuable for the MISO market to explore the potential to incorporate transition constraints within the clearing engine itself as part of the optimization enhancements. The model could represent the delivery of such ramp products during transitions from pumping to generation or vice versa, building on analogous models of ramping during transition of combined-cycle gas turbines (CCGT) that have been explored by the project team, and therefore facilitating enhanced management and utilization of the transition of PSHs.

The operation of PSH has implications for long-term, capital planning which is becoming increasingly dependent on assumptions about resource operating profiles and utilization. The team also worked with the MISO planning groups to understand how optimization models might impact planning processes, and to conduct an initial assessment of how optimization models might be reflected in the production cost and transmission planning processes.

III. Accomplishments and Milestone Summary

As detailed in the Statement of Project Objectives (SOPO), all milestones and deliverables are listed in the below table, with completion status indicated.

Number	Milestone Description	Status
Milestone 1.1	Establish prototype DA SCUC model with PSH optimization that can meet solution quality and performance requirement.	Completed
Milestone 2.1	Establish mathematical formulations to incorporate price forecasts beyond the end of the study window for PSH optimization purpose	Completed
Milestone 3.1	Establish interleaved DA/RT simulation method for economic planning	Completed
Milestone 4.1	Establish prototype of enhanced PSH model within the SCUC framework	Completed
Deliverable 5.1	A prototype representation of price forecast uncertainty in persistent deviation model of RT dispatch	Completed
Milestone 6.1	Establish deterministic PSH optimization model for economic planning while reflecting market optimization	Completed
Critical Design Review	After Milestone 6.1 is finished, prototype DA SCUC model, new MWh reserve requirement and price forecast, and improved deterministic planning model will be established.	Completed
Milestone 8.1	Establish prototype stochastic SCUC tool equipped with fast computation capability that can accurately determine MW and MWh reserve requirements of systems against uncertainties.	Completed
Deliverable 9.1	A detailed report on long-term value of enhanced PSH model through planning analyses.	Completed

It should be noted that the Critical Design Review was conducted on April 7, 2021. Review comments were addressed and incorporated into the Critical Design Review report. After further review, on May 5, 2021, DOE determined the Critical Design Review criteria have been satisfied and the research team can proceed with the rest of the project.

Detailed accomplishments on each of the milestones and deliverables will be elaborated in Section IV.

IV. Detailed Accomplishments toward Milestones

The project team has made significant accomplishments toward each milestone or deliverable, which are detailed in the following sections IV.A through IV.H respectively.

IV.A. Accomplishments Toward Milestone 1.1

Milestone 1.1: Establish prototype DA SCUC model with PSH optimization that can meet solution quality and performance requirement.

Accomplishments Summary: There are two main accomplishments in this Milestone. (1) The team has prototyped a PSH optimization model for DA SCUC. The model has been implemented using HIPPO software. Tests were carried out with several of the MISO day-ahead cases, which were solved with less than 1% Mixed Integer Programming (MIP) gap at 1200 seconds. These results meet MISO solution quality and performance requirements. The team discussed with the industry advisors about state of charge (SOC) parameter settings and case study assumptions and performed computational and benefit studies on MISO test cases, showing that the model is able to not only reduce the total system dispatch cost but also increase the profit for optimized PSH units. (2) An enhanced formulation of SOC constraints was proposed and tested using MISO day-ahead cases and results demonstrated the benefit in computational performance, which suggests the tighter SOC constraints help to build a tighter model with a smaller feasible region and increase the computational efficiency.

In some of the results presented below, a 0.1% MIP relative gap (i.e., the absolute gap divided by the upper bound) is used as a stopping criterion. It should be pointed out 0.1% MIP relative gap is for well-behaved cases that present less challenges to the solution process. By the MISO operating guide, solutions with MIP relative gap limit lower than 1% will be accepted. For difficult cases, if the relative gap is below 3% or absolute gap is below $24000 at 1200 seconds (i.e., 20 minutes), it is also acceptable. If the gap is above 3%, the time limit will be extended from 1200 seconds to 1800 seconds.

IV.A. 1 Developed deterministic PSH model in SCUC

Pumped storage hydro units (PSHUs) can provide flexibility to the system and facilitate renewable energy resources integration. However, these important and valuable services that are available from PSHUs have not been utilized largely due to the fact that PSHUs have not been fully optimized in the market. In the current MISO day ahead market, PSHUs offer opportunity costs and bid prices for their generation and pump mode, respectively. State of charge limits for their reservoirs are not enforced explicitly by the system operator. Instead, a maximum daily electricity generation limit is submitted and applied to PSHUs for their generation modes. The PSHU owner determines the pump/generate window. To fully leverage the storage services from a PSHU and enhance the market efficiency, we believe it is important to introduce a PSHU model that can be fully optimized in the MISO day-ahead unit commitment problem.

The proposed configuration-based modeling of PSHU represents all feasible operation modes and the state-of-charge (SOC) of a PSHU. A pumped storage hydro plant can contain multiple units and each of them will be modeled individually; however, there are only three operation modes in a PSHU, namely generating, pumping, and offline, which are mutually exclusive as shown in Fig. A.1.1. Transitions are allowed between each pair of these modes as shown in Fig. A.1.1 by the double-headed arrows.

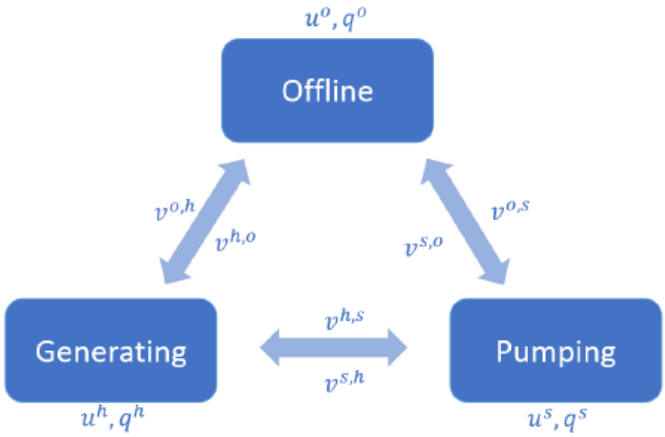

Fig. A.1.1 Mode Transition Diagram of a PSHU in Two Consecutive Time Intervals. There are three operation modes in a PSHU, namely generating, pumping, and offline. Transitions are allowed between each pair of these modes.

Model A.1 describes the proposed deterministic SCUC model that optimizes PSH. It focuses on PSH related modeling, and the specific modeling of other generation plants are not detailed here. The model closely represents the current MISO unit commitment model, and is actually built upon the existing MISO unit commitment model using HIPPO tool.

The objective of the unit commitment problem is to minimize the system operating costs, subject to operational constraints such as system energy balance constraints, state and transition logic constraints, storage energy balance and state of charge (SOC) Constraints, etc. The detailed mathematical model is included in the Appendix for section IV.A.1.

MISO Case Study

In this study we use a MISO case that includes 1,085 generators. Reserve requirements and transmission security constraints are included for all studies. Constraints on individual generators such as, minimum up/down time, maximum start up time, and ramp constraints are included for all units including PSHUs with proposed model.

Computational Analysis: Table A.1.1 shows the computational results of different models[4]:

- HIPPO: A High-Performance Power-Grid Optimization (HIPPO) tool. MISO current pumped storage hydro model is applied (in which model PSHUs offer opportunity costs and bid prices for their specified generation and pump windows);
- HIPPO + PSHU: MISO current model is replaced by proposed pumped storage hydro model in HIPPO described in (A.1.1)-(A.1.14) in the Appendix for section IV.A.1;

[4] All tests were performed on a 2.2-GHz quad-core Intel Xeon CPU E5-2699 with 32 GB RAM (which has similar hardware specifications as the computers used in MISO market clearing process). All optimization problems are solved with Gurobi 8.0.

Table A.1.1. Computational Comparison. Each row shows either the MIP relative gap in percent at 1200s of run time or the time to achieve a 0.1% MIP relative gap.

Case	HIPPO	HIPPO + PSHU
#1	0.11 %	0.16 %
#2	325 sec	400 sec
#3	527 sec	391 sec
#4	519 sec	699 sec
#5	0.13%	0.67%
#6	144 sec	140 sec

The test case and load scenario with the HIPPO model has been benchmarked with MISO production day-ahead market engine. Therefore, HIPPO is used as a benchmark for this study. The PSHU currently provides offer costs and bid prices for their generation and pump modes, respectively. The state of charge of the reservoirs are not enforced by the system operator; instead, the parameter of maximum daily generation is applied. Also, the pump/generate window for the unit are submitted and fixed by the unit owner. In HIPPO + PSH model, the PSHUs are represented by the proposed configuration-based model, the SOC of the units are represented and the PSHUs are fully optimized.

The computational time in both models for six cases are listed in Table A.1.1. If the model can not be solved to the target MIP relative gap at 0.1% within the MISO day ahead market cutoff time at 1200 sec, the MIP relative gap at the cutoff time is listed instead (only for cases #1 and #5). As shown in Table III, compared to the HIPPO model, the MIP relative gap at the cutoff time for the HIPPO+PSHU model slightly increases in case #1 and #5, whereas the computational time for the HIPPO+PSHU model increases only moderately in case #2 and #4.

Benefit Analysis: In this section, the proposed model is benchmarked with the current model in examples based on real data in an actual day in MISO system.

Table A.1.2. System and PSHU Benefit Analysis of HIPPO+PSHU. Positive percentages represent improvement compared to the HIPPO model.

	System Objective [$]	PSHU 1 Profit [$]	PSHU 2 Profit [$]	PSHU 3 Profit [$]
#1	0.4%	1%	10.8%	6%
#2	0.042%	0%	5.92%	−6.04%
#3	0.18%	0.57%	0%	NA
#4	0.188%	0.17%	97%	0.3%
#5	0.67%	2.45%	*	13%
#6	0.107%	0.84%	10.8%	NA

To make a fair comparison between the proposed model and the current model, given a start state of a reservoir and round-trip efficiency of each of the PSHUs in the study, the realized state of the reservoir at the last hour of the day from the results of the current model is applied to the proposed model. That is, the total energy charged to or discharged from the reservoir in each day in the simulation are the same for both models. To lay out a more realistic benefit analysis, the minimum SOC is calculated as the start state of the reservoir minus the effect of the generation cleared by the current model considering the efficiency. Similarly, the maximum SOC is the start

state of the reservoir plus pumping cleared by the current model considering the efficiency. The PSHU parameters in the proposed model are summarized below.

- The SOC of a reservoir at the beginning of the day hour 0 is given.
- The SOC of a reservoir at the end of the day at hour 24 is calculated from the results of the current model and is fixed for the proposed model.
- The SOC min and max are calculated from the results of the current model and are fixed for the proposed model.
- All the other unit parameters (such as min up/ down time, ramp rate etc.) in the proposed model are copied from the production offer in the current model.

The benefits of the proposed model are quantified and summarized in Table A.1.2. Shown in the table, the system objective has been reduced for every case when the proposed model is applied. Notice that the bid and cost from a PSHU indicated by the first term in (1) is excluded from the objective solved under the current model.

The unit commitment solutions of the rest of the generation units in the system other than the three PSHUs in MISO[5] are fixed to the same values as obtained in the current model, such that the results shown in Table A.1.2 mainly reflects the impacts of the proposed model on the PSHUs. The reduction in system objective from the proposed model is shown as the percentage of the system objective of the current model. At the same time, the profit increment for the PSHU owners from the proposed model are shown as percentages of their profits result from current model. The profit reduction for PSHU 3 in case #2, as shown in Table A.1.2, results from the existence of multiple optimal solutions within the MIP relative gap. Similar situations happened in the operation of MISO day-ahead market, a market procedure is developed to detect such condition and fetch alternative solutions for the unit [A.1]. PSHU 3 is not cleared from both models in case #3 and case #6. The profits for PSHU 2 in case #5 from the proposed model is several times the profit from the current model as indicated by * in Table A.1.2. However, this is likely due to the challenges in constructing the bids and offers under uncertainties and it is not a general benefit introduced by the proposed model.

Overall, compared to the current model, the proposed model only increases the computational burden moderately but improves both the system objective and the unit profits. In addition, the scenarios used in the study are from historical data library and have less renewable capacity than currently installed in MISO. According to the current MISO generation interconnection queue [A.2], significant additional amounts of renewable units are likely to be interconnected in the near future. In a system with more variation and intermittency, the value of the flexibility from a PSHU is expected to be further increased with the proposed model. The study described in this subsection has been published in the IEEE Transactions in Power Systems [A.3].

IV.A. 2 Tighter formulation of constraints in PSH model.

There are typically many choices for formulating the linear constraints in a model such as the SOC limit constraints described in (A.1.11) in the Appendix for section IV.A.1, but for computational efficiency it is best to seek constraints that, as closely as possible, match the so-called "convex hull" of the feasible region. The convex hull of the feasible region is defined to be the smallest convex set that contains the feasible region. To consider the convex hull, first define

[5] The three PSHUs include the Ludington station owned and operated by Detroit Edison and Consumers Energy respectively, and Taum Sauk station owned by Ameren.

the "continuous relaxation" to be the region obtained by replacing the binary variables with continuous variables. The continuous relaxation involves linear constraints on continuous variables and is convex. Therefore, the convex hull is contained in the continuous relaxation, but the convex hull can be strictly contained in the continuous relaxation. Using a representation of the linear constraints that is as "tight" as possible, ideally the convex hull, will generally improve the computational efficiency of solving such problems compared to a formulation with a continuous relaxation that strictly contains the convex hull. Further, we proposed a tighter version of the state of charge (SOC) constraints for the PSH as follows, using the notation introduced in section A.1. The previous constraint (A.1.11) in the Appendix for section IV.A.1 is now replaced with constraints (A.2.1) and (A.2.2).

$$e_{r,t-1} + \sum_{g \in G_{psh,r}} q_{gt}^{pump} \eta_g^{pump} \leq \overline{E}, \forall r, \forall t \in [t_2, T] \tag{A.2.1}$$

$$e_{r,t-1} - \sum_{g \in G_{psh,r}} \frac{q_{gt}^{gen}}{\eta_g^{gen}} \geq \underline{E}, \forall r, \forall t \in [t_2, T] \tag{A.2.2}$$

We have confirmed that (A.2.1)-(A.2.2) are valid and proved that these tightened constraints are moderately beneficial numerically based on the test cases considered. In particular, the continuous relaxation of the problem (that allows the commitment variables to range continuously between 0 and 1 instead of being binary) will typically have a solution that is binary-valued when using (A.2.1)-(A.2.2). This property suggests improvement of the peformance of unit commitment software using the tightened constraints, which is demosntrated through numerical results discussed in the next subsection. Further analysis clarified that computational difficulty of the PSH model is driven by a combination of two factors: mutual exclusivity of generation and pumping modes, and SOC constraints.

Empirical results for tightened state-of-charge constraints in PSH model

We implemented and tested several MISO cases and we ran each case with each model for multiple times to collect statistical results on computational time. All the system reserve requirements and transmission security constraints are included. We perform all tests on the same 2.2-GHz quad-core Intel Xeon CPU E5-2699 with 32 GB Ram that was used for the previous MISO case studies; all optimization problems are again solved with Gurobi 8.0.

Seven 36-hour MISO day-ahead market cases with different load and generator scenarios are solved. Ideally the cases are expected to be solved within 1200 seconds and with a 1% or lower MIP relative gap. Each case is solved with three different variant models:

1. "*Without SOC*," without SOC explicilty represented (PSH submits an offer and bid for their unit and PSH is in charge of their own SOC),
2. "*Standard SOC*," with the conventional SOC formulation constraint (A.1.11), and
3. "*Tightened SOC Constraints*," with the newly proposed tighter SOC in (A.2.1)-(A.2.2).

Due to the intrinsic randomness built into a Mixed Integer Programming solver like Gurobi, we test each model for each case five times to have more robust results. A parameter named Random Seed Number in Gurobi is designed to introduce a perturbation that typically leads to different solution paths. Therefore the Random Seed Number is set to a different number (from one to five) every time a model is tested with the same case. For each model and case, the average wall clock MIP stopping times and its sample standard deviation over the five tests are listed in Table A.2.1.

Table A.2.1. Average stopping time and sample standard deviation of Tighter SOC Constraints for Model Variants.

Case	Without SOC	Standard SOC		Tightened SOC		Stand.-Tight.
	Stopping Time [s] (STD)	LP Objective [$]	Stopping Time [s] (STD)	Tight.-Stand. LP Obj. [$]	Stopping Time [s] (STD)	Stopping Time [s] (STD)
1	333(16)	9.5×10^6	409(14)	11	425(27)	−16(21)
2	234(9)	17.5×10^6	262(9)	3,447	285(10)	−23(14)
3	353(23)	14.2×10^6	409(22)	572	382(13)	27(20)
4	302(16)	6.2×10^6	1835(1312)	952	1201(1070)	634(2100)
5	3709(24)	1.4×10^6	3420(569)	0	3663(11)	−243(565)
6	513(252)	16.4×10^6	761(275)	770	660(199)	101(303)
7	219(14)	10.9×10^6	224(45)	18	241(34)	3(57)

The MIP relative gap is set to 1% for cases 1 to 5. The MIP relative gap is set to 0.1% for cases 6 and 7. The MISO production MIP relative gap target is 0.1%; however, cases 1 to 5 are very hard cases and the solver cannot get a solution close to the MIP relative gap of 0.1% within the cutoff time of 3600 seconds. Therefore, a 1% gap is set for those cases instead in order that the solver could get a solution in a reasonable time and the results can be used to compare between models.

A higher LP objective indicates a tighter model and a smaller stopping time indicates that the MIP solver could find a feasible solution within the relative gap in less time. The LP objective and the time taken to get a feasible solution within the relative gap for both models varies with different cases. The fifth column in Table A.2.1 shows the differences between the Tightened SOC model optimal LP objective minus the Standard SOC model optimal LP objective. The results empirically verify that the LP objective of the model with the tightened SOC constraints is always equal to or higher than the LP objective of the model with the standard SOC constraints.

The MIP stopping times shown in Table A.2.1 show that the tightened model has a moderate effect on computational burden, mostly either maintaining roughly the same or somewhat reducing the computational burden, with the exception of case 5. In four out of the seven cases (cases 1 to 3 and case 7), the average stopping time for the standard model and the tightened model are within 50 seconds of each other. For cases 4 and 6, the tightened model is solved faster than the standard model by more than 100 seconds on average. For these two cases, it is observed that the LP objective of the tightened model is signifcantly higher than the standard model indicating that the tightened model provides a better lower bound when the MIP starts. That is likely to contribute to the tightened model's better MIP stopping time performance for cases 4 and 6.

Table A.2.2. Numerical comparison for standard and tightened SOC constraints in MISO case 5.

	Standard SOC		Tightened - Standard	
Case	Objective [$]	Lower Bound [$]	Objective [$]	Lower Bound [$]
5	1.4×10^6	1.4×10^6	22,992	1,841

For case 5, the tightened model is solved slower than the standard model on average. Notice that the LP objectives are the same for both the standard model and the tightened model in case 5. That means the tightened model is not as helpful in case 5 as it is for the other cases, at least at the root node.

To assess the consistency between the result for each run, the average and the sample standard deviation (listed in the paranthesis in each cell) of the stopping time differences (the result of the standard model minus the result of the tightened model) are listed in the last column in Table A.2.1. Except for case 4, the sample standard deviations (STD) are relatively low. That indicates that, except for case 4, the conclusion from the average stopping time does not come from a single or a few runs with extreme results. For case 4, the large STD comes from the fact that the tightened model is solved much slower (more than 2000 seconds) than the standard model in one particular run, while the tightened model is consistently solved faster than the standard model in the other four runs.

Case 5 is an extremely hard case and the solver could not get a solution close to even the 1% MIP relative gap for most of the runs for both the standard and the tightened model. Therefore, the average of the objective and the best lower bound for each model at the cutoff time, or at the time a solution with a less than 1% MIP relative gap was found before the cutoff time (only occurs in one run with the standard model) are listed in Table A.2.2 for a further comparison. Notice that the differences on objective and lower bound between the two models (the result of the tightened SOC minus the result of the Standard SOC model) are listed in the last two columns of the table. The objective of this case is relatively small (about one tenth of most of the other cases). The lower objective is due to the presence of virtual bids/offers and due to violation penalties. In this case it is observed that although the tightened SOC model provides a better (higher) lower bound, it does not help the solver to find a better (lower) objective.

The MIP solver explores the solutions in an iterative process. The way this iterative process is designed and applied in the MIP solver may affect the outcome. However, it is difficult to address that without access to the solver. To summarize, the numerical results of the tested cases in Table A.2.1 show that, with one exception in the seven cases considered, the tightened SOC constraints typically have approximately neutral or improved impact on the computation time. The study results described in this subsection has been summarized in a journal paper and it is submitted and currently under review [A.4].

References:

[A.1] Y. Chen, A. Casto, F. Wang, Q. Wang, X. Wang, and J. Wan, “Improving large scale day-ahead security constrained unit commitment performance,” IEEE Transactions on Power Systems, vol. 31, no. 6, pp. 4732–4743, 2016.

[A.2] MISO, "MISO GIQ web overview," 2019, https://www.misoenergy.org/planning/generator-interconnection/GI Queue/[Online; posted 2019].

[A.3] B.Huang, Y.Chen and R. Baldick, "A Configuration Based Pumped Storage Hydro Model in the MISO Day-Ahead Market", IEEE Trans. Power Syst. July, 2021.

[A.4] R. Baldick, Y.Chen and B.Huang, Optimization Formulations for Storage Devices. Available online: http://www.optimization-online.org/DB_FILE/2021/07/8502.pdf.

IV.B. Accomplishments Toward Milestone 2.1

Milestone 2.1: Establish mathematical formulations to incorporate price forecasts beyond the end of the study window for PSH optimization purpose.

Accomplishments Summary: There are two main accomplishments in this Milestone. (1) The team has prototyped a Look-ahead Commitment (LAC) simulation in HIPPO software. (2) A deterministic PSH optimization model is developed in the LAC formulation. A single point price forecast is used in the model to provide guidance to the PSH in the series of LAC simulation.

IV.B.1 The LAC Rolling Window Simulation in HIPPO

In an operating day, uncertainties on system demand and generation balance arise due to load and generation variations. Those uncertainties are reflected in the uncertainties of LMP. We propose to incorporate a locational marginal price (LMP) forecast into the look-ahead commitment (LAC) problem. A LAC rolling window simulation platform is essential for such implementation and case studies.

A high-performance unit commitment software, HIPPO, is used and further developed to perform the LAC simulations. HIPPO is co-developed by Pacific Northwest National Laboratory (PNNL), MISO and a MIP solver vendor Gurobi to solve large-scale security constrained unit commitment (SCUC) and economic dispatch (SCED) problem for a day ahead (DA) market. The software is built to solve large SCUC and SCED problems for the DA window that includes up to 36 hourly intervals. However, the function to solve a series of rolling LAC windows in a real-time (RT) frame during the day is not available. Based on the original HIPPO code, we have developed the module for the LAC rolling window simulations in HIPPO. The framework of the LAC simulation and the validation results using MISO system data is included in this subsection.

The framework of the LAC rolling window simulation in HIPPO

The framework of the LAC rolling window simulation in HIPPO is illustrated in Fig. B.1.1. To keep minimum modifications to the model structures in HIPPO, each of the LAC rolling window is defined as follows: fix each of the variables outside the LAC window to a previously determined value and allow the variables inside the LAC window to be optimized. In this way, the SCUC or SCED problem is solved with every interval of the entire horizon T for each rolling LAC window so that the constraints remain mostly unchanged. Although variables in every interval are included in the problem for each LAC window, the LAC problem can be solved fast since the only "free" variables are the ones inside the LAC window. Only the unit commitment variables after the LAC window are fixed to the DA solution such that the long lead units can satisfy all binary constraints. At the same time, some of the time-coupled constraints that link the variables after the

LAC to the variables inside LAC such as ramping constraints are disabled to prevent major impacts from the fixed variables after the LAC.

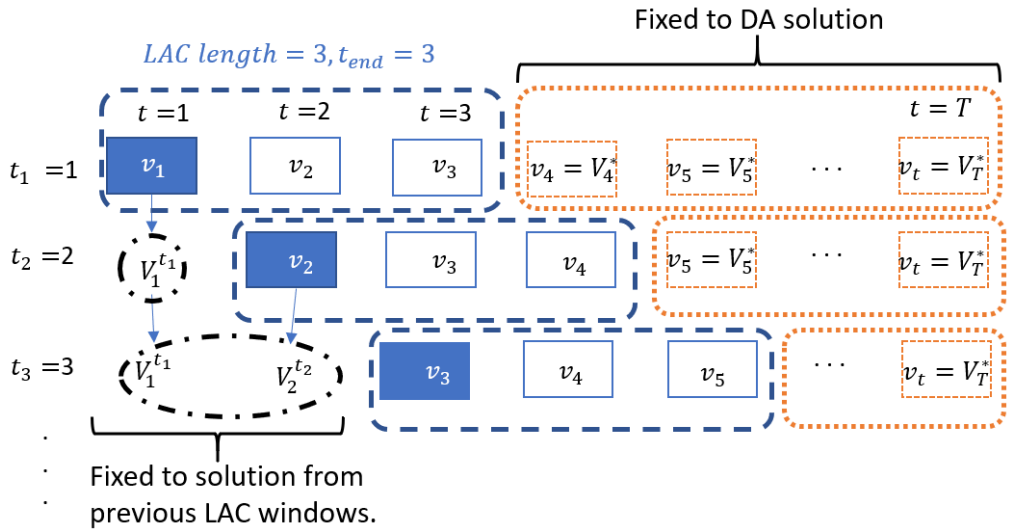

Fig. B.1.1. LAC Rolling Window Simulation Framework in HIPPO. A LAC window is marked by a blue dashed rectangle. The LAC window is moving forward one interval at a time indicated by its position in each time indexed row.

The system variables are indicated in the boxes in Fig. B.1.1. The system variables include the unit commitment and dispatch variables for generators $\mathcal{P}_{gen}, \mathcal{U}_{gen}$ and for PSH units $\mathcal{P}_{psh}, \mathcal{U}_{psh}$, which are defined for each interval for the entire horizon in study: $v_t \in \{\mathcal{P}_{gen}, \mathcal{U}_{gen}, \mathcal{P}_{psh}, \mathcal{U}_{psh} \dots\}, \forall t \in T$. The LAC windows are highlighted by the dashed blue lines in Fig. B.1.1. As an example, there are three intervals included in each LAC window in the figure but the number of intervals in a LAC window is a parameter and can be changed to any integer value between 1 and the total number of intervals T. Notice that the problem is solved with every interval of the entire horizon T represented. However, the intervals after the LAC window highlighted by the dashed orange lines are fixed to a DA solution that is available before the LAC rolling simulation starts.

Although LAC has sub-hour intervals in practice, we first solve a LAC formulation with hourly intervals as a simplification. The hourly intervals allow straightforward comparison of results with DA solutions and it is easier to validate. We can apply sub-hour intervals to the LAC simulation later. The first LAC problem starts at $t_1 = 1$ and it is indicated by the first row of the boxes representing variables in each of the intervals in Fig. B.1.1. Assuming the length of the LAC window is 3 hours, the unit commitment variables after the LAC window is $t \in [4, T]$ and they are fixed to the DA solutions V^*. The LAC window is highlighted by the dashed rectangle and the intervals after the LAC where the solutions are fixed to DA solutions are highlighted in the dotted rectangle in the first row in Fig.B.1.1. After the first LAC problem is solved, the solutions to the variables of the first interval inside the LAC window, that is v_1 written in white font and highlighted in the box filled with blue background, is saved and set as the fixed value $V_1^{t_1}$ to the variables in interval 1 in the next and following LAC problems shown in the dot dashed black circle. Then the second LAC window starts at $t_1 = 2$, with the variables in the first interval v_1

fixed to the solution from the previous window $V_1^{t_1}$ and the commitment variables after the LAC window fixed to the DA solutions $V_t^*, t \in [5, T]$. The variables in the second LAC window are $v_t, t \in [2,4]$. Notice that as the LAC window slides forward at each step, the solution in the first interval inside the previous LAC window is fixed to the variables in the same interval of the current LAC problem and the first interval after the previous LAC window is included in the current LAC window and is "free" to be optimized. After the second LAC window is solved, similarly, the solutions to the variables of the first interval inside the LAC window, that is v_2 written in white font and highlighted in the box filled with the blue background, is saved as $V_2^{t_2}$. Along with the solution of the first interval from the first LAC window $V_1^{t_1}$, $V_1^{t_1}$ and $V_2^{t_2}$ are set as the fixed values for the variables in intervals 1 and 2 in the next and following LAC problems shown in the dot dashed black ellipse. The LAC simulation rolls forward one interval at a time in a similar way until the last interval inside the LAC window reaches the last interval of the entire horizon T.

HIPPO LAC Simulation Validation Results

The framework of the LAC rolling window in HIPPO is first tested and validated with a MISO case with identical case data in DA and LAC cases. Later, the implementation of a deterministic LAC PSH model will be described in section IV.B.2 of this report. The stochastic LAC PSH model and the RT system information update in the LAC simulation is introduced in section IV.E.

The details of the validation results are included in the Appendix for section IV.B.1. The simulation results confirmed that the unit dispatch results from the LAC rolling windows repeat the DA solutions. Once the real-time information such as RT demand is introduced to the LAC rolling window, the case data will differ between the DA and LAC and consequently the solution from LAC would be expected to be different from DA solution. It would be harder to detect if there are any mistakes made in the rolling window program with multiple moving pieces such as changing data. Therefore, it is prudent to test in this middle step to confirm the rolling window structure works correctly.

IV.B.2 A Deterministic PSH Optimization Models in LAC Using Single Point Price Forecast

The research team has explored several model options for the PSH optimization in a LAC problem. The approach of using locational marginal price (LMP) forecast to provide guidance to the PSHU in a LAC is used. The critical question to answer is how to manage the SOC at the end of a LAC window. The end of LAC SOC is important because, as an inter-temporal variable, it determines how much energy is left in the reservoir for the future intervals. The key is to find the best way to effectively reflect the system information from the future (after the LAC window) to the present (inside the current LAC window) so that the LAC could optimize the SOC of the PSHU while being cognizant of the conditions in the future intervals.

Given the availability of historical LMP data in MISO system, a methodology is developed to forecast the LMP at a particular node and it is discussed in details in section IV.E. in this report. In this section, we assume a deterministic single point LMP forecast is available, and we propose a modification based on the PSHU model described in (A.1.1-A.1.14) and a typical LAC formulation to leverage the LMP forecast to optimize the PSHU in a LAC.

$$Objective: Min \sum_{t=t_1}^{t_{end}} C_t(g_t, u_t) - \sum_{t=t_{end}+1}^{T} \sum_{g \in G_{psh}} LMP_{g,t}^{t_0}(q_{g,t}^{gen} - q_{g,t}^{pump}) \quad \text{(B. 2.1)}$$

$$\sum_{k=1}^{K} g_{k,t} + \sum_{g \in G_{psh}} q_{g,t}^{gen} = D_t + \sum_{g \in G_{psh}} q_{g,t}^{pump}, \ \forall t \in [t_1, t_{end}] \quad \text{(B. 2.2)}$$

$$\sum_{k=1}^{K} g_{k,t} = D_t, \ \ \forall t \in [t_{end} + 1, T] \quad \text{(B. 2.3)}$$

$$\text{(A. 1.3)} - \text{(A. 1.11)}, \text{(A. 1.13)}, \text{(A. 1.14)}, \ \ \forall t \in [t_1, T],$$

The first term in (B.2.1) is the objective function for a LAC problem. The production cost $C_t(g_t, u_t)$ is minimized in a LAC window in intervals that start at t_1 and end at t_{end}. Assume the operation and maintanence cost is neglectable for a PSHU, and that the net cost of dispatching a PSHU within the LAC intervals is from the net costs of sale or purchase of energy in the intervals post to a LAC. Such cost is represented in the second term in (B.2.1) as the negative arbitrage profit of the PSHU in the intervals after the LAC starts at $t_{end} + 1$ and stops at the end of the operating day T. The generation of the PSHU at interval t is indicated by $q_{g,t}^{gen}$ and the pump demand of the unit is indicated by $q_{g,t}^{pump}$. The LMP at the node where the PSHU is connected is forecasted for the intervals after the LAC window and it is noted as $LMP_{g,t}^{t_0}$ $\forall t \in [t_{end} + 1, T]$. The LMP forecast is made and updated at t_0 that is one interval before the start of the every LAC window t_1.

The private constraints for a PSHU model are the same as the DA model described in $\text{(A. 1.3)} - \text{(A. 1.11)}, \text{(A. 1.13)}, \text{(A. 1.14)}$ in the Appendix for section IV.A.1, except those constraints are modeled in the intervals from the start of the LAC window t_1 until the end of the operating day T. Since we currently solve the problem in hourly intervals and the constraint on the number of pump starts (A.1.12) is typically effective in sub-hour timeframe, (A.1.12) is less relevant and therefore it is not included in the model.

The PSHU is fully optimized within the LAC window. In the power balance constraint within the LAC window $\forall t \in [t_1, t_{end}]$, the generation of the PSHU, $q_{g,t}^{gen}$, is included on the left hand side of power balance constraint (B.2.2) and the pumping of te PSHU, $q_{g,t}^{pump}$, is considered as demand on the right hand side of the power balance constraint (B.2.2). The dispatch of the PSHU in the intervals after the LAC relies on the LMP forecast and are not optimized with the rest of the system. Therefore, the generation and pumping of the PSHU in the intervals post to the LAC window $\forall t \in [t_{end} + 1, T]$ are not included in the power balance constraint as shown in (B.2.3).

It is observed that the proposed PSHU LAC model (B.2.1) – (B.2.3) heavily relies on the quality of the single point forecast $LMP_{g,t}^{t_0}$. In practice when the price forecast is not perfect, the formulation will easily lead to a suboptimal solution to the system and reduce the PSHU profit. For brevity, the simulation results of the model using single point forecast (B.2.1) – (B.2.3) are not included in this section, but will be presented in comparison with the stochastic PSH models in section IV.E.

IV.C. Accomplishments Toward Milestone 3.1

Milestone 3.1: Establish interleaved DA/RT simulation method for economic planning.

Accomplishments Summary: (1) The team developed an improved PSH model by including detailed water balance constraints, a more realistic piece-wise linear input-output curve, and

transition time between generating and pumping modes for PSH units. (2) We implemented the proposed detailed PSH model and DA/RT interleaved simulation method in PLEXOS. The value of accurate PSH modeling in long-term chronological production cost simulation model is illustrated using a MISO planning system. Our planning studies show, without head-dependent power bounds modeling, the generate power might exceed physical limits, and the head-dependent power bounds modeling is especially important for low-SOC scenarios. In addition, in chronological production cost simulation, SOC error will accumulate day by day and become unacceptable, demonstrating the need of detailed water-power efficiency modeling for long-term planning studies. (3) Further, we proposes a novel disjunctive convex hull model for input-output curve approximation and numeric studies showed an order of magnitude speedup than the common piece-wise linear approximation methods. (4) The team established a deterministic PSH optimization model for economic planning while reflecting the interactions between day-ahead and real-time markets.

IV.C.1 Improved deterministic PSH model for planning

A realistic PSH input-output curve and the efficiency curve

For the generating mode of PSH, Fig. C.1.1 and Fig. C.1.2 shows the input-output curve and the efficiency curve, respectively, based on plant data provided by industry partners. The maximum power output increases with a higher head and generation efficiency varies in ~5% for different net head levels and flow rates.

For the pumping mode of PSH, Fig. C.1.3 and Fig. C.1.4 shows the input-output curve and the efficiency curve, respectively. Pumping efficiency varies in ~6-7% for different net head levels.

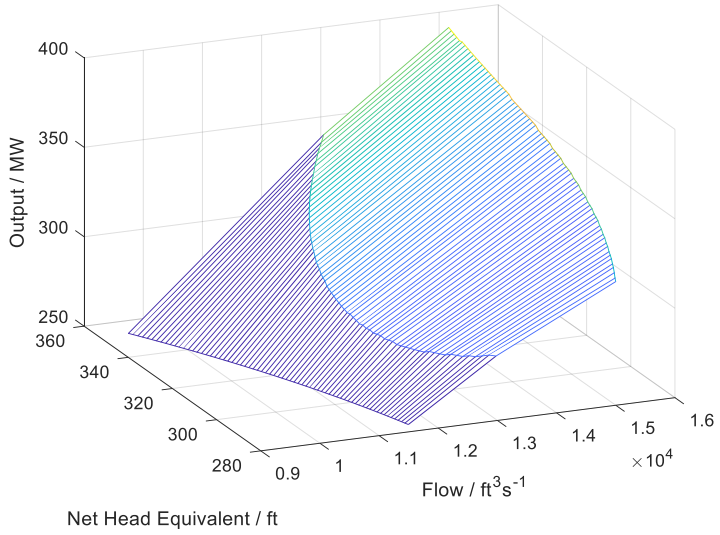

Fig. C.1.1. Input-output Curve for Generating Mode. It describes a generation output function of net head and flow rate. As shown, generation increases as head and flow rate increase. The increasing rate with respect to flow rate first goes up and then comes down.

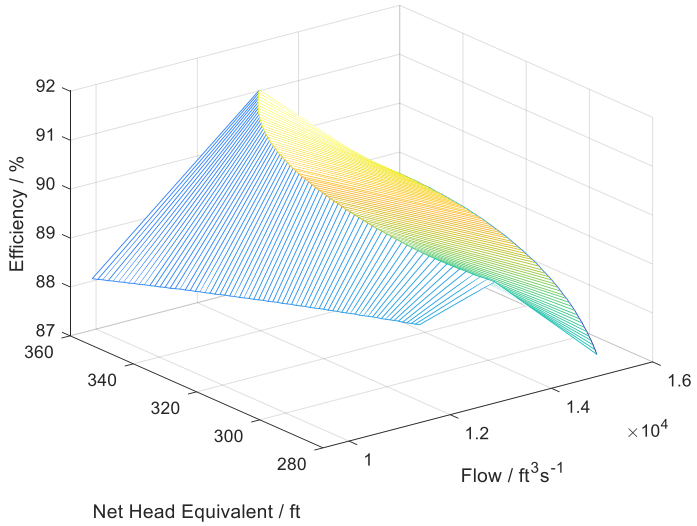

Fig. C.1.2. Efficiency Curve for Generating Mode. Generation efficiency varies in ~5% for different net head levels and flow rates.

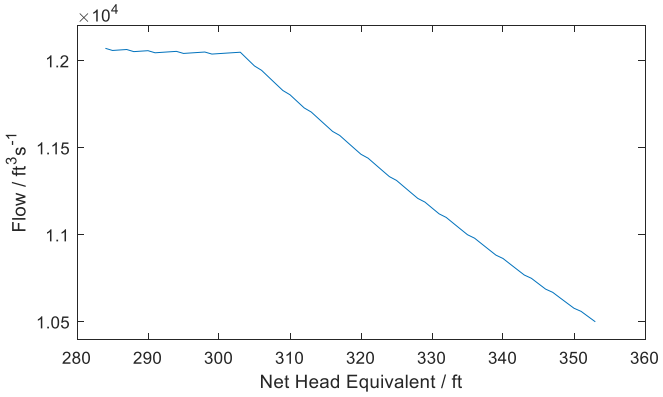

Fig. C.1.3. Input-output Curve for Pumping Mode

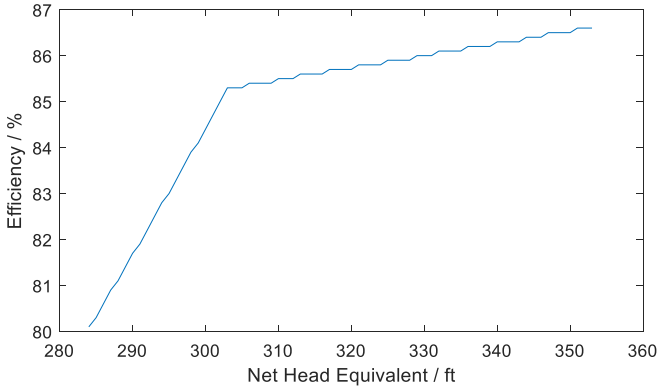

Fig. C.1.4. Efficiency Curve for Pumping Mode. Pumping efficiency varies in ~6-7% for different net head levels.

Zig-zag based piece-wise linear modeling method of input-output curve

In addition to modeling detailed water volume dynamics, bounds and final level, we also modeled the relationship between generating/pumping power, flow rate, and net-head (or water volume). A typical example is shown in Fig. C.1.5, while previously Fig. C.1.1 shows a realistic case. This curve is referred to as an input-output curve, or production function, water-power conversion in the literature. Modeling input-output curve can accurately reflect the efficiency of PSH unit, while it will also bring additional computational burdens since it's nonconvex in general.

We used a zig-zag formulation based piece-wise linear approximation method to model the input-output curve. Compared with the existing piece-wise linear approximation methods for input-output curves in the literature, this Zig-zag based method is compact and strong, thus computational effective.

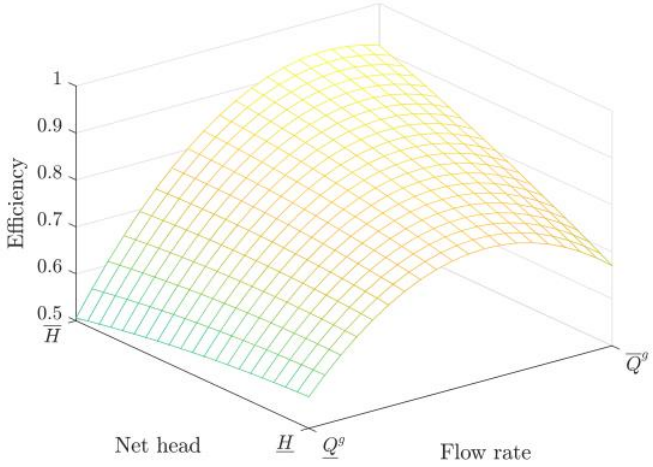

Fig. C.1.5. A typical example of Input Output Curve

In order to test the computational time for zig-zag formulation based piece-wise linear approximation, we performed numerical simulations with different number of pieces, time intervals and operational horizon. The results are shown in Table C.1.1, Table C.1.2, and Table C.1.3, respectively. Compared with the exiting piecewise linear approximation method, zig-zag formulation based input-output curve approximation method can significantly reduce the computational time.

Table C.1.1. Simulation Results for Different Number of Pieces

$m-1$	Zig-zag		Existing	
	Time (s)	Cost (10^3\$)	Time (s)	Cost (10^3\$)
2	3.6	46.15	3.9	46.15
4	4.4	46.12	9.1	46.12
8	25.0	46.12	42.0	46.12
16	52.8	46.12	663.0	46.12

Table C.1.2. Simulation Results for Different Time Intervals

ΔT	Zig-zag		Existing	
	Time (s)	Cost (10^3\$)	Time (s)	Cost (10^3\$)
1 hour	4.1	46.12	7.5	46.12
30 min	22.3	46.02	41.0	46.03
15 min	46.1	45.98	170.0	46.01
5 min	693.3	45.97	> 3600	46.09*

* found a feasible solution that doesn't reach a gap of 0.1% in 3600 seconds.

Table C.1.3. Simulation Results for Different Operational Horizon

T_N (h)	Zig-zag		Existing	
	Time (s)	Cost (10^3\$)	Time (s)	Cost (10^3\$)
24×1	4.4	46.12	9.3	46.12
24×3	67.2	138.18	781.3	138.20
24×7	3378.1	322.42	> 3600	323.29*
24×15	> 3600	691.36*	> 3600	−**

* found a feasible solution that doesn't reach a gap of 0.1% in 3600 seconds.

** no feasible solution found in 3600 seconds.

State transition time and trajectory

Increasing share of renewable energy requires shorter-time-interval and more accurate operation and planning PSH models. Including transition time among different states can improve the flexibility quantification for PSH units. Based on the configuration-based deterministic PSH modeling method mentioned earlier, we modeled the state transition time and trajectory for PSH units.

For illustration, we show the simulation results for short-term dispatch problem with ramp event on a 6-bus system, where the time horizon and the time interval are set as 3 hours and 5 minutes, respectively. We also set a target minimum terminal water level for the upper reservoir.

The load/generation levels, PSH injection power, and PSH status results when state transition times are modeled are shown in (a), (c), (e) subplots of Fig. C.1.6. The corresponding results when state transition times are not considered are shown in (b), (d), (f) subplots of Fig. C.1.6. Coping with the same ramp event, we find PSH unit can switch from generating mode to pumping mode in 5 minutes if state transition times are ignored, which may overestimate the flexibility of PSH units. Considering the state transition time and trajectory, our proposed model can more realistically quantify the flexibility of PSH. Specifically, in subplots (d), (f) of Fig. C.1.6, the PSH unit transits from pump to generate and than from generate to pump, both of which happen in 5 minutes (please see 15th min-30th min, i.e., blocks 4-6[6]). This is unrealistic in practice due to mode transition time requirements of PSH. After modeling the transition process, in subplots (c), (e) of Fig. C.1.6, the unrealitic PSH flexibility through violating the transition time requirement is corrected, thus leading to a more realistic quantification of PSH flexibility.

[6] Note that the resolution of Fig. C.1.6 subplots is 5 minutes. There are 12 blocks in each hour. The 1st block represents 0-5th minutes. Thus, the blocks 4-6 represent 15th-30th minutes.

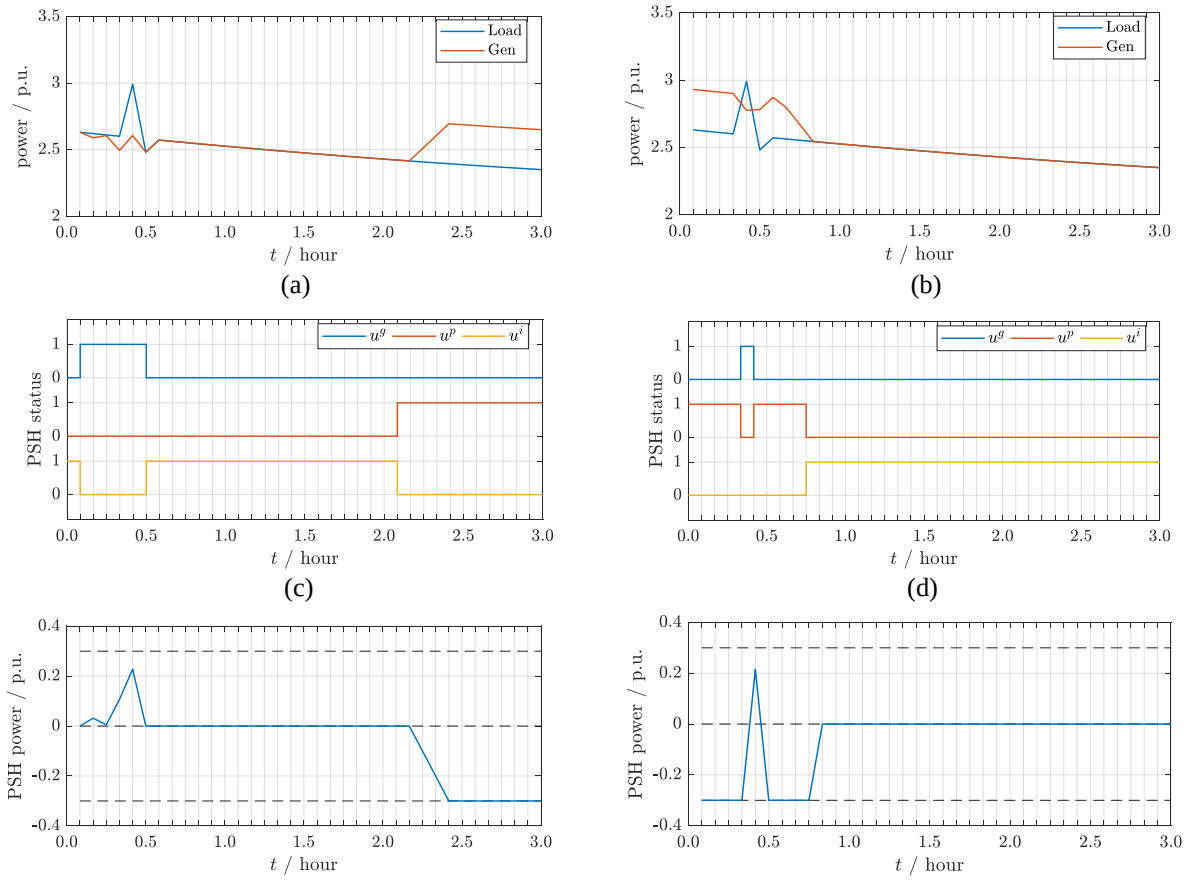

Fig. C.1.6. Results Comparison. For transition time considered case: (a) system load and generation, (c) PSH generating/pumping/idle status, (e) PSH dispatch power. For transition time ignored case: (b) system load and generation, (d) PSH generating/pumping/idle status, (f) PSH dispatch power.

IV.C.2 Impact of enhanced PSH modeling in planning

In our PSH modeling enhancement, there are two important aspects: one is head-dependent power bounds modeling, which quantifies pump power and available generation capacity at each head level, thus avoids the simulation result from violating physical limits; another is variable efficiency modeling, which accurately describes the SOC change given generate or pump power, thus tries to mitigate significant cumulative error in long-term simulations.

Head-dependent power bounds modeling

Based on the real measurement from a realistic PSH unit, the head-dependent maximum generate power and pump power are modeled by off-the-shelf piece-wise linear modeling methods for two-dimensional cases. For maximum generate power, linear constraints are created for the convex feasible region. For pump power, as the fixed pump power for each water head level forms a non-convex feasible region, mixed-integer linear constraints are created due to the non-convexity. We use the zig-zag approximation approach for the mixed-integer piece-wise linear modeling. With an enabling tool we developed, the head-dependent modeling enhancement is

implemented as PLEXOS custom constraints in a MISO planning model (called Eastern Interconnection Seams model).

A comparison analysis was conducted for a realistic PSH with and without head-dependent power bounds modeling. Power bound errors for generate and pump modes are calculated in (C.2.1) and (C.2.2), respectively.

$$\varepsilon_t^{\mathrm{g}} = \sum_{h\in\mathcal{H}^r}\left[p_{h,t}^{\mathrm{g}} - \overline{P}_h^{\mathrm{g}}\left(e_{r,t}\right)\right]^+ \tag{C.2.1}$$

$$\varepsilon_t^{\mathrm{p}} = \sum_{h\in\mathcal{H}^r}\left(p_{h,t}^{\mathrm{p}} - P_h^{\mathrm{p}}\left(e_{r,t}\right)\right) \tag{C.2.2}$$

where, $\varepsilon_t^{\mathrm{g}}$ and $\varepsilon_t^{\mathrm{p}}$ are power bound errors for generate and pump modes, respectively. $p_{h,t}^{\mathrm{g}}$ and $p_{h,t}^{\mathrm{p}}$ are generate and pump power from simulations for unit h at time period t, respectively. $e_{r,t}$ represents SOC of reservoir r at time period t. Given an SOC level $e_{r,t}$, $\overline{P}_h^{\mathrm{g}}\left(e_{r,t}\right)$ and $P_h^{\mathrm{p}}\left(e_{r,t}\right)$ denote maximum generate power and fixed pump power from the original head-dependent power bounds data (in which piecewise linear approximation is not applied), respectively.

As indicated in Fig. C.2.1 (a), without head-dependent power bounds modeling, the generate power might exceed physical limits. The pump power could also have significant errors sometimes. However, with piece-wise linear head-dependent power bounds modeling, the power bound error for the whole 6-unit PSH station can be less than ~5 MW. A low-SOC test is also conducted, which aims to reflect the error for low-SOC operation points, although this scenario is unrealistic to keep for two weeks in practice. The initial SOC is set at a relatively low level (~4 GWh), and the SOC of the upper reservoir follows a daily recycle. As shown in Fig. C.2.1 (b), in the low-SOC test, the amount that PSH generation exceeds its physical limit is larger. Thus, head-dependent power bounds modeling is especially important for low-SOC scenarios.

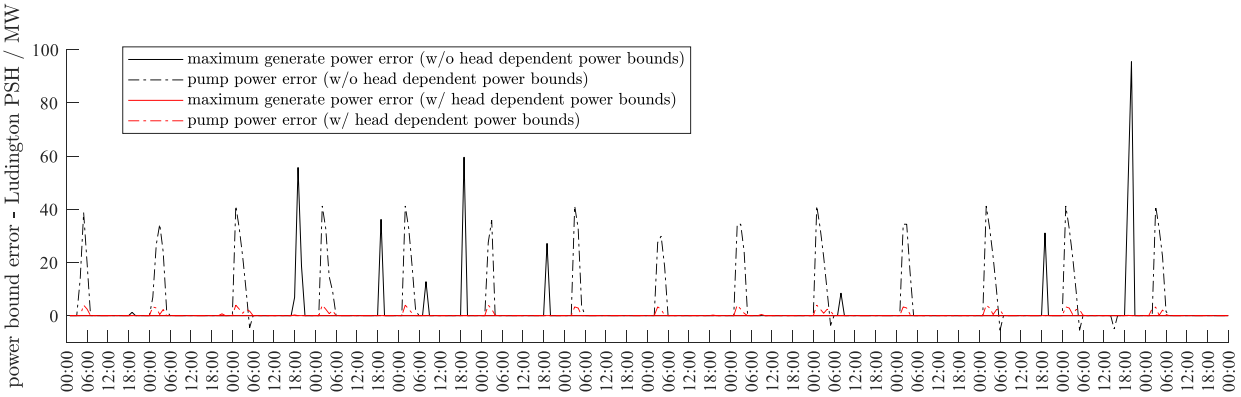

(a) normal-SOC case

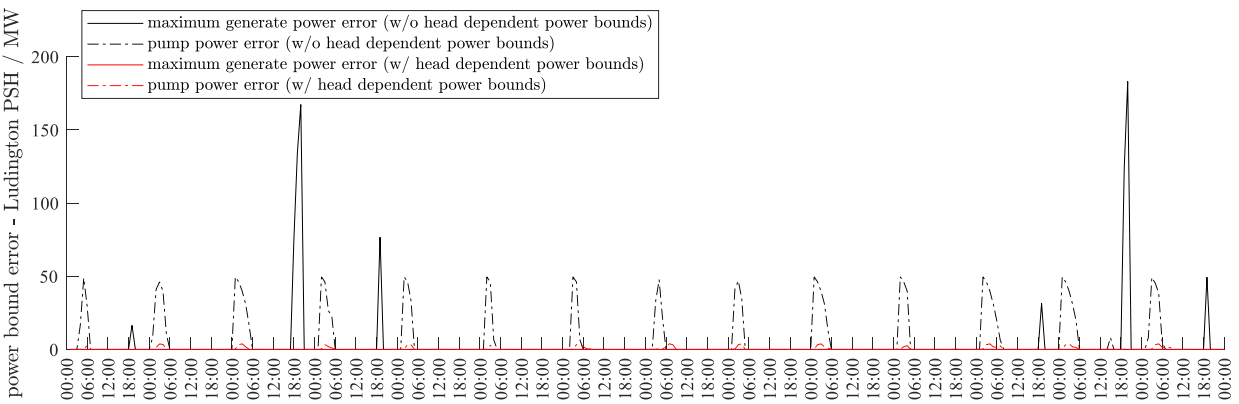

(b) low-SOC case

Fig. C.2.1. Errors with and without head-dependent power bounds modeling. Without head-dependent power bounds modeling, the generate power might exceed physical limits. The pump power could also have significant errors sometimes

Variable efficiency modeling

The constant efficiency modeling serves as the current practice for PSH modeling in MISO planning studies. The variable efficiency modeling would bring additional computational burdens, however, can accurately quantify the relation of water-power conversions. Variable efficiency modeling and its acceleration method have been investigated in previus quarters, the value of variable efficiency modeling is presented here.

The numerical test is conducted as follows, 1) run a production cost simulation using the constant efficiency PSH model, and get the resulting SOC and MW-output; 2) with the same MW-output, re-simulate an SOC curve using the variable efficiency PSH data. As shown in Fig. C.2.2 (a), the SOC difference becomes larger with time in the long-term simulation, and the two SOC curves vary significantly after one week.

In the current practice of PSH plant operations, the water level of the upper reservior is measured and adjusted every day at midnight. To participate in the market, PSH owners will adjust SOC every day; however, this process is difficult to consider in long-term planning models. In order to analyze the impact of efficiency modeling in both operation and planning models, in our numerical simulation, cumulative SOC error is cleared daily for a DA dispatch simulation. As indicated in Fig. C.2.2 (b), for the operation model, SOC error is relatively under control in most days, as the SOC will be adjusted daily. For the chronological production cost simulation model, SOC error will be accumulated. Therefore, detailed water-power efficiency modeling is more important in long-term simulations.

As introduced before, a low-SOC test is also conducted to observe the SOC error for low-SOC operation points. In Fig. C.2.3, SOC error from the low-SOC test is much larger than that from the normal-SOC test. Thus, variable efficiency modeling is more important for low-SOC scenarios. In addition, one real PSH schedule from MISO state estimation during a 15-day period is used for validation. Cumulative SOC error curves are calculated using both constant and variable efficiency models. As shown in Fig. C.2.4, the same conclusion can be obtained as that from the simulation data.

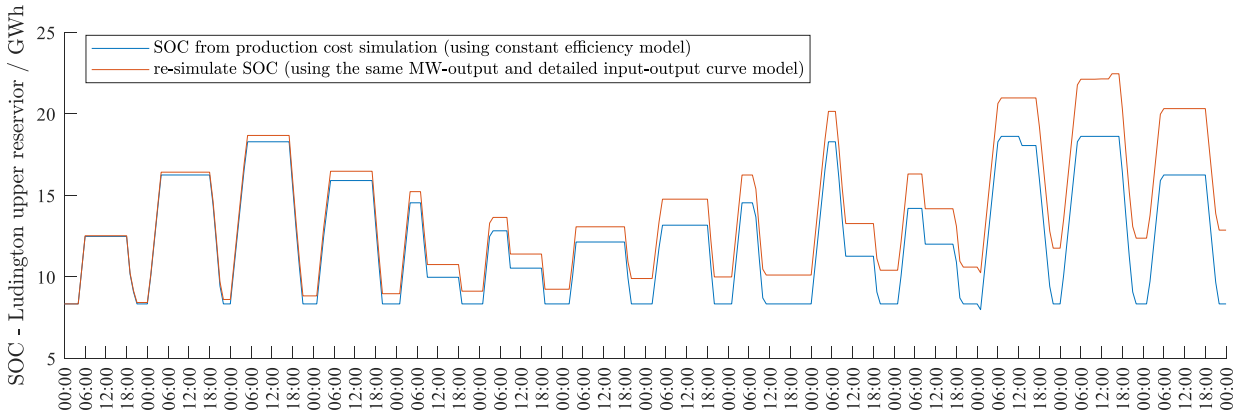

(a) SOC comparison

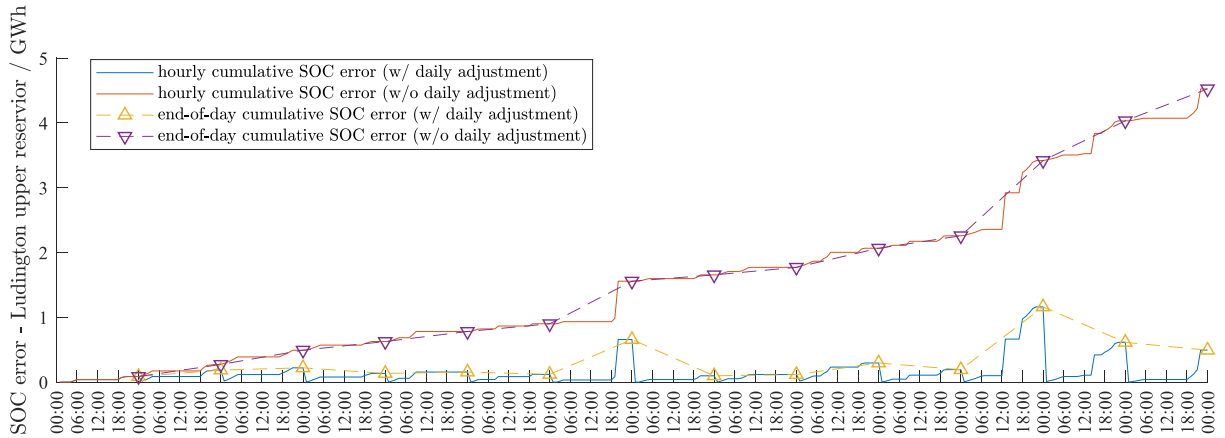

(b) SOC cumulative error comparison

Fig. C.2.2. SOC and cumulative SOC error. SOC difference becomes larger with time in the long-term simulation. In operations, SOC error is relatively under control in most days, as the SOC will be adjusted daily. For the chronological production cost simulation model, SOC error will keep accumulating over time.

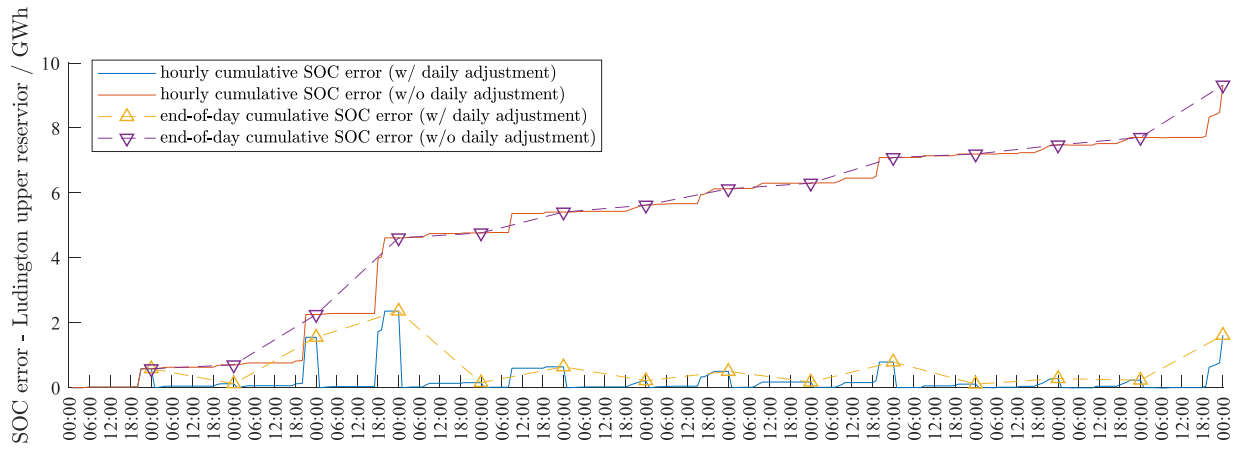

Fig. C.2.3. cumulative SOC error comparison (low SOC case)

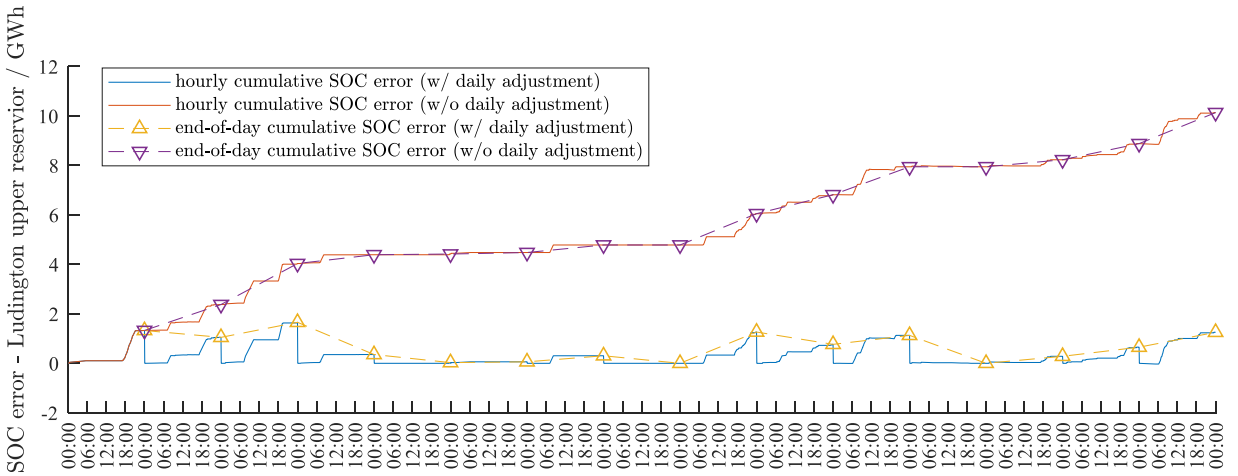

Fig. C.2.4. cumulative SOC error comparison (realistic data)

IV.C.3 Further improved PSH input-output curve modeling with approximate convex decomposition method

To further improve the computational performance, the team proposed a novel disjunctive convex hull model for input-output curve approximation in conjunction with approximate convex decomposition method. In contrast to direct piece-wise linear approximation methods, the proposed method exploit the partial convex properties of the input-output curve. At the same time, we take advantage of the integer variable modeling to preserve approximating accuracy for non-convex part of the curve, which can appropriately address the accuracy issue from the convex hull approximation method. Detailed modeling can be found in the 2020 Q4 Quarterly Report.

To facilitate a numerical performance comparison, the input-output curve is approximated by three methods: piece-wise linear approximation method (PWL), convex hull approximation method (CH), and the proposed disjunctive convex hull approximation method with approximate

convex decomposition (DCH). In Fig. C.3.1, (a), (b), and (c) shows how our proposed disjunctive convex hull approach models the input-output curve under different tolerance settings. Note our disjunctive convex hull approach with $\text{tol}^{\text{g}} = 10$, as shown in Fig. C.3.1 (a), is equivalent to the traditional convex hull approximation method. As a matter of fact, different parameter settings, such as the number of pieces in PWL and the tolerance in CH, affect the number of binary variables, thus the solution time. On the other hand, they also have impacts on the approximation accuracy. So, the estimation error and computation time for the aforementioned approximation methods are needed to be compared for different parameter settings.

On the *accuracy* side, a summary of maximum estimation errors for these methods is shown in Table C.3.1. As indicated, the estimation error for both DCH and PWL methods can be reduced with larger tolerance and a larger number of pieces, respectively. The CH approach, i.e. DCH approach with $\text{tol}^{\text{g}} = 10$, has a relatively large error. Taking the *solution time* into account, the PWL method didn't converge in 2 hours even for a 5×5-piece case, as shown in Table C.3.1. Our proposed DCH method has better performance in solution time than the PWL method under similar estimation error settings. For example, the DCH method with $\text{tol}^{\text{g}} = 2.5$ has similar accuracy in comparison to the PWL method with 15×15 or 20×20 pieces, however, it can be solved much faster.

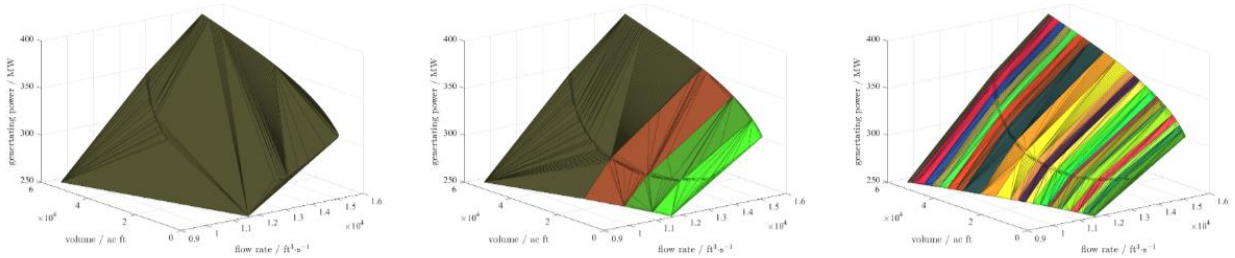

Fig. C.3.1. Input-output curve modeling: subplots (a), (b), and (c) are disjunctive convex modeling for $\text{tol}^{\text{g}} = 10,2.5,0.5$, respectively.

Table C.3.1. Performance Comparison.

DCH				PWL		
tol $^{\text{g}}$	max error (MW)	# of comp.	time (s)	n	max error (MW)	time (s)
10(CH)	5.878	1	122.8	5	9.510	> 7200
2.5	2.496	4	1636.9	10	4.625	> 7200
1.5	1.267	7	4371.0	15	2.804	> 7200
0.5	0.487	24	> 7200	20	2.296	> 7200

IV.C.4 Establish interleaved DA/RT simulation for economic planning

Synthesize RT load

Both DA hourly load variation trend and randomness are considered in synthesizing RT load. The procedure is as follows: First, generate trends from DA data, i.e., using linear interpolation or other methods to generate a 5-min resolution RT load trend curve $D_t^{\text{RT Trend}}$. Second, generate

randomness via inverse sampling of a particular distribution, e.g., for normal distribution the RT load with randomness can be generated by (C.4.1).

$$D_t^{\mathrm{RT}} = \left(1 + cdf_{\mu,\sigma}^{-1}(\zeta)\right) D_t^{\mathrm{RT\ Trend}} \tag{C.4.1}$$

where, $cdf_{\mu,\sigma}^{-1}(\cdot)$ is the inverse cumulative distribution function with mean value μ and standard deviation σ, variable ζ follows a uniform distribution in [0, 1].

The proposed RT load synthesizing method is validated using the authentic RT load and the synthesized RT load from DA load. As shown in Fig. C.4.1, for a company level RT load, the proposed method can well capture the trend of RT load, and generate a certain degree of randomness.

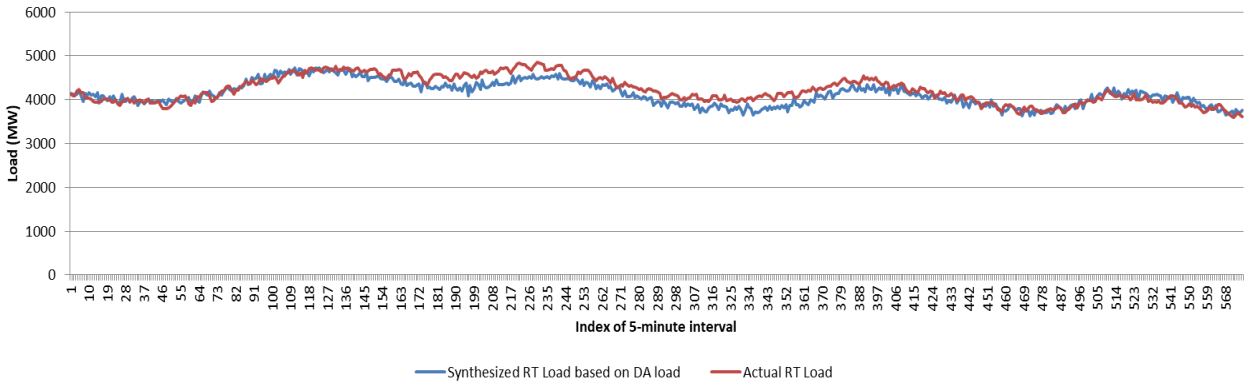

Fig. C.4.1 validation with a company-level load

Procedure of DA/RT interleaved simulation

To capture the interaction between DA and RT markets, an interleaved simulation method is established for the MISO planning model. As shown in Fig. C.4.2, DA and RT market optimizations are run sequentially with information exchanges.

The information passed from the DA market to the RT market includes DA unit commitment for traditional generators and PSH DA information (can be generate/pump commitment, MW-output, upper reservoir shadow price depending on the employed PSH RT operation strategy). From the RT market to the DA market, the RT end state is automatically passed by PLEXOS (including but not limited to MW-output, SOC, and on/off hours). Note currently the model assumes the RT end state is fully known by the DA model.

Detailed MISO planning case study and benefit analysis are presented in section IV.F with an enhaced PSH modeling included.

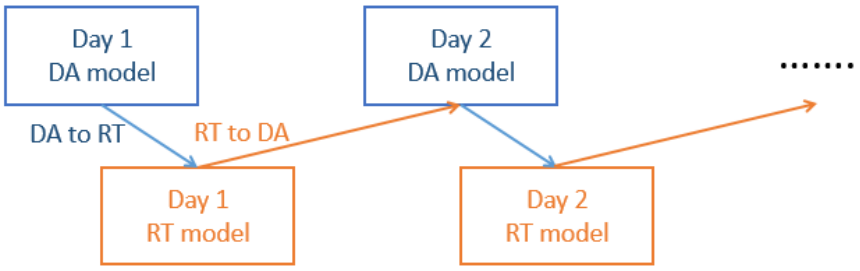

Fig. C.4.2 procedure of DA/RT interleaved simulation

IV.D. Accomplishments Toward Milestone 4.1

Milestone 4.1: Establish prototype of enhanced PSH model within the SCUC framework. The SCUC framework including the key proposed functionalities will be ready for further testing and evaluation on the MISO system.

Accomplishments Summary: (1) The team proposed the MWh reserve constraint concept for PSH units in the day-ahead SCUC model to address the potential SOC boundary violation issue in real-time ED, as a result of RT uncertainties. (2) We developed the energy reserve secure constraints of PSHs in the day-ahead SCUC model. Using MISO's historical data, we developed energy reserve requirement for modeling the secure reserve constraints. (3) Based on the uniform hourly SOC deviation method, we use a PSH profit maximization model with price forecasts to evaluate the impacts of energy reserve secure constraints on profits of PSH owners. Numerical results show that the inclusion of energy reserve secure constraints can improve system security against uncertainties and contingencies, and meanwhile does not necessarily reduce profits of PSH units.

IV.D. 1 The need for energy reserve

Please note: in this document, energy reserve and MWh reserve are used interchangeably. To illustrate a possible scenario when the PSH SOC boundary may be violated due to deviation in RT from DA schedule, we took an actual PSH station data on a winter day of 2019 as an example, as shown in Fig. D.1.1. Because currently MISO does not monitor/record the SOC information and thus the initial SOC value on this day is unavailable, we assume the initial SOC is 9,313 MWh in both DA and RT. The red lines in Fig. D.1.1 represent SOC information in DA, and blue lines are SOC in RT. From this figure, we can see that more energy and reserve are cleared in RT than in DA. If the initial SOC in RT is less than (9,313 – 5,497) MWh, the terminal SOC will be lower than 0 MWh, violating the SOC lower limit (assuming it is 0MWh) at the end of the operating day. Indeed, if spinning reserve is called in one hour of RT (for example, the maximum hourly spinning reserve in this day is 120MW) and initial SOC < (9,313 – 5,497 – 120) MWh, the SOC violation will occur. If spinning reserve in all 24 hours are fully called for deployment and the initial SOC < (9,313 – 5,136) MWh, the SOC violation would occur.

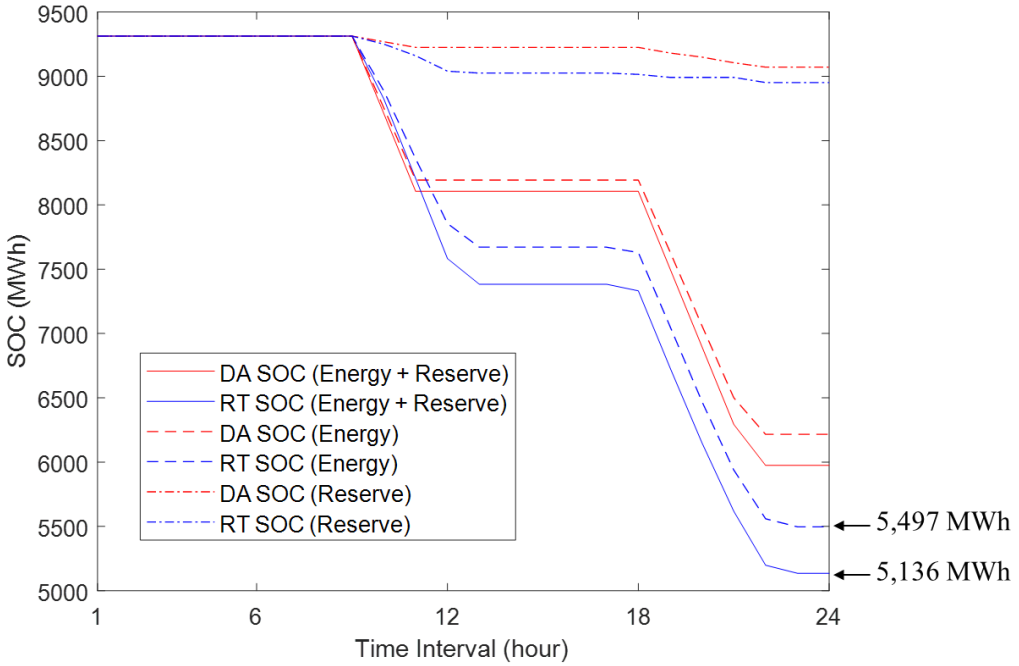

Fig. D.1.1 A hypothetical scenario to illutrate possible SOC boundary violation

Indeed, large SOC deviations between MISO's DA and RT markets are observed in the historical data. To understand the possible cause of the SOC deviation, we tried to understand the consistency between the DA and RT commitment statuses. The historical data in 2019 for this PSH owner with six PSH units was processed for statistical analysis. The hourly commitment results of PSH units in DA and RT are presented in Fig. D.1.2, as an overview of consistent and inconsistent commitments in DA and RT. Three kinds of commitment situations in DA and RT are shown in this figure. The orange dots represent that PSH units are operated in generating mode in both DA and RT, i.e., the commitments in DA and RT are consistent. The green and blue dots stand for inconsistent commitments in DA and RT. Specifically, the green dots mean PSH units are operated in the generating mode in DA, while in RT they are either in pumping or idle mode. The blue ones describe the opposite situation. When there is inconsistent commitment status between DA and RT, a large deviation in SOC is likely to be observed. Such SOC deviations need to be considered in developing the MWh reserve constraints in order to avoid potential SOC boundary violations.

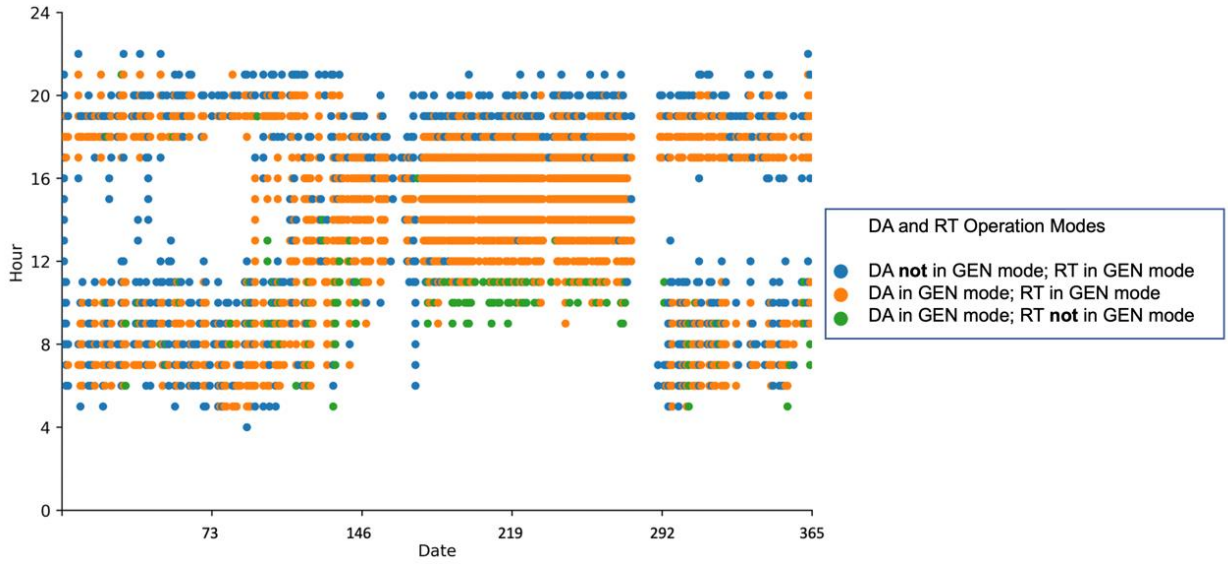

Fig. D.1.2 DA and RT commitment status of the studied PSH in 2019. Legend represents the PSH commitment status in RT and DA. For instance, "DA not in GEN mode; RT in GEN mode" legend means the PSH is not in generation mode in DA market, and it is in generation mode in RT market.

From Fig. D.1.2, we can see that the inconsistent commitments did occur significantly, especially during the beginning and ending hours of a generation period, which could result in large MWh deviations between DA SOC and RT SOC. It should also be noted that, even when the commitment statuses between DA and RT are consistent, the SOC deviation may still occur due to different dispatch levels in DA and RT. Due to the market complications, it is hard to tell whether a SOC deviation is caused by renewable forecast errors, load forecast errors, or interchange and generation uncertainties. To this end, we designed several statistical methods to directly process historical PSH data, and performed scenario selection and reduction approaches to obtain the statistical results of MWh deviation caused by uncertainties, whose details were included in 2020 Q3 Quarterly Report and not included in this final report for conciseness. Besides, it could be observed that, in warm monthes PSH has one continuous generating period in each day and the commitments in DA and RT are mostly consistent, while in cold monthes PSH may have multiple inconsecutive generating periods in a single day and the commitments in DA and RT are usually inconsistent.

IV.D. 2 Formulate secure energy reserve requirement

The energy reserve secure constraints can be represented as follows:

$$E^{LB} + E_t^{M+} \leq E_t \leq E^{UB} + E_t^{M-} \quad \text{(D.2.1)}$$

where E_t is the scheduled SOC of time t; E_t^{M-} and E_t^{M+} respectively are the head room and floor room to be held in advance for securing the real-time operations. The values of head room and floor room for each time interval will be evaluated via the historical data.

If the values of head room and floor room will be evaluated via the historical data of generation and pumping modes separately, (D.2.1) becomes

$$E^{LB} + F_t^G \leq E_t \leq E^{UB} - F_t^P \quad \text{(D.2.2)}$$

where F_t^G is the floor room at time *t*, which is valued by the MISO historical SOC deviation data of the generation mode, and the head room F_t^P at time *t* is calculated by the MISO historical SOC deviation data of the pumping mode.

From formula (D.2.2), two different methods are developed to calculate F_t^G and F_t^P. Initially a uniform hourly SOC deviation constraint (**Method 1**) was developed. Later on, based on observations from MISO historical data that the levels of SOC deviation can be quite different during different periods of the PSH operation modes, a three-section hourly SOC deviation constraint (**Method 2**) was developed to describe the hourly deviation during beginning/ intermediate/ending periods of the generation/pumping mode. **Method 2** is expected to be more accurate and less conservative.

The **Method 1** is

$$F_t^G = \sum_{\tau=t}^{NT} F_{r,t}^G \qquad \& \qquad F_t^P = \sum_{\tau=t}^{NT} F_{r,t}^P \tag{D.2.3}$$

where F_t^G/ F_t^P is the hourly reserve for generation/ pumping mode at time t.

The **Method 2** is

$$F_t^G = \sum_{\tau=t}^{NT} (F_t^{G,B} + F_t^{G,I} + F_t^{G,E}) \qquad \& \qquad F_t^P = \sum_{\tau=t}^{NT} (F_t^{P,B} + F_t^{P,I} + F_t^{P,E}) \tag{D.2.4}$$

where $F_t^{G,B}/F_t^{G,I}/F_t^{G,E}$ is the hourly reserve for beginning hour/intermiate hours/ending hour of the generation mode, and $F_t^{P,B}/F_t^{P,I}/F_t^{P,E}$ is the hourly reserve for beginning hour/intermiate hours/ ending hour of the pumping mode. We can consider (D.2.4) as a general representation of (D.2.3). That is, if the hourly deviations of the beginning, intermediate, and ending hours of generation/pumping mode are the same, (D.2.4) is degradaded to (D.2.3).

We proposed two different sets of deviation constraint formulations based on the above two methods. The formulation for **Method 1** "uniform hourly SOC deviation constraints" is described as follow (Note: Details of the formulation, illustrative example, and statistical analysis for **Method 2** "three-section hourly SOC deviation constraints" were included in 2020 Q4 Quarterly Report, and not included in this final report for conciseness.).

Uniform hourly SOC deviation constraint formulation for Method 1

In this subsection, we present the uniform hourly SOC deviation constraint formulation for **Method 1**, which shows that when the PSH is on the generation/ pumping mode, a uniformly hourly deviation boundary can be constructed at each time:

Floor Room for Generation Mode:

$$F_{r,t}^G \geq \Delta_r^G \cdot ur_{r,t}^G \tag{D.2.5}$$

Head Room for Pumping Mode:

$$F_{r,t}^P \geq \Delta_r^P \cdot ur_{r,t}^P \tag{D.2.6}$$

Final Floor/Head Room Formulation:

$$E_r^{LB} + \sum_{\tau=t}^{NT} F_{r,\tau}^G \leq E_{r,t} \leq E_r^{UB} - \sum_{\tau=t}^{NT} F_{r,\tau}^P \tag{D.2.7}$$

Here we define $ur_{r,t}^G$ and $ur_{r,t}^P$ as continuous variables, which indeed can only take binary values as restricted by other constraints for PSHs. It is 1 if reservoir r is in generation/pumping mode at time t. Δ_r^G/Δ_r^P is the unique hourly deviation value for generation/pumping mode. $F_{r,t}^G$/ $F_{r,t}^P$ is the hourly reserve for generation/pumping mode at time *t*. $E_{r,t}$ is the scheduled SOC of time *t* for reservoir r.

Variable $ur_{r,t}^G/ur_{r,t}^P$ describes whether the reservoir is operated in generation/pumping mode. The unique hourly deviation values for generation/pumping mode Δ_r^G/Δ_r^P are evaluated by the historical data with a certain confidence level.

Statistical Analysis

The head/floor room value for each time interval is calculated based on historical data in the pumping/generation period. Specifically, for the headroom, we collect and evaluate historical SOC deviation for each time interval in the pumping period; For the floor room, it is from the generation period. The unique hourly deviation values for generation/pumping mode Δ_r^G/Δ_r^P are evaluated by the historical data with a certain confidence level. The statistical results presented below are obtained with a 95% confidence level.

Fig. I.D.4.1 shows the data analysis of SOC deviation for generation/pumping mode during the historical PSH DA and RT data in 2019. The left subfigure is the histogram of the historical SOC deviation of the generation mode, and the right subfigure is the histogram of the historical SOC deviation of the pumping mode.

```
mean       60.333180
count    1414.000000
std       179.143915
Name: SOC_together, dtype: float64
------------------------------
mean                      60.3332
count                        1414
std                       179.144
ci95_hi     [411.4552528888061]
ci95_lo    [-290.7888926813568]
Name: SOC_together, dtype: object
```

```
mean       14.436623
count    1102.000000
std       207.084638
Name: SOC_together, dtype: float64
------------------------------
mean                      14.4366
count                        1102
std                       207.085
ci95_hi     [420.3225135849308]
ci95_lo    [-391.4492679708957]
Name: SOC_together, dtype: object
```

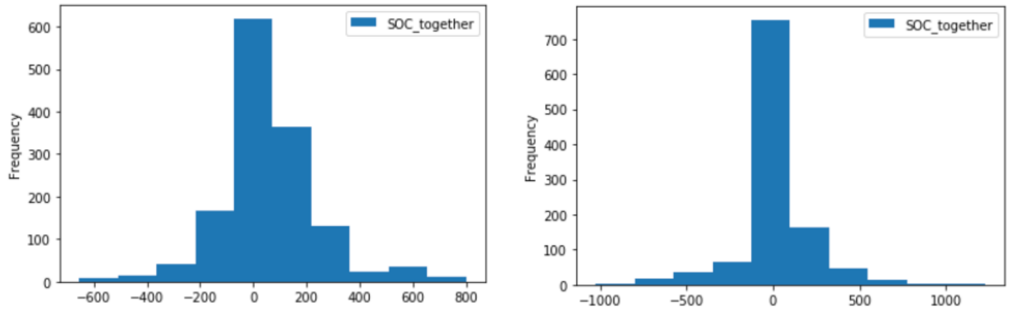

Fig. D.2.1. Histgram for historical SOC deviation of generation/pumping mode

Tables D.1.I and D.1.II show the statistical results of the floor and head rooms. The floor room is calculated by the 95% lower confidence bound of the histogram of generation mode in the left subfigure of Fig. D.2.1. The head room is calculated by the 95% higher confidence bound of the histogram of pumping mode in the right subfigure of Fig D.2.1. For instance, we can see from Tables D.1.I that if in the DA schedule the generation duration is 4 hours, the floor room will hold 1,163.2MWh. When the PSH is on the pumping mode for 1-4 hours, the floor rooms range from 420.3MWh to 1,681.2 WMh. As will be illustrated in the following subections, the model with energy reserve secure constraints will not necessarily reduce profits of PSH owners. Indeed, the profit could be the same or even higher than the one without energy reserve secure constraints.

Table. D.1.I. Statistical results of floor room

GEN period duration (hours)	Floor Room (MWh)	Conservative Ratio_Gen
1	290.8	1.6%

4	1,163.2, 872.4, 581.6, and 290.8 for GEN hours 1-4	6.2%, 4.7%, 3.1%, 1.6%

Table. D.1.II. Statistical results of head room

PUMP period duration (hours)	Head Room (MWh)	Conservative Ratio_Pump
1	420.3	2.3%
4	1,681.2, 1,260.9, 840.6, and 420.3 for PUMP hours 1-4	9%, 6.8%, 4.5%, 2.3%

Besides the above uniform hourly SOC deviation constraint formulation for **Method 1**, we also explored a refined **Method 2**: three-section hourly SOC deviation constraints. This is motivated by the observations from MISO historical data that the levels of SOC deviation can be quite different during different periods of the PSH operation modes. The three-section hourly SOC deviation constraints describe the variant hourly deviation boundaries during beginning/ intermiate/ending periods of the generation/ pumping mode. Details of the formulation, illustrative example, and statistical analysis were included in 2020 Q4 Quarterly Report, and not included in this report for conciseness. The **Method 2** "three-section hourly SOC deviation constraint" could provide better solutions, in terms of smaller conservative ratio, than the **Method 1** "uniform hourly SOC deviation constraint".

IV.D. 3 Impact of modeling reserve secure constraint

We use the PSH profit maximization problem with price forecasts as an example to understand the potential financial impacts of energy security constraints to PSH owners. We add the uniform hourly SOC deviation constraints, i.e., constraints (D.2.1)-(D.2.3) and (D.2.5)-(D.2.7), as well as additional binary variables, to the profit maximization model, which leads to an MILP formulation. $LMP_{t_0,s,t}$ is forecasted LMP for hour *t* in scenario s conducted at hour t_0, which are described in section IV.E.

The PSH profit maximization mode is detailed as follows:

$$max \sum_{s=s_0}^{s_N} \sum_g p_s LMP_{t_0,s,t_0} psh_{g,t_0} + \sum_{s=s_0}^{s_N} \sum_{t=t_0+1}^{T} \sum_g p_s LMP_{t_0,s,t} psh_{g,s,t}$$

s.t.
$$\underline{P}_{pump} u_{g,t_0}^{pump} + \underline{P}_{gen} u_{g,t_0}^{gen} \le psh_{g,t_0} \le \overline{P}_{pump} u_{g,t_0}^{pump} + \overline{P}_{gen} u_{g,t_0}^{gen}, (\underline{\alpha}_0)$$
$$\underline{P}_{pump} u_{g,s,t}^{pump} + \underline{P}_{gen} u_{g,s,t}^{gen} \le psh_{g,s,t} \le \overline{P}_{pump} u_{g,s,t}^{pump} + \overline{P}_{gen} u_{g,s,t}^{gen} \forall t \in [t_1, T], \forall s, \ (\underline{\alpha}_{t,s}, \overline{\alpha}_{t,s})$$
$$e_{r,t_0} + \sum_g psh_{g,t_0} - E_{start} = 0, \forall r \quad (\gamma_0)$$
$$e_{r,s,t_0+1} + \sum_g psh_{g,s,t_0+1} - e_{r,t_0} = 0, \forall s, \forall r \quad (\gamma_{t,s})$$
$$e_{r,s,t} + \sum_g psh_{g,s,t} - e_{r,s,t-1} = 0, \ \forall t \in [t_0 + 2, T], \forall s, \forall r \quad (\gamma_{t,s})$$
$$E_{r,T} - e_{r,s,T} = 0, \quad \forall s, \forall r. \quad (\gamma_{T,s})$$
$$E_r^{LB} + \sum_{\tau=t_0}^{NT} F_{r,s,\tau}^G \le e_{r,t_0} \le E_r^{UB} - \sum_{\tau=t_0}^{NT} F_{r,s,\tau}^P, \forall s, \forall r, (\theta_{0,s})$$
$$E_r^{LB} + \sum_{\tau=t}^{NT} F_{r,s,\tau}^G \le e_{r,s,t} \le E_r^{UB} - \sum_{\tau=t}^{NT} F_{r,s,\tau}^P \ \forall t \in [t_1, T], \forall s, \forall r, \ (\underline{\theta}_{t,s}, \overline{\theta}_{,t,s})$$

Binary Constraints:

$$\sum_{m\in M_g} u^m_{g,t_0} = 1\,,\ \sum_{m\in M_g} u^m_{g,s,t} = 1\,,\quad \forall g \in G, \forall t \in T\backslash t_0, \forall s$$
$$u^m_{g,t_0} = \sum_{n\in M_g^{F,m}} v^{n,m}_{g,t_0} - \sum_{n\in M_g^{F,m}} v^{m,n}_{g,t_0}$$
$$u^m_{g,s,t} - u^m_{g,s,t-1} = \sum_{n\in M_g^{F,m}} v^{n,m}_{g,s,t} - \sum_{n\in M_g^{F,m}} v^{m,n}_{g,s,t}, \forall s, \forall t \in T\backslash t_0$$
$$\sum_{m\in M_g}\sum_{n\in M_g^{F,m}} v^{m,n}_{g,t_0} \le 1\,, \sum_{m\in M_g}\sum_{n\in M_g^{F,m}} v^{m,n}_{g,s,t} \le 1\,,\ \forall s, \forall t \in T\backslash t_0$$
$$ur^{pump}_{r,t_0} + ur^{gen}_{r,t_0} \le 1.\ \ \forall r \in \mathcal{R}$$
$$ur^{pump}_{r,s,t} + ur^{gen}_{r,s,t} \le 1.\ \ \forall r \in \mathcal{R}, \forall t \in T\backslash t_0, \forall s$$
$$u^m_{g,t_0} \le ur^m_{r,t_0}, \forall r \in \mathcal{R}, \forall g \in G_{psh,r}, \forall m \in \{gen, pump\}$$
$$u^m_{g,s,t} \le ur^m_{r,s,t}, \forall r \in \mathcal{R}, \forall g \in G_{psh,r}, \forall m \in \{gen, pump\}, \forall t \in T\backslash t_0, \forall s$$

Energy Reserve Secure Constraints:

$$F^G_{r,t_0} \ge \Delta^G_r \cdot ur^G_{r,t_0}, F^P_{r,t_0} \ge \Delta^P_r \cdot ur^P_{r,t_0}$$
$$F^G_{r,s,t} \ge \Delta^G_r \cdot ur^G_{r,s,t}, \forall s, \forall t \in [t_1, T\,]$$
$$F^P_{r,s,t} \ge \Delta^P_r \cdot ur^P_{r,s,t}, \forall s, \forall t \in [t_1, T\,]$$

Case Study

We use actual MISO data to evaluate the potential financial impacts of new energy security constraints to PSH owners. It should be noted that this study takes real-time price forecasting results from section IV.E as input, and tests for 5 different typical days have been conducted to provide insights and confirmations. The total DA+RT realized profits on a sample day in spring 2020 are reported in Table D.3.1, calculated as $\sum_{t=1}^{T} LMP^{DA}_t \cdot (g^{DA}_t - p^{DA}_t) + LMP^{RT}_t \cdot [(g^{RT}_t - p^{RT}_t) - (g^{DA}_t - p^{DA}_t)]$, where g^{RT}_t and p^{RT}_t are generating and pumping dispatches of the unit in RT optimized from the above mode and LMP^{DA}_t/LMP^{RT}_t represnets the actual DA/RT LMP. In this test, PSHs are considered as price takers (i.e., the inclusion of the above energy reserve secure constraints will not impact the actual DA/RT LMPs. The price making case will be further explored in milestone 8.1.

From Table D.3.1, we can see that including energy reserve secure constraints does not necessarily reduce the profit of PSH owners. For instance, with the head/floor room of 50/70MWh, the profit is $11,335 for this PSH from the real-time market on this day, which is the same as the one without energy reserve secure constraints. Moreover, when the head/floor room raises to 250MWh, the profits from our proposed model is $12,392, higher than $11,335 without these constraints. This clearly shows the PSH's potential in increasing their profits by holding some energy through the proposed energy reserve secure constraints. That is, including energy reserve secure constraints potentially could not only improve system security against uncertainties and contingencies, but also in some cases increase profits of PSH units.

We consider there may be circumstances when PSH profit decreases. Presumably, when future price is lower than current price, it should be more profitable to generate now than in the future. In this case, when the PSH is dispatched at lower level in DA market due to MWh reserve requirement, it may result in reduced profit as some generation is dispatched at a lower price in the future instead of being dispatched at a higher price now.

Table. D.3.1. Profit maximization case study

0(gen)&0(pump)/3000MWh	After the Fact	Rolling Window (50 scenarios)	Rolling Window (single prediction)	Stay with DA LMP

Profits ($)	17,017	11,335	12,456	10,977
50(gen)&70(pump)	**After the Fact**	**Rolling Window (50 scenarios)**	**Rolling Window (single prediction)**	**Stay with DA LMP**
Profits ($)	17,017	11,335	12,456	10,977
250(gen)&250(pump)	**After the Fact**	**Rolling Window (50 scenarios)**	**Rolling Window (single prediction)**	**Stay with DA LMP**
Profits ($)	16,678	12,392	12,447	11,369

Table D.3.1. shows the impact of MWh on PSH's profit via **Method 1** Uniform hourly SOC deviation constraints. We use three MWh reserve withheld values (0/0, 50/70, and 250/250 MWh), and compare with the baseline (stay with DA LMP, i.e., do. not deviate from the DA positions) as well as the perfect simulation (after the fact, i.e., the best profit PSH owner can get if it can fully foresee the actual RT price ahead of time). We conducted two rolling window tests, one with 1 scenario, one with 50 scenarios. In both tests, the results are higher than the profits of baseline ("stay with DA LMP"), and comes closer to the ideal profit ("after the fact"). The full explanation of this table, together with other test results, can be found in the 2020 Q4 Quarterly Report.

IV.E. Accomplishments Toward Deliverable 5.1

Deliverable 5.1: A prototype representation of price forecast uncertainty in persistent deviation model of RT dispatch.

Accomplishments Summary: There are a few accomplishments achieved for this Milestone. (1) Based on the deterministic PSHU model achieved in Milestone 2.1, the team developed stochastic PSHU models in LAC, where probabilistic price forecast is used to incorporate RT uncertainties. (2) An ARIMAX based forecast model has been developed for real-time (RT) LMP single point forecast. Next, the methodology for probabilistic LMP forecast is introduced. We innovatively applied scenario generation methods to generate a series of trajectory lines, which collectively represent a range of potential RT-LMP predictions over the forecast horizon, with associated probabilities. Further, based on the single point and probabilistic LMP forecast, an intra hour LMP forecast has been developed. (3) Based on the discussion with industry advisors, a risk management formulation is developed to address the concern of the profit lost in the RT market. Based on the LAC simulation in HIPPO that is achieved in Milestone 2.1, the team prototyped the proposed stochastic PSHU model and the risk management formulation. Case studies are developed, the preliminary results show the value of capturing uncertainties in the stochastic PSHU model and improvement in the system objective. The results demonstrate the effect of the risk management formulation in improving system objective and avoiding negative profits for the PSHU.

IV.E.1 A Stochastic PSH Model in LAC Using Probabilistic Price Forecast

In section IV.B, a deterministic PSH model is proposed in LAC using the single point price forecast. In this section, we propose a stochastic PSH model to incorporate the uncertainty in the

RT market for intervals occurring after the LAC intervals. The methdology to generate the probabilistic price forecast is summarized in subsection IV.E.3 in this report. Therefore, in this subsection we assume a probabilistic LMP forecast is given.

The formulation of the stochastic PSH model in LAC is listed below (E.1.1)-(E.1.18).

$$Objective: Min \sum_{t=t_1}^{t_{end}} C_t(g_t, u_t) - \sum_{s=s_1}^{s_N} \sum_{t=t_{end}+1}^{T} \sum_{g \in G_{psh}} p_s LMP_{g,s,t}^{t_0}(q_{g,s,t}^{gen} - q_{g,s,t}^{pump}) \quad \text{(E. 1.1)}$$

Similar to the deterministic PSH model in a LAC, the first term in (E.1.1) is the objective function for a LAC problem. The production cost $C_t(g_t, u_t)$ is minimized in a LAC window in intervals that start at t_1 and end at t_{end}. Assume the operation and maintanence cost is negligable for a PSHU, and that the net cost of dispatching a PSHU in the LAC intervals due to the net costs of sale or purchase of energy in the intervals post to the LAC intervals. This net cost is represented in the second term in (E.1.1) as the negative arbitrage profit of the PSHU in the intervals after the LAC that starts at $t_{end} + 1$ and stops at the end of the operating day T. Notice that the second term in (E.1.1) now includes the cost/negative profit of the PSHU for multiple scenarios that are weighted by the probability of each scenario p_s. Different PSHU generation and pumping values are allowed in each scenario. It is acknowledged that, strictly speaking, causality is violated by the implicit assumption that the generation and pumping values can be chosen for all intervals in a given scenario.

The generation and pump demand of the PSHU during the intervals after the LAC are defined for each scenario $q_{g,s,t}^{gen}$, $q_{g,s,t}^{pump}$. The probabilistic LMP forecast $LMP_{g,s,t}^{t_0}$ is provided for each interval after the LAC and the forecast is updated at t_0 that is one interval before the start of each LAC window t_1.

Power Balance Constraints:

$$\sum_{k=1}^{K} g_{k,t} + \sum_{g \in G_{psh}} q_{g,t}^{gen} = D_t + \sum_{g \in G_{psh}} q_{g,t}^{pump}, \ \forall t \in [t_1, t_{end}] \quad \text{(E. 1.2)}$$

$$\sum_{k=1}^{K} g_{k,t} = D_t, \ \forall t \in [t_{end} + 1, T] \quad \text{(E. 1.2}^*\text{)}$$

Similar to the deterministic PSHU model, the PSHU is fully optimized within the LAC window given a deterministic forecast of the demand within the LAC window. In the power balance constraint within the LAC window $\forall t \in [t_1, t_{end}]$, the deterministic generation of the PSHU, $q_{g,t}^{gen}$, is included on the left hand side of power balance constraint (B.2.2) and the determinstic pumping load of the PSHU, $q_{g,t}^{pump}$, is considered as demand on the right hand side of the power balance constraint (B.2.2). The dispatch of the PSHU in the intervals after the LAC relies on the LMP forecast and are not optimized with the rest of the system. Therefore, the generation and pumping of the PSHU in the intervals post to the LAC window $\forall t \in [t_{end} + 1, T]$ are not included in the power balance constraint (B.2.3).

The Private Constraints for a PSHU within a LAC:

$$\text{(A. 1.3)} - \text{(A. 1.11)}, \text{(A. 1.13)}, \text{(A. 1.14)}, \ \forall t \in [t_1, t_{end}],$$

The private constraints for a PSHU model are the same as the DA model described in $(\text{A. } 1.3) - (\text{A. } 1.11), (\text{A. } 1.13), (\text{A. } 1.14)$ in the Appendix for section IV.A.1, except those constraints are modeled in the intervals from the start of the LAC window t_1 until the end of the operating day T. Since we currently solve the problem in hourly intervals and the constraint on the number of pump starts (A.1.12) is typically only binding in the sub-hour timeframe, (A.1.12) is less relevant and therefore it is not included in the model.

The private constraints for a PSHU model are defined for each scenario in the intervals after the LAC and they are described in the rest of this subsection. In the following, we would focus on the explanation related to the stochastic scenarios, the detailed description of each of the constraints can be found in $(\text{A. } 1.3) - (\text{A. } 1.11), (\text{A. } 1.13)$ and $(\text{A. } 1.14)$ in this report.

PSH Unit Commitment and Transition Mutual Exclusivity Constraints After a LAC Window:

$$\sum_{m \in M_g} u_{g,s,t}^{m} = 1, \forall g \in G_{psh}, \forall s \in S, \forall t \in [t_{end}+1, T], \qquad (\text{E. } 1.3)$$

$$\sum_{m \in M} \sum_{n \in M_g^{F,m}} v_{s,t}^{n,m} \leq 1, \forall g \in G_{psh}, \forall s \in S, \forall t \in [t_{end}+1, T], (\text{E. } 1.4)$$

Different to the deterministic model, in the intervals after the LAC window, starting at $t_{end} + 1$ until the end of the operating day T, the private constraints for the PSHU are modeled for each scenario s. Mutual exclusivity constraints on the unit commitment variables and transition variables are presented in (E.1.3) and (E.1.4) respectively.

PSH Transition Logic After a LAC Window:

$$u_{g,s,t_{end}+1}^{m} - u_{g,t_{end}}^{m} = \sum_{n \in M_g^{F,m}} v_{g,s,t_{end}+1}^{n,m} - \sum_{n \in M_g^{F,m}} v_{g,s,t_{end}+1}^{m,n}, \forall g \in G_{psh}, \forall m \in M_g, \forall s \in S, \qquad (\text{E. } 1.5^{*})$$

$$u_{g,s,t}^{m} - u_{g,s,t-1}^{m} = \sum_{n \in M_g^{F,m}} v_{g,s,t}^{n,m} - \sum_{n \in M_g^{F,m}} v_{g,s,t}^{m,n}, \forall g \in G_{psh}, \forall m \in M, \forall s \in S, \forall t \in [t_{end}+2, T], \qquad (\text{E. } 1.5)$$

In the intervals after the LAC window, from $t_{end} + 2$ until the end of the operating day T, the PSH transition logic constraints are modeled for each scenario s in (E. 1.5). Since the transition logic constraint is inter-temporal, we need to specifically address the constraint when it crosses between the interval within a LAC window and the interval after the LAC w.indow. In (E. 1.5^{*}), the transition between modes from the last interval of the LAC, t_{end}, and the first interval after the LAC, $t_{end} + 1$, are defined for each scenario s. Notice that the commitment variable within LAC $u_{g,t_{end}}^{m}$ is deterministic and both the unit commitment and transition variables after the LAC are defined for each scenario, $u_{g,s,t_{end}+1}^{m}$, $v_{g,s,t_{end}+1}^{n,m}$. Therefore, using (E. 1.5^{*}), every stochastic unit commitment variable in the intervals after LAC is linked to the last deterministic unit commitment variable within the LAC by the corresponding stochastic transition variables.

PSH Output Box Constraints:

$$u_{g,s,t}^{pump}\underline{Q_g^{pump}} \le q_{g,s,t}^{pump} \le u_{g,s,t}^{pump}\overline{Q_g}^{pump},\ \forall r \in R, \forall s \in S, \forall g \in G_{psh,r}, \forall s \in S, \forall t \in [t_{end}+1, T], \quad \text{(E. 1.6)}$$

$$u_{g,s,t}^{gen}\underline{Q_g^{gen}} \le q_{g,s,t}^{gen} \le u_{g,s,t}^{gen}\overline{Q_g}^{gen},\ \forall r \in R, \forall s \in S, \forall g \in G_{psh,r}, \forall s \in S, \forall t \in [t_{end}+1, T], \quad \text{(E. 1.7)}$$

In the intervals after the LAC window starts at $t_{end}+1$ until the end of the operating day T, the upper and lower limit for pumping and generating in a PSHU are modeled for each scenario s in (E.1.6) and (E.1.7).

PSH Reservoir State-of-charge (SOC) Constraints:

$$e_{r,s,t_{end}+1} + \sum_{g \in G_{psh},r} \frac{q_{g,t_{end}}^{gen}}{\eta^{gen}} - \sum_{g \in G_{psh},r} q_{g,t_{end}}^{pump} * \eta^{pump} - e_{r,t_{end}} = 0,\ \forall r \in R, \forall s \in S, \quad \text{(E. 1.8*)}$$

$$e_{r,s,t+1} + \sum_{g \in G_{psh},r} \frac{q_{g,s,t}^{gen}}{\eta^{gen}} - \sum_{g \in G_{psh},r} q_{g,s,t}^{pump} * \eta^{pump} - e_{r,s,t} = 0,\ \forall r \in R, \forall s \in S,\ \forall t \in [t_{end}+1, T], \quad \text{(E. 1.8)}$$

In the intervals after the LAC window, starting at $t_{end}+1$ until the end of the operating day T, the SOC constraints are modeled for each scenario s in (E. 1.8). For the inter-temporal SOC constraint, similar to the transition logic constraint, we need to specifically address the constraint when it crosses between the interval within a LAC window and the interval after the LAC window. In (E. 1.8*), the SOC changes from the last interval of the LAC, t_{end}, and the first interval after the LAC, $t_{end}+1$, are defined for each scenario s. Notice that the SOC variable and generation and pumping variables at the last interval of LAC ($e_{r,t_{end}}, q_{g,t_{end}}^{gen}, q_{g,t_{end}}^{pump}$) are deterministic and the SOC in the first interval after LAC is defined for each scenario, $e_{r,s,t_{end}}$. Therefore, using (E. 1.8*), every stochastic SOC variable in the intervals after LAC is linked to the last deterministic SOC variable within the LAC.

$$E_{r,T+1} - e_{r,s,T+1} = 0, \forall r \in R, \forall s \in S, \quad \text{(E. 1.9)}$$

$$\underline{E} \le e_{r,s,t} \le \overline{E},\ \forall r \in R, \forall s \in S, \forall t \in [t_{end}+1, T], \text{(E. 1.10)}$$

The SOC variable at the end of the day $T+1$, $e_{r,s,T+1}$, is fixed to the given target $E_{r,T+1}$,that is the SOC at the end of the day in the DA solution, in each scenario in (E.1.9). In the intervals after the LAC window, the upper and lower limit is enforced to each SOC variable for each scenario in (E.1.10).

PSH Ramp Up/Down Constraints:

$$q_{g,t}^{gen} - q_{g,t-1}^{gen} \le RRup_{g,t}, \forall g \in G_{psh}, \forall t \in [0, t_{end}], \qquad (E. 1.11)$$

$$q_{g,t-1}^{gen} - q_{g,t}^{gen} \leq RRdown_{g,t}, \forall g \in G_{psh}, \forall t \in [0, t_{end}], \quad \text{(E. 1.12)}$$

$$q_{g,s,t_{end}+1}^{gen} - q_{g,t_{end}}^{gen} \leq RRup_{g,t_{end}+1}, \forall g \in G_{psh}, \forall s \in S, \quad \text{(E. 1.13)}$$
$$q_{g,t_{end}}^{gen} - q_{g,s,t_{end}+1}^{gen} \leq RRdown_{g,t_{end}+1}, \forall g \in G_{psh}, \forall s \in S, \text{(E. 1.14)}$$

$$q_{g,s,t}^{gen} - q_{g,s,t-1}^{gen} \leq RRup_{g,t}, \forall s \in S, \forall t \in [t_{end} + 2, T], \quad \text{(E. 1.15)}$$
$$q_{g,s,t-1}^{gen} - q_{g,s,t}^{gen} \leq RRdown_{g,t}, \forall s \in S, \forall t \in [t_{end} + 2, T], \text{(E. 1.16)}$$

Ramp up/down constraints within the LAC window are determinstc and they are listed in (E. 1.11) and (E. 1.12). The ramp up/down constraints at the boundary between the last interval of LAC t_{end} and the first interval after LAC $t_{end} + 1$ are listed in (E. 1.13) and (E. 1.14) (these ramping constraints are not enforced for the non-PSH units in the system). The Ramp up/down constraints after the LAC window are defined for each scenario in (E. 1.15) and (E. 1.16).

Plant Level Mutual Exclusivity Constraints:

$$ur_{r,s,t}^{pump} + ur_{r,s,t}^{gen} \leq 1, \forall r \in R, \forall s \in S, \forall t \in [t_{end} + 1, T], \text{(E. 1.17)}$$
$$u_{g,s,t}^{m} \leq ur_{r,s,t}^{m}, \forall r \in R, \forall g \in G_{psh,r}, \forall s \in S, \forall t \in [t_{end} + 1, T], \forall m \in \{gen, pump\}, \text{(E. 1.18)}$$

In the intervals after the LAC window, the plant level mutual exclusivity constraints are defined for each scenario in (E.1.17) and (E.1.18).

IV.E.2 Single Point Forecast Methodology for Locational Marginal Price (LMP)

We analyzed historical LMP data from 2017 to 2019 for the locational nodes of the PSHU in the study. In the dataset we have historical real-time and day-ahead prices on hourly basis.

IV.E.2.1 Time Series Analysis

For this problem, we are dealing with time series forecasting. Because data points in time series are collected at sequential time periods, there is potential for correlation between observations. This is one of the main properties that distinguishes time series data from cross-sectional data.

Components of Time Series

Time series data typically includes a level, trend, seasonality, residual or noise. Before we illustrate each of those components, it's important to note that not all time series data will include every one of these components.

Level: Assuming if there were a straight line, baseline value of timeseries is called its level which refers to the mean of data.

Trend: The increasing or decreasing behavior of the series over time shows its trend. If the data has no trend, then it is called a Stationary dataset. In other words, it has constant mean and variance, and covariance is independent of time.

Seasonality: The presence of variations that occur at specific regular intervals that are correlated with the calendar, which could be quarterly, monthly, weekly, daily, hourly and so on. Not all time series have a seasonal component.

Residual: The variability in the observations that cannot be explained by the model.

When the fluctuation and variation of time series increase or decrease over time and shows dependency to the Level of time series, then we are dealing with a Multiplicative time series:

Multiplicative Model: Time series = (Trend) * (Seasonality) * (Noise).

On the other hand, Additive models are the ones in which variation in the time series stay almost constant over time, and can be interpreted as following:

Additive Model: Time series = (Trend) + (Seasonality) + (Noise)

Since our time series data does not increase or decrease over time it fits in the category of additive model for data decomposition. We can calculate the correlation for time series observations with observations from previous lags. Because the correlation of the time series observations is calculated with values of the same series at previous times, this is called an autocorrelation. Auto Correlation Function (ACF) considers all the above components while finding correlations and describes how well the present value of the series is related with its past values.

IV.E.2.2. Methodology for Single Point LMP Forecasting

The main objective is forecasting the price deviation between real-time and day-ahead Locational Marginal Price (LMP). For that purpose, if we are able to provide a good point forecast for real-time-LMP then we can readily calculate the expected deviation of the forecasted real-time from the given day-ahead-LMP.

As described above, in this context we are dealing with a times series forecasting problem. There are a lot of methods and techniques to analyze and forecast time series. One of the most used is a methodology based on Autoregressive Integrated Moving Average (ARIMA) model. In this method, the historical data of univariate time series are used to analyze its own trend and forecast future cycle. The ARIMA model is one of the most used methodologies for analyzing time series. This is mostly because it offers great flexibility in analyzing various time series and because it can achieve accurate forecasts, too. The other advantage is that for analyzing single time series it uses its own historical data. Applying ARIMA(p,d,q) methods and finding the right parameters for autoregressive lags (p), moving average lags (q), and order of differencing (d) was studied. When an ARIMA model includes other time series as input variables, the model is sometimes referred to as an ARIMAX model. Usually including extra independent variable (covariant) X into the model brings much better results than simple ARIMA model. Here the choices for exogenous variable could be the Load forecast, and day-ahead-LMP, or both.

Given time series data y_t(RT-LMP) and exogeneous data x_t(DA-LMP and Load), where p is the number of auto-regressive lags, d is the degree of differencing, and q is the number of moving average lags.

$$y_t = \sum_{i=1}^{p} \varphi_i \, y_{t-i} + \sum_{j=1}^{q} \theta_j \, \epsilon_{t-j} + \sum_{m=1}^{M} \beta_m \, x_{m,t} + \epsilon_t, \quad \epsilon \sim \aleph(0, \sigma^2), \qquad (\text{E. } 2.\ 1)$$

- Here ϵ, is the residual which is assumed to be normally distributed, with $\aleph(0, \sigma^2)$ defined to be the normal distribution with mean zero and variance σ^2.
- The partial auto correlation function (**PACF) and ACF** plots can be used to estimate the **AR**-part**, i.e. p-value,** and the **MA**-part**, i.e. q-value,** respectively.
- Here the choices for exogenous variable could be the Load forecast, and Day-Ahead LMP.

We initially explored the three alternatives of including both exogenous variables of Load and DA-LMP together, and also including each one individually. The empirical result is that DA-LMP

plays the main role as a predictive variable. Moreover, including just the one exogenous variable of DA-LMP provides as good a prediction result as including both Load and DA-LMP. As a result, our final choice for covariate X-variable in the ARIMAX model is the DA-LMP.

For each daily price prediction, we consider the past 6 days as our training data to fit the right ARIMAX(p,d,q) model and predict RT-LMP for the following day. In order to evaluate the model, we compare the predicted results versus the data unseen by the prediction model, namely the test set for RT-LMPs for intervals in the following day.

In general, a perfect forecast is the one which fits exactly on the test set. However, the problem is that in reality this is not achivable. The main distinction of forecasting is that the future is unknown and the best a forecasting model could do is learning the most from the given historical data and do the prediction for future based on that. The result of prediction model is shown as the red curve of Fig. E.2.1. It demonstrates that the forecasted RT-LMP is tracing the path of the actual RT-LMP shown in blue which is called the test set. In the current time series analysis we captured the performance of our Seasonal-ARIMAX methodologies by computing some metrics such as, Mean-Absolute-Error (MAE), and Root-Mean-Square-Error (RMSE). The errors of our daily forecating analysis show an acceptable range which we can rely on ARIMAX as our point forecast methodology to predict RT-LMP. It should be pointed out that, for PSH, the key is to determine the hours of charging and discharging. Price forecast needs to properly capture the peak and valley within a day with enough spread to cover round trip efficiency. RMSE was used to evaluate the performance of ARIMAX as our choice to forecast the RT-LMP. We tried to fit two models, namely ARIMA and ARIMAX, on more than 200 days of study year 2019, and computed RMSE for both models. It was observed that in 82% of test days, the RMSE for ARIMAX was smaller than ARIMA. Moreover, it is notable that in the other 12% of days the performance of ARIMAX compared to ARIMA was not significantly worse. Consequently, we chose ARIMAX in all subsequent forecasts.

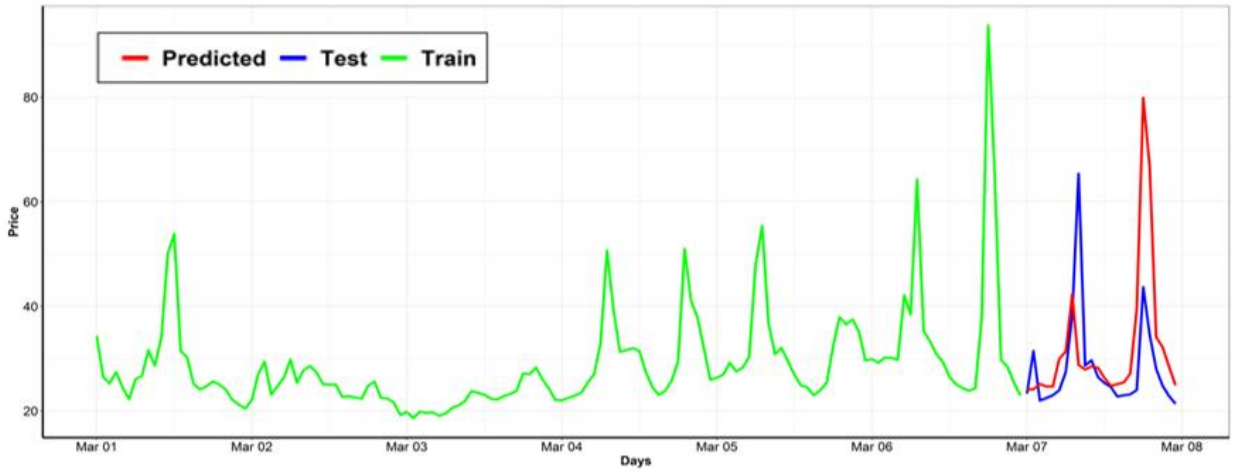

Fig. E.2.1. Time Series Forecast of RT-LMP for day of March 7th, 2019 using ARIMAX method with X being DA-LMP. In total, six days of RT LMP data is used as training data and the prediction is made on the last day shown in the figure. The forecasted RT-LMP is tracing the path of the actual RT-LMP.

IV.E.3 Probabilistic LMP Forecasting Methodology

Probablistic forecasts are used to reflect the uncertainty range for the existing deterministic/point forecast approach. The issue is that usually the general form of probabilistic forecasts, such as quantile regression, neglect the interdependence structure of forecast errors in look ahead times. Creating statistical scenarios based on the transformed prediction errors in Normal space and capturing the interdependence structure of these prediction errors by their associated covariance matrix is the probabilistic methodology that we used to capture the uncertainty associated with the point forecasts. The steps to generate statistical scenarios based on the given deterministic point forecasted LMP are included in the Appendix for section IV.E.3.

As a result, the interdependent structure of errors can be summarized in a unique covariance matrix. Following steps of generating statistical scenarios proposed in [E.1], we will generate a series of trajectory lines, which collectively represent a range of potential RT-LMP predictions over the forecast horizon, with associated probabilities. Fig. E.3.1 shows the associated scenarios reflecting both the prediction uncertainty and the interdependence structure of predictions errors.

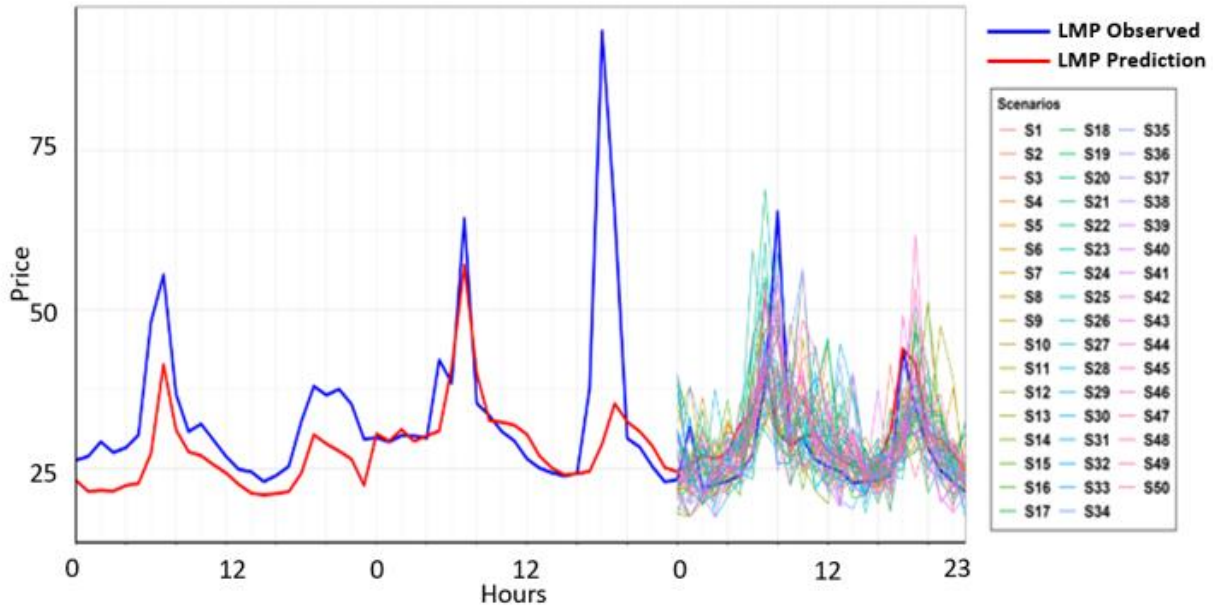

Fig. E.3.1. Real-Time LMP point prediction with 50 alternative statistical scenarios for March 7th, 2019. The RT LMP single point forecast of three days and the probabilistic forecast of the last day are plotted.

IV.E.4 Intra-hour Single Point Price Forecast:

For each daily price prediction, we consider the past 6 days as our training data to fit the right ARIMAX(p,d,q) model and predict RT-LMP for the following day. Now that the point forecast for RT-LMP in each forecast horizon, 24 hours, is available. We need to up-sample and interpolate the results and get the values of RT-LMP forecast for intra-hour points in every 15 minutes time interval. Detailed methodology is included in the Appendix for section IV.E.4.

Table E.4.1 demonstrates a quick look on how our final results for intra-hour RT-LMP would look like. As Table E.4.1 shows, the first column is the original hourly RT-LMP forecast values as a result of applying ARIMAX approach. Then, in the next columnm, we use the linear interpolation on the hourly forecasted RT-LMP values to get the intra-hour LMP values for all

those intra-hours. However, since the hourly average constraint is not yet considered in these 15-minute RT-LMP values, we make sure to derive the intra-hour values which meet the averaging constraint. Finally, the last column demonstrates a new profile for 15-min intra-hour RT-LMP which the average of each four intra-hour values is equal to value of the corresponding beginning hour RT-LMP.

Table. E.4.1. RT-LMP Point Forecast and its associated 50 scenarios based on 15-minute time intervals

TIME_EST	RT-LMP Forecast (hourly)	Interpolated Intrah-hour Forecast	Intrahhr Forecast, meet the hourly Avg constraint	Final hourly & Intra-hr Forecast
4/15/2019 0:00	21.81834601			21.81834601
4/15/2019 0:15		21.6699551	22.04093237	22.04093237
4/15/2019 0:30		21.52156419	21.89254146	21.89254146
4/15/2019 0:45		21.37317328	21.74415055	21.74415055
4/15/2019 1:00	21.22478237		21.59575965	21.22478237
4/15/2019 1:15		21.3461717	21.04269838	21.04269838
4/15/2019 1:30		21.46756103	21.16408771	21.16408771
4/15/2019 1:45		21.58895035	21.28547704	21.28547704
4/15/2019 2:00	21.71033968		21.40686636	21.71033968
4/15/2019 2:15		21.78432818	21.59935694	21.59935694
4/15/2019 2:30		21.85831667	21.67334543	21.67334543
4/15/2019 2:45		21.93230517	21.74733393	21.74733393
4/15/2019 3:00	22.00629366		21.82132242	22.00629366
4/15/2019 3:15		22.37543179	21.45258647	21.45258647
4/15/2019 3:30		22.74456992	21.8217246	21.8217246
4/15/2019 3:45		23.11370804	22.19086273	22.19086273
4/15/2019 4:00	23.48284617		22.56000085	23.48284617

Fig. E.4.1 presents RT-LMP single point forecast and its associated statistical scenarios to capture uncertainties for 15-minues time intervals.

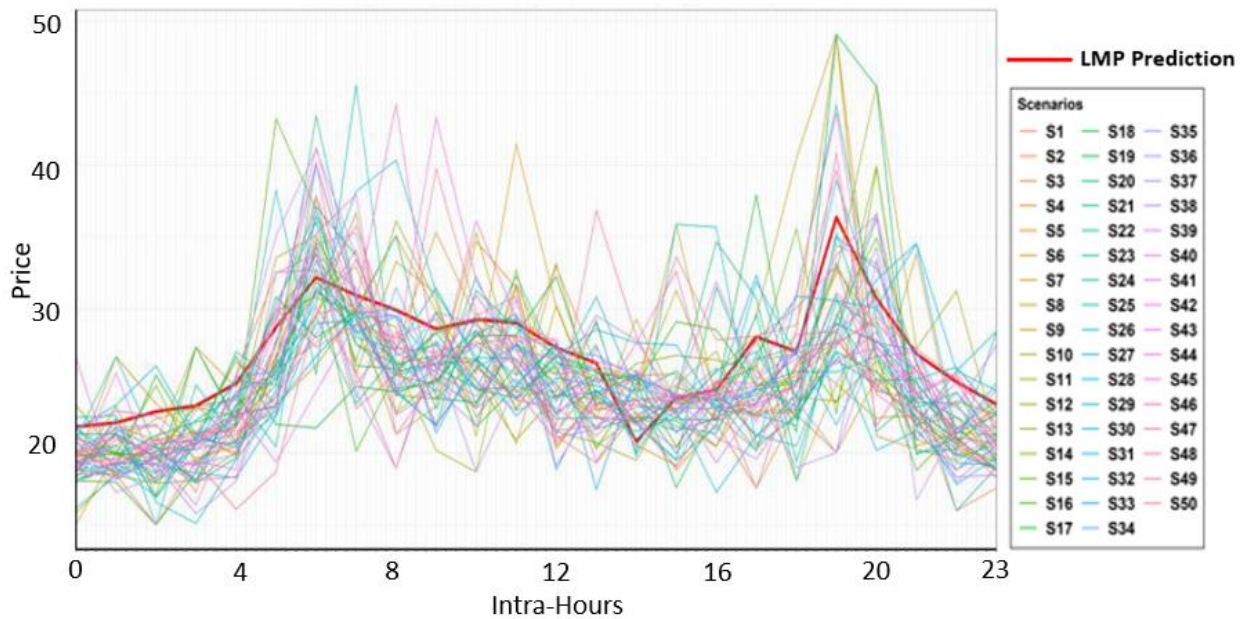

Fig. E.4.1 RT-LMP Point Forecast and its associated 50 scenarios based on 15-minute time intervals

IV.E.5 Deterministic Forecasting for Multi-Day Ahead Forecasting

Problem Description: The effort of forecasting Day-Ahead LMP in a forecast horizon of multiple days ahead, is helpful in identifying end of state of charge (SOC) values to faciliate multi-day ahead scheduling. Having access for DA-LMP forecast beyond day-ahead (24-36 hours), will help to decide the best schedule in day-ahead.

The goal is to learn the below function W from the data and obtain forecasts of day ahead prices for t+h, where $\mathbf{h} \in \{\mathbf{1}, \mathbf{2}, \dots, \boldsymbol{H}\}$.

$$y_{\{t+h\}} = W\left(y_t, \ \dots, \ y_{\{t-n+1\}}\right) + \epsilon_t$$

ARIMAX method is used to model multi-day ahead LMP single point forecasting and results are compared with those from another method of time-series analysis named Facebook Prophet. The details of the ARIMAX-based multi-day ahead LMP single point forecasting method and Facebook Prophet are included in the Appendix for section IV.E.5.

To compare the performance of our existing ARIMAX model with Facebook Prophet, we ran an analysis using both approaches. Moreover, we generated a new set of outputs by taking their weighted average given ¾ weight to the ARIMAX and ¼ weight to the outputs of Facebook Prophet. Fig. E.5.1. shows the results of all three aforementioned single point forecasting along with the realized LMP values.

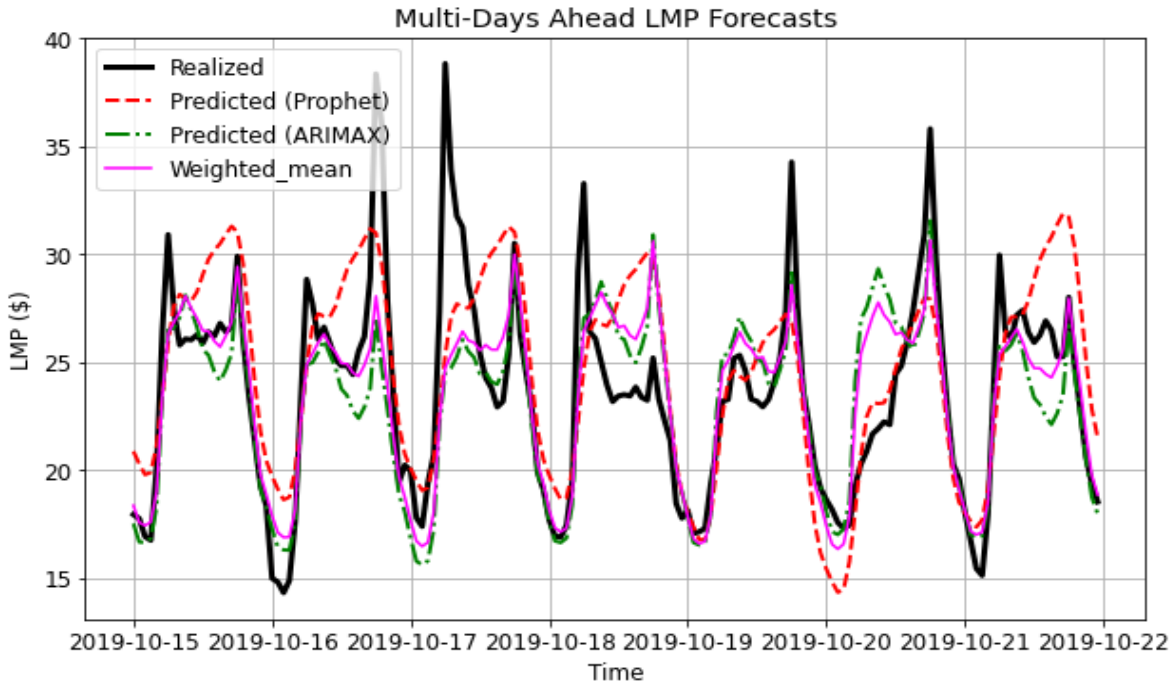

Fig. E.5.1. The realized LMP along with three forecasted results, namely ARIMAX, Prophet, and the weighted average of both.

From Fig. E.5.1, it can be seen that ARIMAX captures the trend and also the peaks and turning points of the realized RT-LMP much better than Facebook Prophet. And the output as a result of taking the average mean of these two approaches shows even better results than the ARIMAX. This observation was consistent in running the above comparison analysis for many random days

in all four seasons. We also measured the observed performance of these methodologies using Root-Mean-Square-Error. The numbers out of RMSE are also confirming our visual observations as described:

RMSE_Facebook Prophet:	3.5011
RMSE_ARIMAX:	3.0121
RMSE_Weighted Avg:	2.8479

IV.E.6 Probabilistic Forecasting for Multi-Day Ahead Forecasting

The scenarios associated to the weighted average single point forecast, as described in previous section, are shown in Fig E.6.1 with 50 colors along with the point forecast shown in solid red and the realized LMP in solid blue. These statistical scenarios reflect the prediction uncertainty.

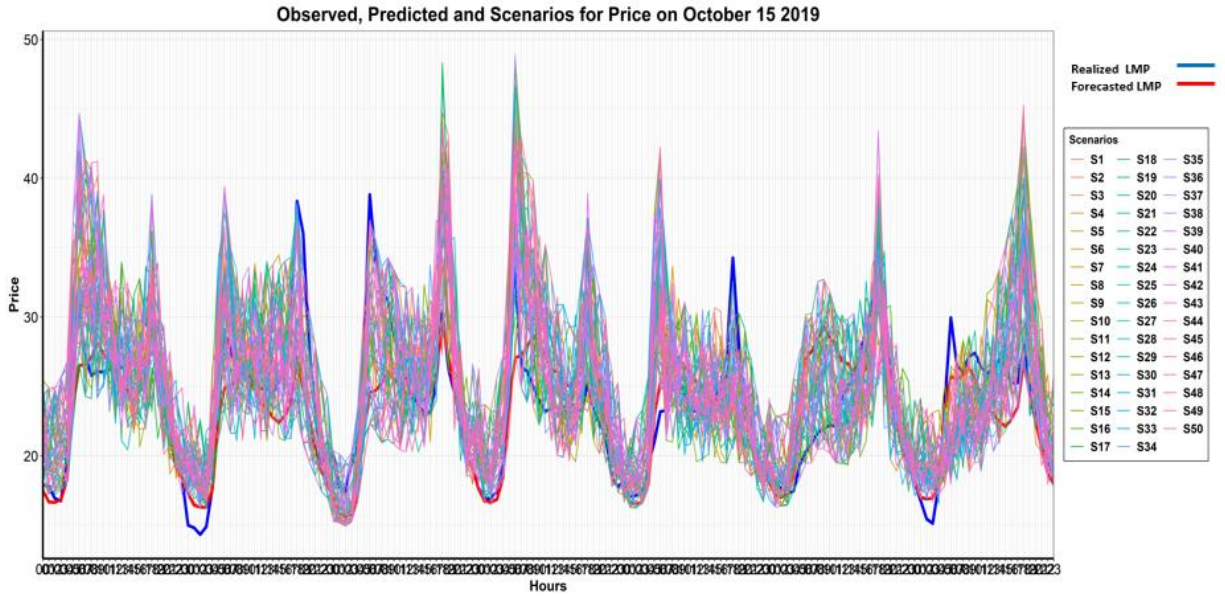

Fig. E.6.1. Statistical scenarios associated to the single point forecast for multi-days ahead prediction. These statistical scenarios reflect the prediction uncertainty.

IV.E.7 A Robust Risk-management Formulation

In our discussion with industry advisors, some PSHUs are reluctant to participate in the real-time market. One of the major concerns is the exposure to the uncertain RT LMP may cause the unit to lose profit in the RT market. To address this risk-averse concern, after discussion with the industry advisors, we have developed a robust risk-management formulation that can be applied to the stochastic PSHU model in LAC as we described in section IV.E.1.

$$Objective: Min \sum_{t=t_1}^{t_{end}} C_t(g_t, u_t) + \sum_{r \in R} w_r \,, \text{(E. 7.1)}$$

$$w_r \geq -\sum_{t=t_{end}+1}^{T} \sum_{g \in G_{psh,r}} LMP_{g,s,t}^{t_0}\left[\left(q_{g,s,t}^{gen} - q_{g,s,t}^{pump}\right) - \left(q_{g,t}^{gen,DA} - q_{g,t}^{pump,DA}\right)\right], \forall r \in R, \forall s \in [s_1, s_N]. \quad \text{(E. 7.2)}$$

Subject to (E.1.2)-(E.1.18)

In the risk-management formulation, the objective is updated in (E.7.1). Notice that the first term is the system production costs and that is the same compared to the stochastic model in (E.1.1). The difference is in the second term in the objective function. In (E.1.1), the cost/negative profit of the PSHU in the intervals after the LAC is weighted by the probability of each scenario. Therefore, the model presented in (E.1.1) is a risk-neutral formulation. However, in (E.7.1), the cost of each PSH plant r is represented by variables w_r. The cost variable is then constrained in (E.7.2). The right-hand side of (E.7.2) is the negative profit of the PSHU in the RT market after the LAC intervals in each scenario. The RT profit is calculated as RT LMP forecast at each scenario $LMP_{g,s,t}^{t_0}$ times with gen/pump difference between its solution in RT market in a scenario $\left(q_{g,s,t}^{gen} - q_{g,s,t}^{pump}\right)$ and the solution in the DA market $\left(q_{g,t}^{gen,DA} - q_{g,t}^{pump,DA}\right)$. Constraint (E.7.2) limits each cost variable w_r to be the cumulative cost of the PSHU from the first interval after LAC $t_{end} + 1$ to the end of the day T in the worst-case scenario (that is the largest cost to the system or the lowest profits to the PSHU) based on the probabilistic LMP forecast. Therefore, since the worst-case PSHU cost is minimized in the objective, it is a robust or risk averse formulation. The rest of the stochastic PSHU model remained unchanged from (E.1.2)-(E.1.18).

With the proposed risk-management formulation in (E.7.1) and (E.7.2), the solution for a PSHU will only deviate from the DA solution if it is profitable indicated by every post-LAC price scenario. Therefore, (E.7.1) and (E.7.2) address the concern of profit loss in the RT market from the industry advisors. As in Section IV.E.1, it is acknowledged that, strictly speaking, causality is violated by the implicit assumption that the generation and pumping values can be chosen for all intervals in a given scenario.

IV.E.8 LAC simulation Case Studies and Preliminary Results

The HIPPO based LAC simulation platform is introduced in section IV.B.1. In this section, we first introduce the input data preparation for the LAC simulation. Then, a case study with four models will be presented. The four models include the deterministic PSHLAC model described in section IV.B.2, the stochastic PSH LAC model described in section IV.E.1, the risk management formulation described in section IV.E.7, and a perfect case benchmark model that we will introduce in this section.

Simulation Setup

It is necessary to update the real-time (RT) system condition in the LAC rolling window simulation. However, there were only day-ahead (DA) market cases available to HIPPO since it was initially developed for studies in a DA market. Therefore, a first task is to prepare the real-time system condition data as input to the LAC simulation.

To ensure that the RT data is valid and consistent with the DA system, we develop the real-time system condition data in steps. For a large system like the MISO system with a large set of

input data, the security constrained unit commitment (SCUC) model is very large, and the model can easily become infeasible due to inconsistent input data. Because the real-time system data we are collecting hasn't been used either in the HIPPO software or for the purpose of LAC rolling window simulation, it could be very difficult to detect the cause of model infeasibility and to troubleshoot if we update all different system input data at once. In contrast, taking a step at a time to update the real-time system data allows us to collect feedback from the model and make adjustment if it is necessary.

Since RT demand is one of the data sets that distinctly represents a RT case, we first prepared RT demand data as input to the LAC rolling window simulation. We took advantage of existing software named ODC that is internally used in MISO for RT market benchmark purpose. Because ODC also takes RT MISO system data as input, we can take the RT system input data from a report that is generated by ODC and translate the data into a form that HIPPO can read. After a successful simulation run with the RT demand, we prepared and input the RT generator data to the LAC simulation. The RT generator data is another set of input that is important to represent the system conditions. In a similar way, the existing software ODC is used to prepare the RT generator input for our HIPPO based LAC simulation. It is noted that some approximations are made to clean the input data and resolve some inconsistency and to attain feasible solutions. As a result, only a part of the generator data has been successfully passed to feed in the HIPPO based LAC simulation.

A day in the existing DA case library is first picked, and then the RT demand and generator data for the same day are taken from the report from ODC and they are prepared for input to HIPPO. At the current stage of the study, we decide to first keep the hourly interval study to keep the simulation simpler and we can extend to 15-minute intervals later. Therefore, the RT demand and generator data are both prepared in hourly intervals. So far, we have updated the RT demand and generator data and kept the rest of the DA input data in the LAC simulation. Similarly, the other system settings are kept consistent with the way it is designed for the DA market. For example, the virtual bids and dispatchable demand are kept in the current LAC simulation to keep the problem feasible. We continue to refine and update the RT data on generators and other system conditions to bring the simulation closer to a realistic LAC.

Two PSH plants are included in this study. The parameters of the units are matched with production data.

Case Studies

First, a day is picked from the HIPPO DA case library and the DA case is solved in HIPPO. Then the RT demand and generator input data for the same day is prepared for the LAC rolling window simulation in HIPPO. Finally, the historical RT LMP data for the same day is attained and both the single point and probability LMP forecast is generated by the methodology described in sections IV.E.2 and IV.E.3. Notice that only the most important but partial of the RT system data is prepared and read into the LAC while the LMP forecasts are made based on realistic historical LMP data. Therefore, there is a gap between the partial RT system represented in the LAC and the RT LMP forecast that is made from the realistic RT system data. This gap will be reduced as we continue to refine the RT input data for the LAC simulation.

Case studies are developed with in total four models. Three models were described in the previous sections, and they are the deterministic PSH LAC model (in section IV.B.2), the risk-neutral stochastic PSH LAC model (in section IV.E.1) and the risk-averse stochastic PSH LAC model (in section IV.E.7). In addition, a perfect forecast model is developed to set the benchmark and gauge the maximum benefits of incorporating a PSHU in the LAC problem.

DA Solution and Profit

The DA case is solved before the LAC simulation starts. The DA solutions are used in the risk averse stochastic PSH LAC model (E.7.2). The DA profits can be calculated in (E.8.1)

$$Profits_g^{DA} = \sum_{t=1}^{T} LMP_{g,t}^{DA} * (q_{g,t}^{gen,DA} - q_{g,t}^{pump,DA}), \forall g \in G_{psh} \quad \text{(E.8.1)}$$

where $LMP_{g,t}^{DA}$ is the DA locational marginal price (LMP) for the PSHU at interval t, $q_{g,t}^{gen,DA}$ and $q_{g,t}^{pump,DA}$ are the generation and the pump load of the PSHU g at interval t in the DA solutions.

Perfect Model

In the perfect model, the LAC is solved in a series of rolling windows such that each of them contains three hourly intervals. The generators other than the PSHUs are optimized within the LAC three-hour window. The LAC window is solved and slides forward one hour at a time. The solution of the first interval inside each LAC is implemented and saved to be fixed in the following windows.

The PSHU is fully optimized in the horizon that starts at the beginning of each LAC window and ends at the last interval of the day. That the PSHU is fully optimized means all the unit constraints are fully represented in the system wide optimization including the unit output limits, ramp limits and limits on the state of charge (SOC) etc. The end of the day SOC is set to meet the end of the day target in the DA solution. Notice that we don't incorporate the price forecast in this perfect case, instead, we assume the after the fact RT system conditions (the RT demand and generator conditions) are known to PSHUs when each LAC is solved. With the full awareness to the real time market system condition, the PSHU can be put to the best position by the optimization. Therefore, in comparison to cases where price forecast is used to guide the PSHU's output in a LAC, the solution from a perfect case should guarantee the lowest system objective value and the highest profits for a PSHU.

The system objective value is stored after the last LAC window has been solved. If the PSHU deviates from its DA position in LAC, the PSHU would gain (or lose) profits from the RT market. Therefore, the profits for the benchmark are composed by a DA component and a RT component as follows.

$$Profits_g^{LAC} = \sum_{t=1}^{T} LMP_{g,t}^{DA} * (q_{g,t}^{gen,DA} - q_{g,t}^{pump,DA}) + LMP_{g,t}^{RT} * [(q_{g,t}^{gen,LAC} - q_{g,t}^{pump,LAC}) - (q_{g,t}^{gen,DA} - q_{g,t}^{pump,DA})], \forall g \in G_{psh} \quad \text{(E.8.2)}$$

where $LMP_{g,t}^{RT}$ is the realized RT LMP for the PSHU at interval t, $q_{g,t}^{gen,LAC}$ and $q_{g,t}^{pump,LAC}$ are the generation and pump load of the PSHU at interval t in the LAC solution, respectively. Notice that the first term on the right-hand side of (E.8.2) is the same as the right-hand side of (E.8.1) that represents the DA profits for the unit. The second term on the right-hand side of (E.8.2) is the RT profits for the PSHU and that is the RT LMP times with the dispatch difference between the unit net output in the LAC and the unit net output in the DA.

Some Other System Conditions in LAC

Except for a few constraints summarized in Table E.8.1, the unit commitment and economic dispatch model for the rest of the system remains unchanged in each LAC simulation. The

transmission constraint is only considered inside each LAC window. Only in the Perfect Case, the PSHU is included in the power balance constraint for every interval starting from the beginning of the LAC until the end of the day. For the three models that uses price forecast, the PSHU is included in the power balance constraint only inside each LAC window. The system reserve requirement is only considered inside each LAC window. The ramp rate for the rest of the units (other than the PSHUs) in the system are modeled only inside each LAC window as well.

Table E.8.1. System Conditions Settings in Each Model

	Transmission Constraint	Load Balance	Reserve (Reg, Spin, Supp)	Ramp Rate for the Rest of the Units
Perfect Case	Only in LAC	PSH is Counted Till T	Only in LAC	Only in LAC
Deterministic PSH	Only in LAC	PSH is Counted Only in LAC	Only in LAC	Only in LAC
Risk-neutral Stochastic PSH	Only in LAC	PSH is Counted Only in LAC	Only in LAC	Only in LAC
Risk-averse Stochastic PSH	Only in LAC	PSH is Counted Only in LAC	Only in LAC	Only in LAC

Preliminary Simulation Results

A series of three hour LAC windows are solved sequentially. The simulation ends at the last LAC window that starts from 22nd hourly interval and contains the last three hours of the day. (In actual practice, the LAC would also be performed for the window starting at the 23rd and 24th hourly interval and would include data relevant to the next day; however, we did not have that next day DA and RT data available, so we used the LAC window starting at the 22nd hour to set the RT decisions for all three hours.) After in total twenty-two LAC problems been sequentially solved for all models, the system objective values and the unit profits are collected and compared in Table E.8.2 and Table E.8.3 respectively.

Table E.8.2. LAC System Objective Results.

	Change compared to the Perfect Case	Change in Percentage compared to the Perfect Case
Deterministic PSH	+21959.2	+7.1%
Risk-neutral Stochastic PSH	+10374.9	+3.3%
Risk-averse Stochastic PSH	+4221.5	+1.3%

As described earlier, the Perfect Case should give the best system objective. Therefore, the objective value of the Perfect Case is set as the benchmark. The objective of the other three models are compared and the difference (increase and percentage) are listed in Table E.8.2. It is observed that the deterministic PSH model using the single point forecast gives the highest (worst) objective. With the probabilistic price forecast applied, the risk-neutral stochastic PSH improves the objective compared to the deterministic PSH model. Furthermore, with the robust risk management formulation applied to the stochastic PSH model, the objective is improved further and is close to the result from the Perfect Case. Notice that only part of the RT system data is represented in the LAC simulation, therefore the LMP forecast that is based on the actual RT system may differ significantly from the represented RT system in the LAC. It makes sense that the risk-averse PSH model does better than the risk-neutral model when the LMP forecast is relatively "off". However, in the case when the represented RT system is closer to the actual system

that the LMP forecast is based on, we expect that a good LMP forecast would help the risk-neutral PSH model to achieve a better objective than the risk-averse PSH model. We will update the results in more case studies in a later paper.

Table E.8.3. PSHU Profits Results.

	RT Profits [$]
Perfect Case	
PSHU1	1484
PSHU2	-735
Deterministic PSH	
PSHU1	-7581
PSHU2	-10653
Risk-neutral Stochastic PSH	
PSHU1	-2387
PSHU2	-5454
Risk-averse Stochastic PSH	
PSHU1	610
PSHU2	-1894

The profits for the two PSH plants are listed in Table E.8.3, the DA profits are calculated by (E.8.1) and the RT profits are calculated by (E.8.2). The RT profits for each model are listed in the second column. In the perfect case, PSHU1 gains some RT profits while PSHU2 loses a small amount of profit in the RT market. Notice that both PSHU1 and PSHU2 are connected at the same node, multiple optimal solutions exist, and so it is likely that there is a solution where both units make a small amount of positive RT profits. It is observed that even in the Perfect Case, the PSH deviation from the DA solution is not significant and results in a small profit gain in the RT market. This is largely due to the fact that only part of the RT system data is represented in the LAC simulation such that the system condition in LAC is not too much different to the DA.

Among the three proposed models, the Risk-averse Stochastic PSH model gives the best RT profits. The deterministic PSH model results in worse profits due to RT dispatch for both units. That is partly because the model considers only the single point LMP forecast. When the probabilistic price forecast with total 50 scenarios is applied in the Risk-neutral Stochastic PSH model, both units still lose profits in the RT market but the situation is significantly relieved compared to the result from the deterministic model. In addition, after the robust risk-management formulation is applied in the risk-averse stochastic PSH model, one of the PSHUs has a small negative RT profits, and the other PSHU gains a small amount of positive RT profit. Notice that the margin of the RT profits is very small shown in the results of the Perfect Case, and the results from the Risk-averse stochastic PSH model is very close to the Perfect Case.

The unit dispatch solutions for plant PSHU1 and PSHU2 from the simulation with the risk-averse stochastic model are plotted in Fig. E.8.1 and Fig. E.8.2. The PSHU outputs are indicated by the solid lines and they align with the units on the left of the figure. The LMP are indicated by the dashed lines and they align with the units on the right of the figure. The DA solutions are in blue and LAC solutions are in red. For both PSHU plants, most of the LAC solutions are either the same (where the red lines overlap with the blue lines) or very close to the DA solution.

The most significant differences between the LAC and DA solutions for both PSHU are highlighted in the dashed rectangles in Figs. E.8.1 and E.8.2 and they can be summarized as follows. First of all, compared to the DA results, the ramp of the morning peak in the LAC are

slower and they can be observed by the comparison of LMPs in DA and LAC. This change from DA to LAC is reflected in the LAC solution. In the LAC solution, the generation of both units at interval 5 are less than the DA solution as highlighted in the first dashed rectangle from left to right in both figures. Second, in the LAC solution, both units generate more in the morning peak hour at interval 6 shown in the second dashed rectangle from left to right in both figures. Third, both units have some activities in the mid-day (gen and pump for PSHU1 and pump for PSHU2) in the LAC while they are kept offline in the DA solution as highlighted in the third dashed rectangle from left to right in both figures.

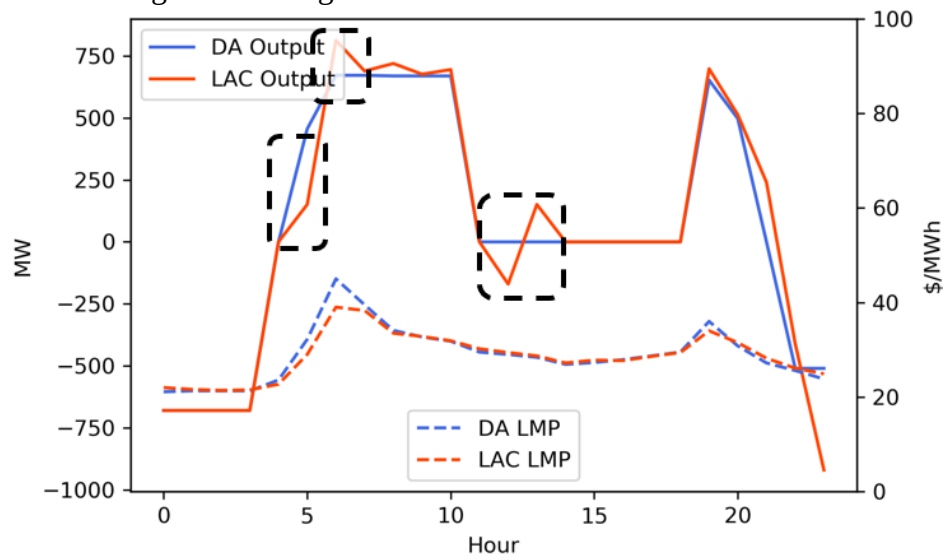

Fig. E.8.1 DA and LAC Solution for PSHU1. The dispatch differences between the DA and LAC solution are highlighted in the black dashed rectangles. The changes in LAC dispatch solutions reflect that the PSHU is adapted to the updated LAC LMP shown in the dashed red lines.

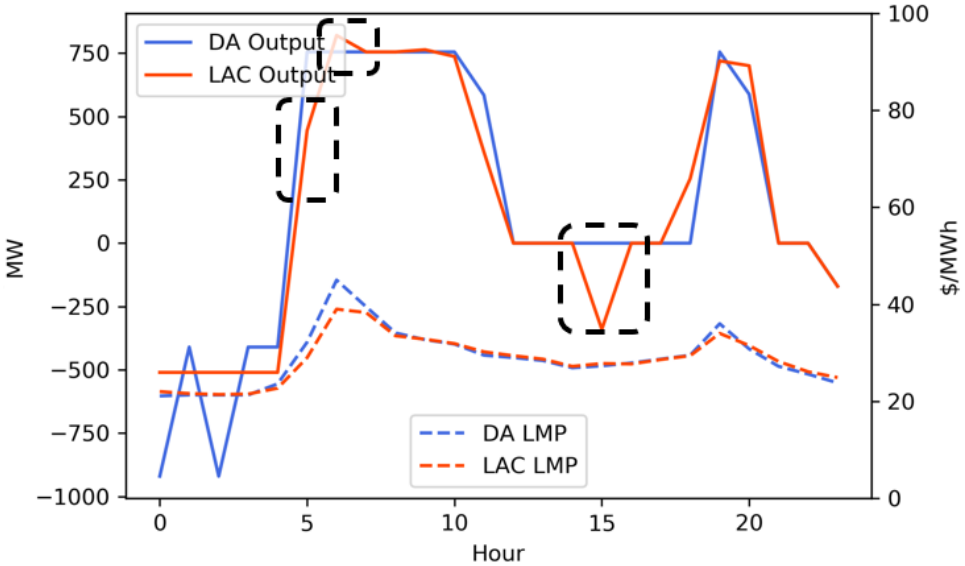

Fig. E.8.2 DA and LAC Solution for PSHU2. The dispatch differences between the DA and LAC solution are highlighted in the black dashed rectangles. The changes in LAC dispatch solutions reflect that the PSHU is adapted to the updated LAC LMP shown in the dashed red lines.

Compared to the DA solution, the first and second deviations at both units in the LAC solution show cases where the probabilistic price forecast accurately captured the changed system

conditions in RT and helped to take the right decision for both units; that is, to generate less when the morning peak ramp is slower and generate more in the peak hour. Those actions would contribute to the improved system objective and the increased RT profits at the units. Compared to the DA solution, the third deviations in the LAC solution for both units don't perfectly align with the RT system condition indicated by the LAC LMP. That indicates the probabilistic LMP forecasts in the corresponding LAC windows consistently deviate from the realized LAC LMP or that another issue, such as the size of the MIP relative gap, drive the outcomes in this case.

In summary, with the risk-neutral stochastic PSH model, the dispatch of the PSHU in the LAC simulation deviates from the DA solution as designed. The risk-neutral stochastic PSH model helps to bring the system objective close to the perfect case and avoid large negative RT profits for one PSHU and achieved a small positive RT profits for the other PSHU. With the current RT system data in the LAC simulation, the DA system condition and the RT system condition in LAC are relatively close. Therefore, the value of the adjustment on the PSHU dispatch in LAC is marginal as indicated by the results from the perfect case. We plan to continuously refine the RT data in LAC simulations that would reduce the gap between the model in the LAC simulation and the realistic system condition. In addition, more cases where the DA and RT system conditions are significantly different will be studied. We will update those results in a later paper that will be submitted for a journal publication.

References:

[E.1] P. Pinson, G. P. (2009). From probabilistic forecasts to statistical scenarios of short-term wind power. *Wind Energy 12(1)*, 51-62.

[E.2] S. Delikaraoglo, P. P. (2014). High-quality Wind Power Scenario Forecasts for Decision-making Under Uncertainty in Power Systems. *13th International Workshop on Large-Scale Integration of Wind Power and Transmission Networks*.

IV.F. Accomplishments Toward Milestone 6.1

Milestone 6.1: Establish deterministic PSH optimization model for economic planning while reflecting market optimization.

Accomplishments Summary: (1) In section IV.C, the team established a deterministic PSH optimization model for economic planning while reflecting DA and RT market optimizations in a MISO system using PLEXOS. Based on this, the team establishes a PSH optimization model with market optimizations enhancements (e.g., incorporating price forecast and MWh reserve). Tests are conducted in revised planning models for a MISO planning case. (2) MWh reserve modeling was included for MISO system using PLEXOS. Numerical simulation shows the benefit of modeling MWh reserve in MISO planning model is to make sure the SOC would not violate its limit given certain reserve deployment assumptions. (3) A value-of-water based approach was used for the RT operation of PSH units to exploit the flexibility of storage resources. Test results show defining a value-of-water function for RT can enable the flexibility of PSH and reduce the overall system cost in the RT market. (4) Furthermore, we explored the benefit of MWh reserve in real-time rolling horizon optimization. Combining with a value-of-water based rolling horizon framework, we analyzed the benefit of withholding energy in a test system.

IV.F.1 Incorporating MWh-reserve for PSH in planning studies

MWh-reserve modeling

Based on the MWh reserve modeling method in section IV.D, a MWh reserve formulation is implemented in PLEXOS. We assume PSH units can provide both upward and downward reserve in the generating mode, and zero reserve in the pumping mode due to the fixed-power pump. As shown in (F.1.1), the lower limit of the upper reservoir is improved with the consideration of possible reserve deployments. The storage should withhold a certain amount of energy to avoid SOC lower limit violation in time period *t*, If reserve was deployed *k* time periods before.

$$E_r^{\min} + \frac{1}{\eta^g} \cdot \sum_{h \in \mathcal{H}^r} rsv_{h,t-k}^{\text{guDA}} \leq e_{r,t} \quad \forall r \in \mathcal{R},\ \forall t \in \mathcal{T} \tag{F.1.1}$$

We first evaluate the value of MWh reserve modeling in a small test system. As shown in Fig. F.1.1, the three bus system consists of three generators and one PSH unit. To test two different cases, we designed a low load profile for CASE I, and a high load profile for CASE II in Fig. F.1.2 (a) and Fig. F.1.2 (b), respectively. The SOC schedule results for both cases are shown in Fig. F.1.3. As indicated, in CASE I, the SOC curve from the test with MWh reserve modeling is higher than that from the test without MWh reserve modeling. Hense, MWh reserve modeling can withhold some water to avoid the reservoir from violating its lower limit when there exists reserve deployment. However, in CASE II the two SOC curves are exactly the same. As shown in Table F.1.1, the cleared reserve of PSH turns to zero in CASE II with MWh reserve. Thus, the SOC solution satisfies (F.1.1) when the cleared reserve is zero. Note the key feature of CASE I is that other online conventional generators cannot fully satisfy the system reserve requirement, which is 100 MW. So, the reserve of PSH would be cleared even with the price of withholding more water. However, as the load increase in CASE II, all three generators are online, and the total available capacity of them can cover the system reserve requirement. Then the reserves of other generators are preferred to be deployed than the reserve of PSH.

Through this comparative test, we found when MWh reserve is modeled: 1) PSH might withhold some extra water if the other generator cannot fully cover the system reserve requirement, like CASE I. 2) the reserve of PSH might not be cleared if other generators cannot fully cover the system reserve requirement, like CASE II.

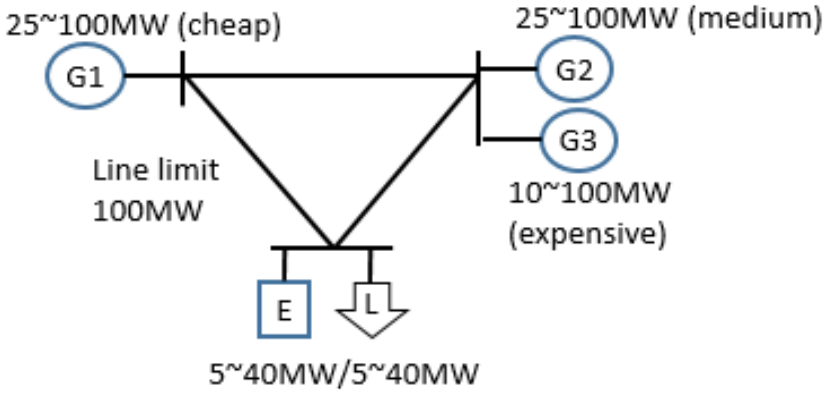

Fig. F.1.1. A 3-bus test system

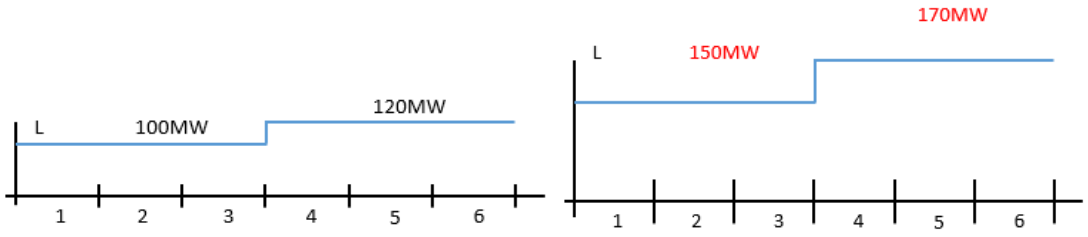

(a) load profile for CASE I (b) load profile for CASE II

Fig. F.1.2 load profiles for two test cases

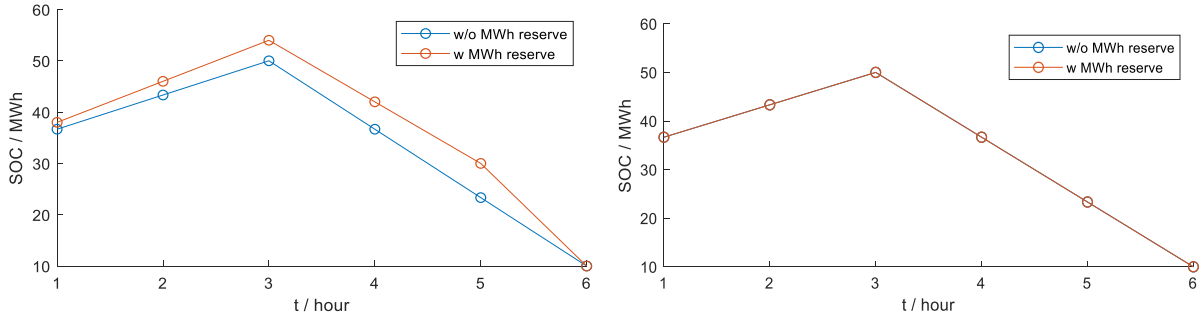

(a) CASE I (b) CASE II

Fig. F.1.3 Scheduled SOC of PSH. MWh reserve modeling can withhold some water to avoid the reservoir from violating its lower limit when there exists reserve deployment.

Table F.1.1 cleared reserve of each unit in CASE II with MWh reserve

Time period (hour)	1	2	3	4	5	6
G1 reserve (MWh)	0.00	0.00	0.00	0.00	0.00	0.00
G2 reserve (MWh)	68.33	25.00	25.00	25.00	25.00	25.00
G3 reserve (MWh)	31.67	75.00	75.00	75.00	75.00	75.00
PSH reserve (MWh)	**0.00**	**0.00**	**0.00**	**0.00**	**0.00**	**0.00**

Test on the revised MISO planning model

The MWh reserve is implemented in a MISO planning model, which is a portion of the interconnection seam study model. The detailed implementation of the MWh reserve is shown in (F.1.2), wherein a four-interval look-back formulation is employed as an example. In our test, the SOC is not explicitly daily recycled. As shown in (F.1.3), only the lower bound of SOC is limited to enable the capability of lifting the SOC curve up.

$$
\begin{aligned}
E_r^{\min} + \frac{1}{\eta^g} \cdot \sum_{h \in \mathcal{H}^r} rsv_{h,t}^{\text{guDA}} &\leq e_{r,t} \quad \forall r \in \mathcal{R},\ \forall t \in \mathcal{T} \\
E_r^{\min} + \frac{1}{\eta^g} \cdot \sum_{h \in \mathcal{H}^r} rsv_{h,t-1}^{\text{guDA}} &\leq e_{r,t} \quad \forall r \in \mathcal{R},\ \forall t \in \mathcal{T} \\
E_r^{\min} + \frac{1}{\eta^g} \cdot \sum_{h \in \mathcal{H}^r} rsv_{h,t-2}^{\text{guDA}} &\leq e_{r,t} \quad \forall r \in \mathcal{R},\ \forall t \in \mathcal{T} \\
E_r^{\min} + \frac{1}{\eta^g} \cdot \sum_{h \in \mathcal{H}^r} rsv_{h,t-3}^{\text{guDA}} &\leq e_{r,t} \quad \forall r \in \mathcal{R},\ \forall t \in \mathcal{T}
\end{aligned} \tag{F.1.2}
$$

$$
e_{r,t_{\text{end}}} \geq E_0 \tag{F.1.3}
$$

The testing results of the cases without and with MWh reserve are shown in Fig. F.1.4 and Fig. F.1.5, respectively. In the test with MWh reserve, the MWh reserve constraint for the ending hour does bind, but the SOC curve doesn't change, which is similar to CASE II in the previous subsection. Also, we noticed that the reserve of PSH at hour 21 changes to 0 after the MWh reserve modeling is included. As the reserves of other generators are sufficient to cover the system reserve requirement in hours 21-24, if reserve can be offered by other generators, the optimal solution tends not to clear PSH's reserve.

Although the scheduled SOC curve doesn't change, the inclusion of MWh reserve modeling does change the cleared reserve of PSH. For the solution from the without MWh reserve test, suppose the reserve of PSH is deployed in the time period 21, the ending SOC would violate its lower limit. However, with MWh reserve modeling, it would not happen as the reserve of PSH is not cleared in the time period 21. The benefit of modeling MWh reserve in MISO planning model is to make sure the SOC would not violate its limit given certain reserve deployment assumptions.

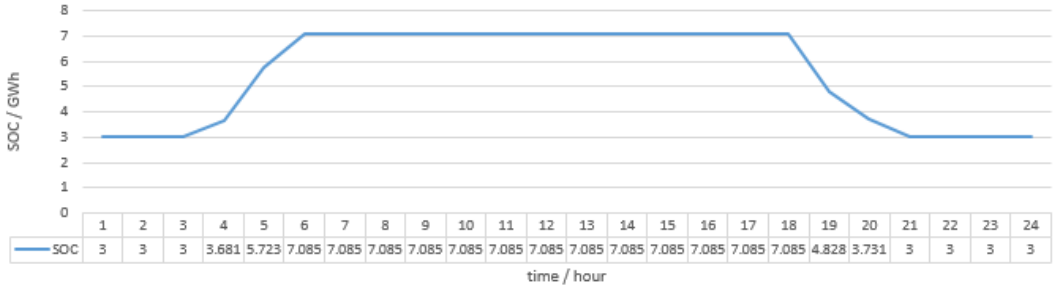

	1	2	3	4	5	6	7	8	9	10	11	12	13	14	15	16	17	18	19	20	21	22	23	24
SOC	3	3	3	3.681	5.723	7.085	7.085	7.085	7.085	7.085	7.085	7.085	7.085	7.085	7.085	7.085	7.085	7.085	4.828	3.731	3	3	3	3

(a) SOC of a realistic PSH station

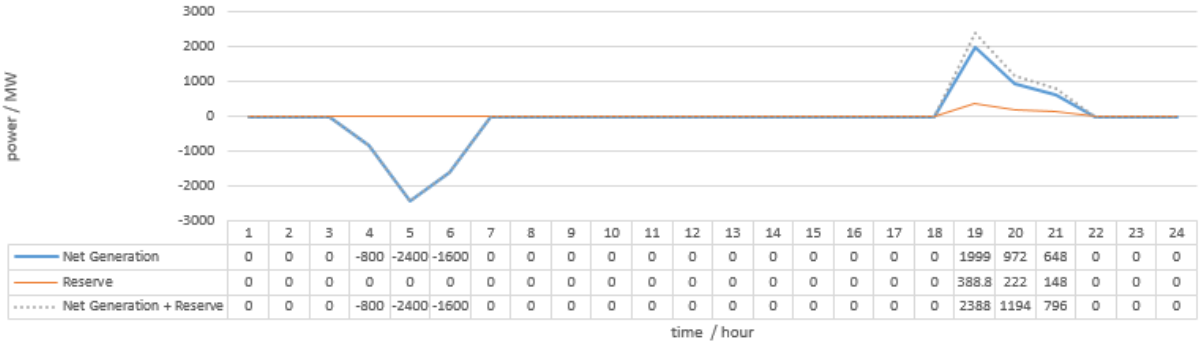

	1	2	3	4	5	6	7	8	9	10	11	12	13	14	15	16	17	18	19	20	21	22	23	24
Net Generation	0	0	0	-800	-2400	-1600	0	0	0	0	0	0	0	0	0	0	0	0	1999	972	648	0	0	0
Reserve	0	0	0	0	0	0	0	0	0	0	0	0	0	0	0	0	0	0	388.8	222	148	0	0	0
Net Generation + Reserve	0	0	0	-800	-2400	-1600	0	0	0	0	0	0	0	0	0	0	0	0	2388	1194	796	0	0	0

(b) energy and reserve dispatch of a realistic PSH station

Fig. F.1.4 simulation result of a realistic PSH station without MWh reserve modeling

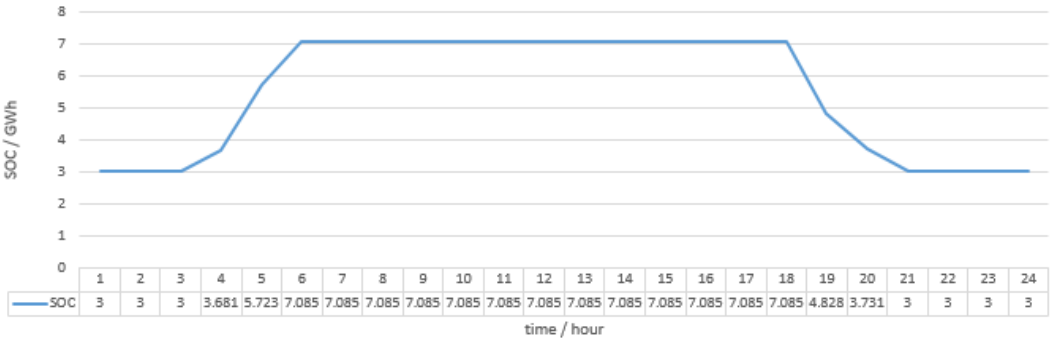

	1	2	3	4	5	6	7	8	9	10	11	12	13	14	15	16	17	18	19	20	21	22	23	24
SOC	3	3	3	3.681	5.723	7.085	7.085	7.085	7.085	7.085	7.085	7.085	7.085	7.085	7.085	7.085	7.085	7.085	4.828	3.731	3	3	3	3

(G) SOC of a realistic PSH station

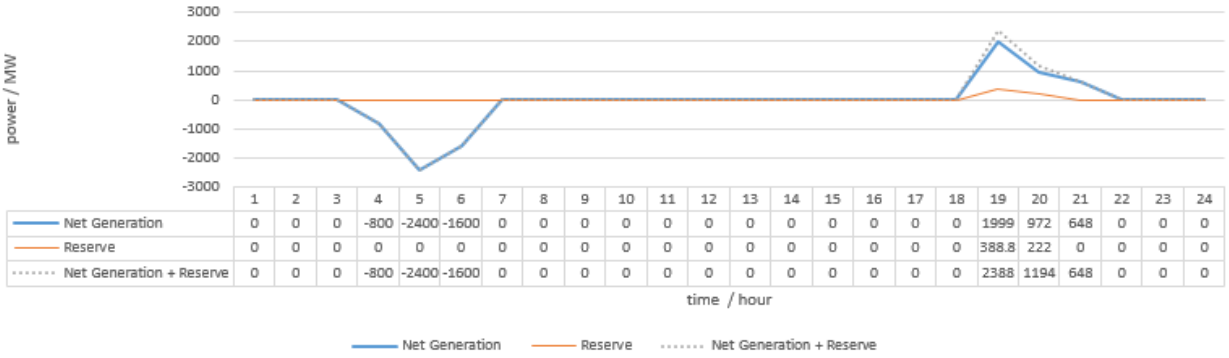

	1	2	3	4	5	6	7	8	9	10	11	12	13	14	15	16	17	18	19	20	21	22	23	24
Net Generation	0	0	0	-800	-2400	-1600	0	0	0	0	0	0	0	0	0	0	0	0	1999	972	648	0	0	0
Reserve	0	0	0	0	0	0	0	0	0	0	0	0	0	0	0	0	0	0	388.8	222	0	0	0	0
Net Generation + Reserve	0	0	0	-800	-2400	-1600	0	0	0	0	0	0	0	0	0	0	0	0	2388	1194	648	0	0	0

(b) energy and reserve dispatch of a realistic PSH station

Fig. F.1.5 simulation result of a realistic PSH station with MWh reserve modeling

IV.F.2 Incorporating real-time value-of-water for PSH in planning studies

Real-time value-of-water modeling

1) current practice: following the DA schedule

Currently, in RT operations, PSH owners attempt to follow the DA schedule as close as possible. As shown in Fig. F.2.1, actual DA and RT schedule of a realistic PSH from in a 15-day period also verifies the aforementioned fact from a long-term perspective. This PSH RT operation strategy works well for power systems with relatively low renewable energy penetration, however, restricts the flexibility of PSH in RT operations when the DA forecast error is large. In our numerical simulations, following the DA generate and pump schedule in RT is regarded as the current practice of PSH RT operation strategy.

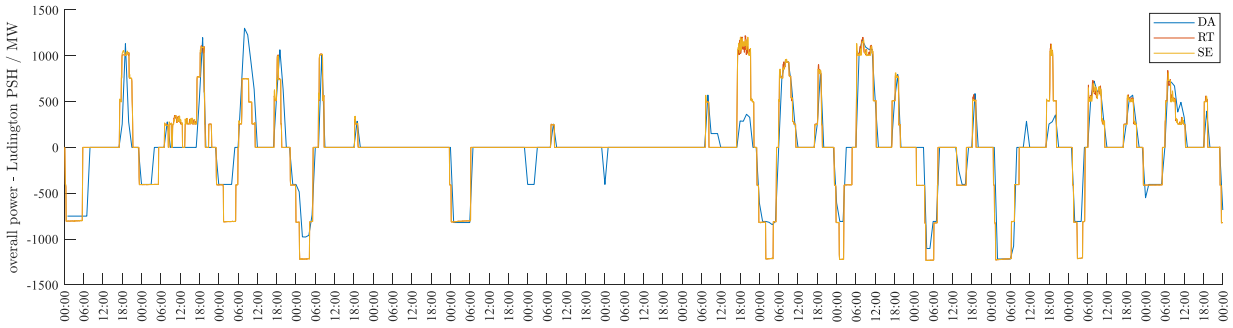

Fig. F.2.1 Actual DA and RT schedule of a realistic PSH. RT operations. RT schedule largely follows the DA schedule.

2) proposed approach: define an appropriate value-of-water function

A value-of-water based rolling horizon DA/RT interleaved framework is developed to reflect the impact of future prices in guiding short-term PSH optimization.

In RT operations, ISOs usually optimize a single time period market clear problem every 5 minutes. Lack of look-ahead ability brings a significant challenge for energy-limited resources if they don't follow the DA schedule. The look-ahead schedule is a good option to consider the future possibilities for the current decision, however, it suffers from heavy computational burdens for practical large-scale power systems to clear the market in less than 5 minutes.

To this end, value-of-water based approach is a promising technical solution to keep the optimization time horizon of market clear problem as one period, while considering the forecast for the future. The value of water (VOW) is an expectation of the water cost in the upper reservoir of PSH.

As investigated in section IV.B, the DA storage shadow price, i.e. the dual variable for the SOC constraint of the upper reservoir, can be used to estimate it for perfect DA prediction and strongly convex cases. In reality, the market model is generally non-convex. In the planning model, we use the DA storage shadow price as a predictive indicator for the future water price, as shown in (F.2.1).

$$VOW_{s,t} \approx \hat{\gamma}_{s,t}^{\mathrm{DA}} \tag{F.2.1}$$

Test the Revised MISO Planning Model

The DA/RT interleaved method and the value-of-water based PSH RT operation strategy are implemented in the Seams model using PLEXOS. The revised model is tested to compare different operation strategies and analyze the value of the interleaved simulation method.

1) flexibility advantage of the value-of-water based PSH RT operation strategy

In our simulation for the current practice of RT operation strategy, PSH units follow their DA generate and pump schedule. As shown in Fig. F.2.2, in RT, MW output and hour-end SOC of

PSH units cannot deviate from their DA schedules. Suppose RT system net-load is far from the DA forecasted value, the system needs the flexibility from PSH to follow the RT net-load, and meanwhile, PSH owner can earn more to follow the price signal and deviate from the DA schedule. In these scenarios, following DA schedule can restrict the flexibility of PSH.

For the proposed value-of-water based approach, VOW is estimated by DA storage shadow price. We first apply VOW for the generate mode, and remain pump schedule following that from DA. As indicated in Fig. F.2.3, PSH can generate even when it is not pre-scheduled in DA. The flexibility of PSH units can be exploited when it is needed.

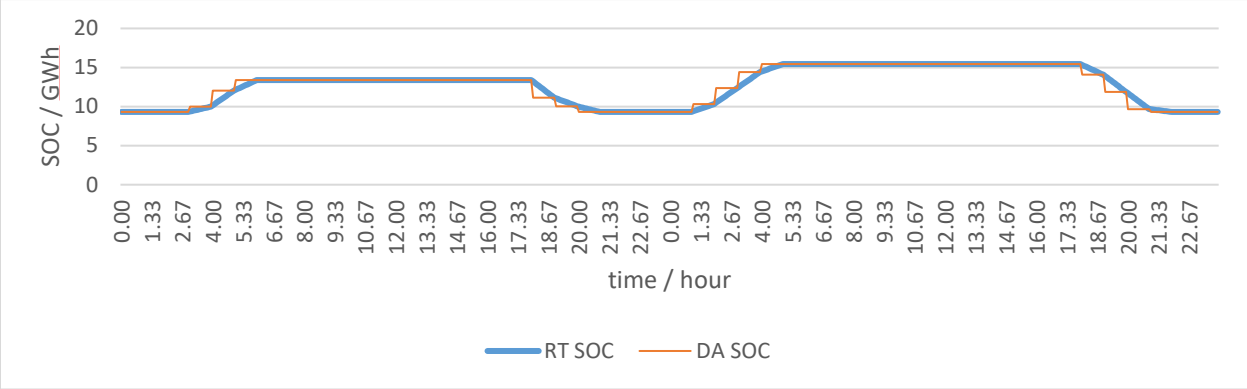

(G) DA and RT SOC

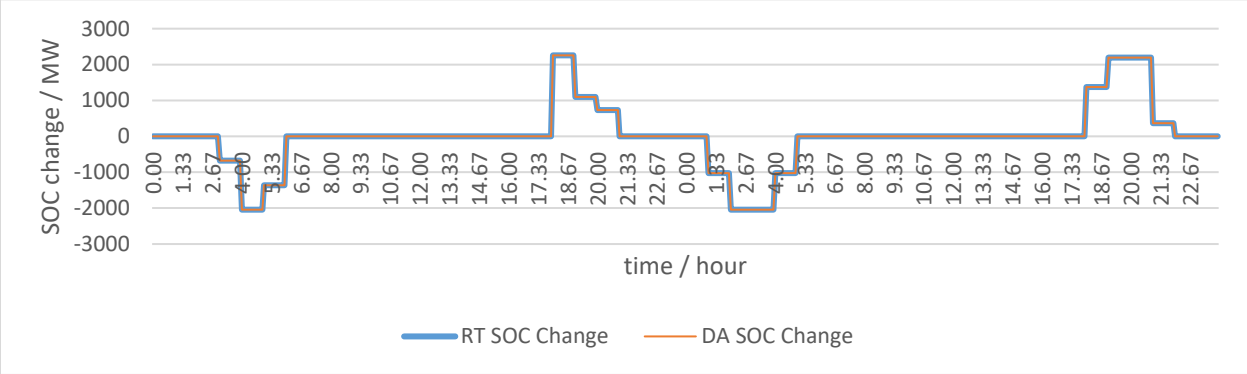

(b) DA and RT SOC change

Fig. F.2.2 Simulated DA and RT dispatch of a realistic PSH (RT follows DA schedule approach)

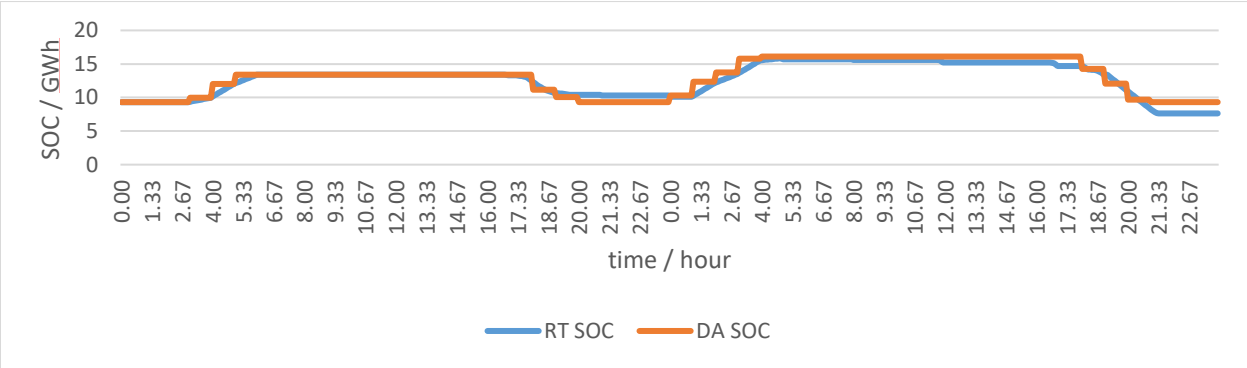

(G) DA and RT SOC

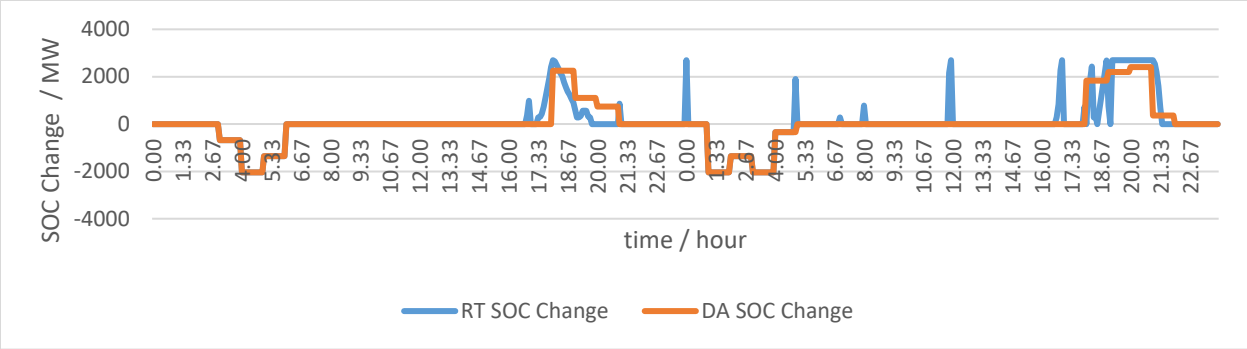

(b) DA and RT SOC change

Fig. F.2.3 Simulated DA and RT dispatch of a realistic PSH (proposed value-of-water based approach where RT generation uses VOW, RT pump follows DA). PSH can generate in RT even when it is not pre-scheduled in DA in order to exploit the flexibility of PSH units.

For different PSH RT operation strategies and different fluctuation levels, RT overall system costs are compared. As indicated in Table F.2.1, in contrast to the current practice (i.e., follow DA schedule), the preliminary result shows that defining a value-of-water function for RT can enable the flexibility of PSH. This can reduce the overall system cost for the RT market. Longer term simulation results are shown later in this report.

Fig. F.2.1 RT cost comparison for different PSH RT operation strategies (2-day result)

PSH RT operation strategy	trend only (10^3 \$)	with error σ = 1% (10^3 \$)	with error σ = 5% (10^3 \$)
follows DA schedule	226,388.020	226,313.814	227,718.326
gen uses VOW, pump follows DA	225,816.761	225,936.243	227,122.333
VOW for both gen and pump	225,794.180	-	-

2) value of the proposed interleaved simulation

A case with larger intra-hour prediction errors in DA, i.e., with a 5% standard deviation in synthesizing the RT load, is also tested. As shown in Fig. F.2.4, PSH units generate more in RT to flexibly address the uncertainty. The interleaved simulation can reflect DA/RT deviation that is brought by DA prediction error. In addition, it can be observed that the initial SOC of the second day starts from the ending SOC of the first day, which indicates the interleaved simulation can reflect the SOC interaction between the RT market of the current day and the DA market of the next day.

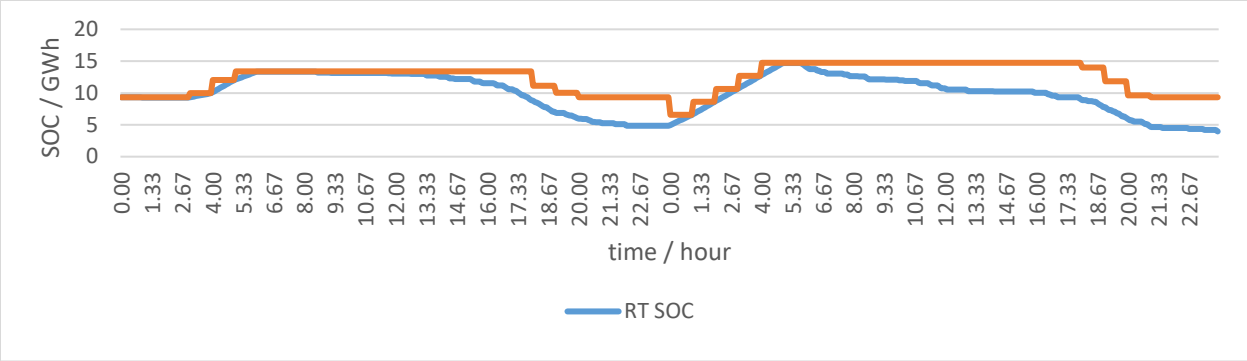

(G) DA and RT SOC

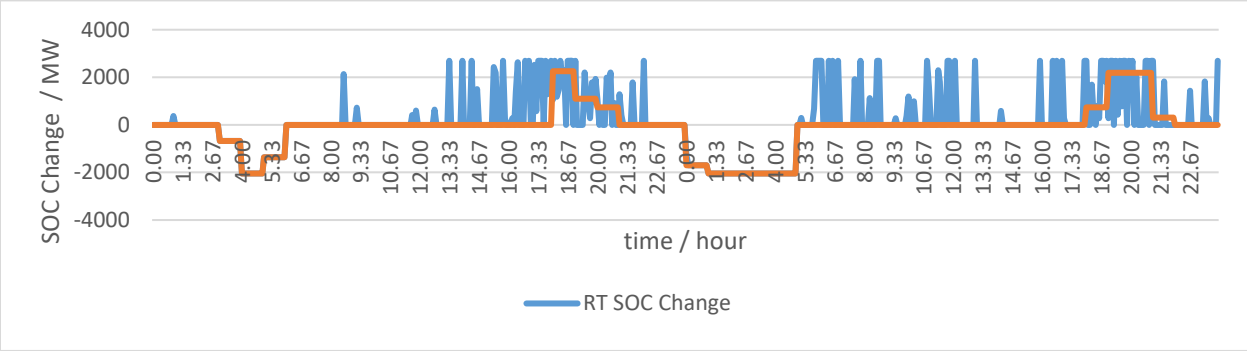

(b) DA and RT SOC change

Fig. F.2.4 Simulated DA and RT dispatch of a realistic PSH (larger DA load prediction error, RT generation uses VOW, RT pump follows DA). The interleaved simulation can reflect the SOC interaction between the RT market of the current day and the DA market of the next day.

3) long term evaluation

We further conducted simulation for longer time periods. With a monthly simulation for each quarter, RT overall system costs are compared for different PSH RT operation strategies. As indicated in Table F.2.2, in contrast to the current practice (i.e., follow DA schedule), the test result shows that defining a value-of-water function for RT can enable the flexibility of PSH. This can reduce the overall system cost for the RT market, with a monthly average of 0.22% reduction. As the only difference between the 'follow DA schedule' and 'VOW' is the RT dispatch approaches for PSH, the cost benefits are thus from better utilizations of PSHUs' flexibility, demonstrating the value of better optimized PSH.

Table F.2.2. RT cost comparison for different PSH RT operation strategies Using DA/RT Interleaved Simulation on MISO planning model for 2024 (with error σ = 5%)

PSH RT operation strategy	January 2024 (10^3 $)	April 2024 (10^3 $)	July 2024 (10^3 $)	October 2024 (10^3 $)
Follows DA schedule	4,303,959	3,161,008	6,752,143	3,424,229
VOW	4,275,751	3,157,345	6,750,693	3,420,599

Cost Reduction ($)	28,208	3,663	1,450	3,630
Cost Reduction (%)	0.66%	0.12%	0.02%	0.11%

IV.F.3 Exploring the benefit of MWh reserve in real-time rolling horizon optimization

In this subsection, we focus on uncertainties, and try to find the benefits of MWh reserve modeling in rolling horizon optimization. In addition to physical violations, we aim to investigate the potential cost increase or revenue decrease that is caused by running out of water.

In RT operation, dualizing the SOC constraint was proposed in previous tasks to decouple the temporal coupling in the SOC constraints. The value of water can be estimated by the DA storage shadow price, i.e., $VOW_{s,t} \approx \hat{\gamma}_{s,t}^{\mathrm{DA}}$. This works well for perfect prediction and strongly convex cases. If uncertainties are further considered in RT, the assumption of perfect prediction does not hold. For testing convenience, we keep the strongly convex assumption (simplified linear constraints and quadratic objectives for problems with both long and short horizons). The ISO clear and PSH owner strategic bid problems that do not consider MWh reserve constraints are shown in (F.3.1) and (F.3.2), respectively. For perfect prediction, adding MWh reserve constraints (F.3.3) would have ISO cost non-decreasing and PSH owners' profit non-increasing. We then analyze cases with uncertainties in a small illustrative case.

$$
\begin{aligned}
\min \quad & \sum_{i\in\mathcal{G}\cup\mathcal{H}} \sum_{t} f\left(p_{i,t}\right) \\
\text{s.t.} \quad & \underline{P}_i \le p_{i,t} \le \overline{P}_i, && \forall i \in \mathcal{G},\ \forall t \in \mathcal{T} \\
& -\underline{P}_i^p \le p_{i,t} \le \overline{P}_i^g, && \forall i \in \mathcal{H},\ \forall t \in \mathcal{T} \\
& e_{r,t} = e_{r,t-1} - \sum_{i\in\mathcal{H}^r} p_{i,t}, && \forall r \in \mathcal{R},\ \forall t \in \mathcal{T} \\
& \underline{E}_r \le e_{r,t} \le \overline{E}_r, && \forall r \in \mathcal{R},\ \forall t \in \mathcal{T} \\
& \sum_{i\in\mathcal{G}\cup\mathcal{H}} g_{i,t} = D_t, && \forall t \in \mathcal{T}
\end{aligned}
\tag{F.3.1}
$$

$$
\begin{aligned}
\max \quad & \lambda \cdot \sum_{i\in\mathcal{H}^r} p_{i,t} - \sum_{i\in\mathcal{H}^r} \sum_{t} f\left(p_{i,t}\right) \\
& -\underline{P}_i^p \le p_{i,t} \le \overline{P}_i^g && \forall i \in \mathcal{H}^r,\ \forall t \\
& e_{r,t} = e_{r,t-1} - \sum_{i\in\mathcal{H}^r} p_{i,t}, && \forall t \\
& \underline{E}_r \le e_{r,t} \le \overline{E}_r, && \forall t
\end{aligned}
\tag{F.3.2}
$$

$$
E_{r,t}^{*} \le e_{r,t}, \qquad \forall r \in \mathcal{R},\ \forall t \in \mathcal{T} \tag{F.3.3}
$$

The small illustrative system contains one PSH with 20MW and 40MWh installed capacity, and three generators as listed in Table F.3.1. The predicted load (or net-load) profile is assumed as shown in Fig. F.3.1. For a perfect prediction case, the rolling-horizon optimization result matches that from long-horizon optimization (we don't elaborate on the result as it has been shown in previous sections).

Table F.3.1 system parameter

unit	Pmax (MW)	b ($/MW)	a ($/MW^2)
G1	100	8.5	0.002
G2	100	9	0.001
G3	30	16	0.0005

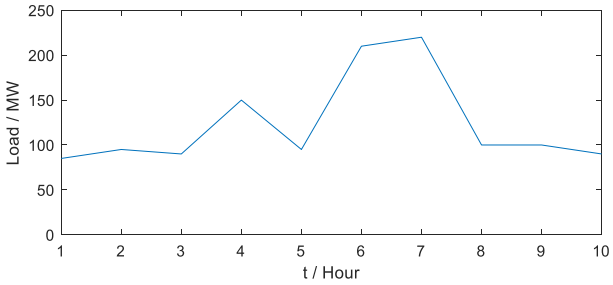

Fig. F.3.1 predicted load profile

We consider the load/net-load uncertainty. Although the load difference is small and LMP patterns are similar (not perfect but good load/LMP predictions), the PSH rolling-horizon schedule misses the highest price because of running out of the water, as shown in Fig. F.3.2. In our rolling horizon dispatch, the value of water from even a very small inaccurate prediction (in our case, close net-load and very similar LMP pattern) might not always correctly guide the PSH schedule. Additional floor room might be needed to avoid PSH from running out of the water before the high price.

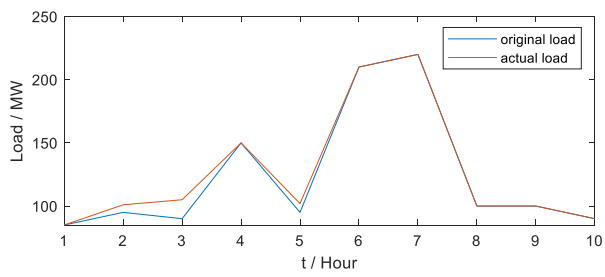

(a)

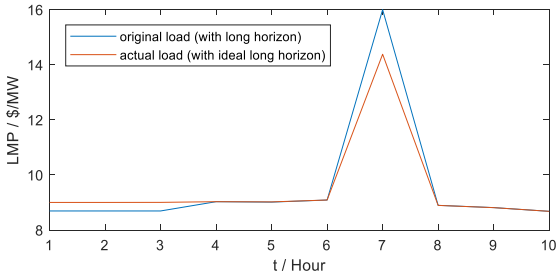

(b)

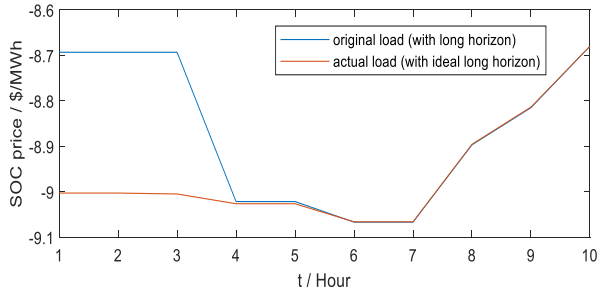

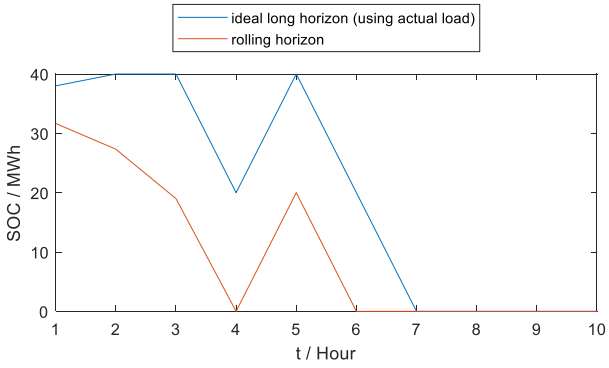

(c) (d)

Fig. F.3.2 load/net-load uncertainty test without MWh reserve (a) load; (b) LMP; (c) SOC price; (d) SOC. The PSH rolling-horizon schedule misses the highest price because of running out of the water.

As the LMP patterns are similar, in this case, we used a simple SOC lower bound strategy, which sets a floor level around the long-horizon SOC solution, as shown in (F.3.4). The main purpose is to check if modeling floor room makes sense in rolling horizon RT dispatch with VOW defined. Considering MWh reserve, as shown in Fig. F.3.3, the PSH doesn't miss the highest price at hour 7. For rolling horizon RT dispatch, ISO cost can be reduced from $10943 to $10801 with the MWh reserve modeling. As the PSH owner, catches the high price, a profit increase can be expected.

$$\min\left\{E^{\min}, \hat{e}_t^{\mathrm{LH}} - \epsilon\right\} \leq e_t \tag{F.3.4}$$

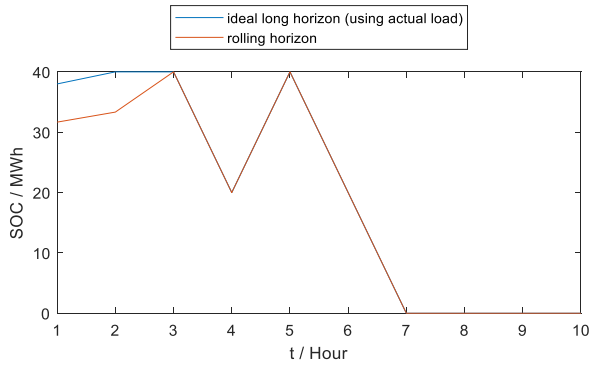

Fig. F.3.3 load/net-load uncertainty test with MWh reserve. The PSH doesn't miss the highest price at hour 7.

Although this the benefit analysis conclusion may not necessarily hold for general uncertainty realizations, it is sufficient to reflect the value of withholding water in particular inaccurate-prediction scenarios.

IV.G. Accomplishments Toward Milestone 8.1

Milestone 8.1: Establish prototype stochastic SCUC tool equipped with fast computation capability that can accurately determine MW and MWh reserve requirements of systems against uncertainties.

Accomplishments Summary: (1) The team has built a stochastic model to incorporate uncertainty SOC considerations in the day-ahead FRAC model to address the potential SOC boundary violation issue in real-time ED, as a result of RT uncertainties. (2) By studying MISO's historical data, the team has introduced new parameters to define scenarios describing DA to RT decrepedancy, which are used to cast a computationally-tractable stochastic model for determining MWh reserve requirements of systems. Numerical results show that including energy reserve secure constraints can improve system flexibility against uncertainties and contingencies, and

meanwhile does not necessarily reduce profits of PSH plants as evaluated by new DA and RT LMPs after including the uncertainty SOC constraints. (3) The team has used ADP to learn SOC-price curves for evaluating the value of water of PSHs outside a finite time horizon. The learned SOC-price curves could be used in the FLAC and LAC models to optimize the SOC levels at the end of the final time horizon, without explicitly simulating uncertainties of future time periods. Numerical results on a one-hour look-ahead PSH profit maximization problem show that the SOC-price curves learned out of the ADP approach could derive better solutions than a rolling based stochastic model while effectively avoiding the needs to explicitly simulate/forecast uncertainties of future time periods.

IV.G.1 Stochastic SOC Headroom and Floor Room of PSHs

This subsection describes the proposed stochastic model to incorporate uncertainty SOC considerations in the DA FRAC model. Specifically, multiple selective historical scenarios are incorporated in the DA FRAC model via chance constraints, in order to leverage solution robustness and economics against potential uncertainties of SOC deployment in the RT market.

A SOC limitation constraint that considers headroom and floor room can be written as:

$$SOC^{LB} + H_t^{LB} \leq soc_t \leq SOC^{UB} - H_t^{UB} \quad \text{(G.1.1)}$$

where soc_t represents the SOC at hour t; SOC^{LB} and SOC^{UB} are respectively its lower and upper bounds; headroom and floor room H_t^{LB} and H_t^{UB} are given values that are learned from history data. All variables are denoted by lower case letters and all parameters are denoted by upper case letters. Our goal is to consider uncertainties within this constraint by adopting a stochastic formulation. Indeed, is would be computationally challenging if directly considering variable soc_t as stochastic, because it is explicitly related with pumping and generating dispatch variables of the PSH (denoted as variable p_t and g_t). If soc_t is defined as a stochastic variable, p_t and g_t will be stochastic variables as well; and since these variables are involved in the power balance constraint of FRAC, the uncertainties will finally spread to the entire FRAC model, resulting in extremely heavy computational burden that is not affordable for the stringent FRAC computational time requirement. Alternatively, manipulating H_t^{LB} and H_t^{UB} may be a feasible option to consider uncertainties. In the following, we consider H_t^{LB} and H_t^{UB} as variables and thereafter rewrite them as h_t^{LB} and h_t^{UB}.

To begin with, a new parameter named "deviation rate" is introduced, which is defined as the ratio of the actual SOC deviation to the maximum possible deviation. The maximum possible deviation will be determined by the PSH's lower power bound (denoted as P^{LB} for pumping and G^{LB} for generating) and power upper bound (denoted as P^{UB} for pumping and G^{UB} for generating) as well as its current dispatch. For example, if a PSH is scheduled in DA at 600MW and its power lower/upper bound is 400MW/800MW, the maximum possible up-deviation (i.e., generating more) is 200MW (i.e., 800MW-600MW), while the maximum possible down-deviation (i.e., generating less) is also 200MW (i.e., 600MW-400MW). With this, if the PSH is dispatched at 700MW in RT, the up-deviation rate can be calculated as (700-600)/200=0.5; While if the PSH is dispatched at 550MW, the down-deviation rate can be calculated as (600-550)/200=0.25.

We use four parameters $R_t^{G,UP}$, $R_t^{G,DN}$, $R_t^{P,UP}$, and $R_t^{P,Dn}$ to denote the up-deviation rate under generating, down-deviation rate under generating, up-deviation rate under pumping, and down-deviation rate under pumping. We further add a subscript s to these variables, which gives $R_{s,t}^{G,UP}$, $R_{s,t}^{G,DN}$, $R_{s,t}^{P,UP}$ and $R_{s,t}^{P,Dn}$, to indicate generated deviation rates under a certain historical scenario s.

In fact, SOC deviations can be induced in two occasions: One is the dispatch discrepancy between DA and RT, but with the same generating/pumping mode; The other is generating/pumping mode switching (e.g., the PSH is scheduled Off in DA, but generates in RT at a certain time interval). The deviation rate is designed to measure first occasion. To deal with the second occasion, we further define four possible mode switching types from DA to RT:

- pumping to Off (I_t^{P-O})
- generating to Off (I_t^{G-O})
- Off to pumping (I_t^{O-P})
- Off to generating (I_t^{O-G})

Mode switching directly from generating to pumping or from pumping to generating has not been seen in the MISO's historical operation data, thus, not considered. In the same way, we add a subscript s to these parameters to indicate generated mode switching under a certain historical scenario s.

Scenario generation for Stochastic SOC Headroom and Floor Room

We borrow the idea of stochastic production simulation (simulating both unit output and unit status) and propose a "dual track" scenario generation procedure. On one track, a scenario will have deviation rates, both up- and down-deviation rates for pumping and generating, generated for each time interval; On the other track, this scenario may also have mode switching for each hour. In a scenario, the mode switching at a certain time interval can be none (i.e., no mode switching happens from DA to RT) or one of the above four possible mode switching types exclusively.

Formulation of Stochastic SOC Constraints

The basic idea of assessing the possible deviation under each scenario is that if a mode switching exists at a certain time interval and is triggered by the schedule under this scenario, its resulting SOC deviation will be counted first; otherwise, only dispatch deviation will be counted. The floor room under a certain scenario s can be formulated as:

$$h_{s,t}^{LB} = R_{s,t}^{G,UP}(G^{UB} \cdot u_t^G - g_t) + R_{s,t}^{P,DN}(p_t - P^{LB} \cdot u_t^P) + G^{UB} \cdot I_{s,t}^{O-G}\left(1 - u_t^G - u_t^p\right) + p_t \cdot I_{s,t}^{P-O}; \quad \text{(G.1.2)}$$

where u_t^G and u_t^p are binary mode indicators for generating and pumping respectively.

The four terms of $h_{s,t}^{LB}$ are explained as follows:

- First term: scheduled as generating in both DA and RT, but generates more in RT;
- Second term: scheduled as pumping in both DA and RT, but pumps less in RT;
- Third term: scheduled as OFF in DA, but starts to generate in RT;
- Fourth term: scheduled as pumping in DA, but quits pumping in RT.

Equation (G.1.2) can be understood as follows:

- If no mode switching occurs ($I_{s,t}^{O-G}$=0 and $I_{s,t}^{P-O}$=0) and the PSH is scheduled as generating at time t, namely u_t^G=1. The first term becomes $R_{s,t}^{G,UP} \cdot (G^{UB} - g_t)$, which calculates the dispatch up-deviation (extra generation); While all other three terms will be 0.
- If no mode switching occurs ($I_{s,t}^{O-G}$=0 and $I_{s,t}^{P-O}$=0) and the PSH is scheduled as pumping at time t, namely u_t^P=1. The second term becomes $R_{s,t}^{P,DN} \cdot (p_t - P^{LB})$, which calculates the dispatch down-deviation (short in pumping); While all other three terms will be 0.

- If $I_{s,t}^{O-G}$=1, but the PSH is scheduled as pumping or generating (i.e., not OFF), the mode switching will not be triggered, and the third term is cancelled out as 0. On the other hand, when the PSH is scheduled OFF (i.e., u_t^G=0 and u_t^p=0), the third term is triggered and equal to G^{UB}, indicating that the PSH starts to generate at the max in RT. G^{UB} represents the most conservative situation and it may be set as other values to mitigate the conservativeness.
- If $I_{s,t}^{P-O}$=1, but the PSH is scheduled other than pumping, the mode switching is not triggered and the fourth term is 0, since p_t will be 0. When the PSH is scheduled as pumping, the fourth term is equal to p_t, indicating that the PSH quits pumping in RT.

It is worthwhile to emphasize that $I_{s,t}^{O-G}$ and $I_{s,t}^{P-O}$ are given parameters, which are derived according to the historical scenarios. $I_{s,t}^{O-G}$ and $I_{s,t}^{P-O}$ can be 0 or 1 depending on the specific scenario.

Following the same logic, $H_{s,t}^{UB}$ can be calculated as:

$$h_{s,t}^{UB} = R_{s,t}^{G,DN}(g_t - G^{LB} \cdot u_t^G) + R_{s,t}^{P,UP}(P^{UB} \cdot u_t^P - p_t) + P^{UB} \cdot I_{s,t}^{O-P} \cdot \left(1 - u_t^G - u_t^p\right) + g_t \cdot I_{s,t}^{G-O}; \quad \text{(G.1.3)}$$

The four terms of $h_{s,t}^{UB}$ represent:

- First term: scheduled as generating in DA and RT, but generates less in RT;
- Second term: scheduled as pumping in DA and RT, but pumps more in RT;
- Third term: scheduled as OFF in DA, but starts to pump in RT;
- Fourth term: scheduled as generating in DA, but quits generating to OFF in RT.

With the above equations, the SOC limitation constraint can be written as:

$$SOC^{LB} + \sum_{k=1}^{t} h_{s,t}^{LB} - s_{s,t}^{LB} \le soc_t \le SOC^{UB} - \sum_{k=1}^{t} h_{s,t}^{UB} + s_{s,t}^{UB} \quad \text{(G.1.4)}$$

Additional auxiliary constraints and final SOC stochastic constraints are included in the Appendix for section IV.G.1.

IV.G.2 Case Study with Stochastic SOC Headroom and Floor Room

The DA FRAC with stochastic SOC limitation constraint is performed on the MISO cases with the HIPPO platform. There are three PSH plants in MISO's system (referred to as PSH-1, PSH-2, and PSH-3 in this study), in which each of the first two contain 3 units and the last one contains 2 units. One sample day in spring 2019 is selected for the study. The scenarios used to formulate the stochastic constraints are selected from historical data of the past three years and the total numbers of scenarios for individual PSHs are listed in Table G.2.1. All scenarios are given on the plant level. With different RT load profiles and settings on the allowance of recommitment/ decommitment of PSH plants in RT, four cases are studied as shown in Table G.2.2. The DA load profile and RT load profile with and without extra wind fluctuations are shown in Fig. G.2.1.

Table G.2.1 The number of selected scenarios

PSH Name	Total Number of Scenarios	Num of Scenarios in 2017	Num of Scenarios in 2018	Num of Scenarios in 2019
PSH-1	30	15	10	5
PSH-2	30	15	10	5

PSH-3	30	15	10	5

Table G.2.2 The four cases and their settings

Case Name	Setting
Normal load + Fixed PSH	UDS load + fixed unit commitment of PSH plants
High load + Fixed PSH	UDS load + wind fluctuation + fixed commitment of PSH plants
Normal load + Committable PSH	UDS load + re-committable/de-committable PSH plants
High load + Committable PSH	UDS load + wind fluctuation + re-committable/de-committable PSH plants

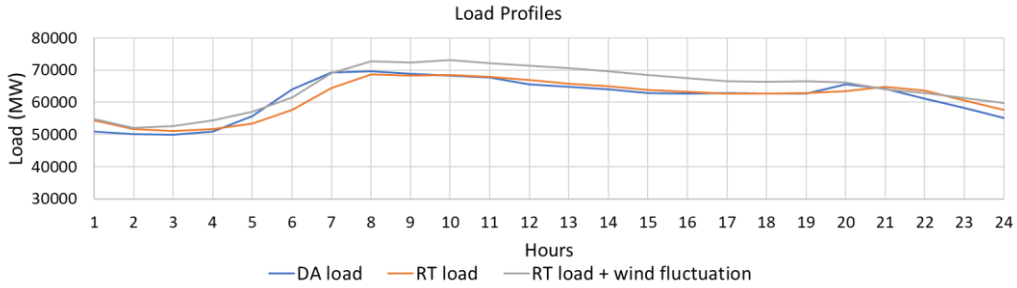

Fig. G.2.1. Load profiles in DA and RT for a sample day in spring 2019

Models with different headroom and floor room settings are differentiated with different N values, and the case without considering headroom and floor room is viewed as the benchmark model and denoted by w/o. In the simulation, M of each PSH is set as 5 times of the reservoir capacity. The MILP gap threshold for all cases is set as 0.1% and the solution time limit is 1200s.

The day-ahead revenue of the three PSHs are shown in Table G.2.3. It is worthwhile to mention that all the above four cases are created for RT, thus all the four cases will share the same DA result from the same DA case. The DA revenue is calculated as Realized profits = $\sum_{t=1}^{T} LMP_t^{DA} \cdot (g_t^{DA} - p_t^{DA})$, where g_t^{DA} and p_t^{DA} are generating and pumping dispatches of the PSH plant and LMP_t^{DA} represnets the DA LMP. It can be seen that even with different settings of N, all the three PSH plants profit less in the DA compared with the benchmark model. This is expected since certain amount of energy has been reserved via the headroom and floor room for the RT use.

Table. G.2.3 DA revenue with different N settings ($).

N	PSH-1	PSH-2	PSH-3	Total
w/o	**153,701**	**96,522**	**67,273**	**317,497**
40%	150,300	96,474	67,530	314,304
30%	150,021	96,440	67,511	313,973
20%	148,971	94,711	66,584	310,267
10%	149,225	94,189	66,534	309,949
0%	147,772	93,506	63,684	304,963

RT schedule results are derived from two different RT market clearing simulation setups: hourly security-constrained economic dispatch (SCED) and 15-min SCED. As their names suggest,

hourly SCED has 1 hour time interval and 15-min SCED has 15 minutes time interval. That is, the latter has a high time resolution.

RT Result with hourly SCED

The DA+RT revenue results of the three PSH plants from hourly SCED are shown in Tables G.2.4-G.2.8, for the four cases under different *N* settings. The DA+RT revenue is calculated as Realized Profits = $\sum_{t=1}^{T} LMP_t^{DA} \cdot (g_t^{DA} - p_t^{DA}) + LMP_t^{RT} \cdot [(g_t^{RT} - p_t^{RT}) - (g_t^{DA} - p_t^{DA})]$, where g_t^{RT} and p_t^{RT} are generating and pumping dispatches of the unit in RT and LMP_t^{RT} represnets the RT LMP.

Table. G.2.4 DA+RT revenue with Normal load + Fixed PSH ($).

N	PSH-1	PSH-2	PSH-3	Total
w/o	**154,636**	**96,766**	**67,273**	**318,676**
40%	150,696	97,114	67,530	315,341
30%	150,146	96,591	67,511	314,249
20%	149,185	95,430	66,584	311,200
10%	149,373	94,366	66,534	310,273
0%	147,772	93,506	63,684	304,963

Table. G.2.5 DA+RT revenue with High load + Fixed PSH ($).

N	PSH-1	PSH-2	PSH-3	Total
w/o	**153,902**	**96,849**	**67,273**	**318,026**
40%	150,810	97,185	67,530	315,525
30%	150,428	97,094	67,511	315,034
20%	149,181	95,574	66,584	311,340
10%	149,412	94,446	66,534	310,393
0%	147,999	94,093	63,764	305,857

Table. G.2.6 DA+RT revenue with Normal load + Committable PSH ($).

N	PSH-1	PSH-2	PSH-3	Total
w/o	**154,958**	**98,310**	**67,353**	**320,623**
40%	154,431	99,270	67,610	321,312
30%	155,151	98,435	68,381	321,968
20%	154,741	97,939	67,289	319,970
10%	154,779	98,430	67,191	320,401
0%	156,149	96,367	67,802	320,319

Table. G.2.7 DA+RT revenue with High load + Committable PSH ($).

N	PSH-1	PSH-2	PSH-3	Total
w/o	**153,865**	**94,367**	**66,856**	**315,089**
40%	156,415	100,186	67,646	324,248
30%	154,974	97,976	68,711	321,662
20%	156,056	100,519	68,027	324,602
10%	156,630	99,274	68,249	324,153

0%	157,962	100,723	68,503	327,189

It can be seen that in the first three cases, all three PSH plants are hard to profit more compared to the benchmark model. In addition, generally, with a higher N, PSH plants are more likely to profit more. On the other hand, in the last case, all three PSH plants profit more. There are two main reasons. The headroom and floor room added in DA in fact reflect reserved flexibility of PSH plants. With the cases that consist of low DA-RT load discrepancy, the need of flexibility in RT would be limited. In addition, fixing commitment of PSH plants puts a restrict on exploiting the reserved flexibility. These two limits do not apply in the last case of High load + Committable PSH, leading to more profit to PSH plants.

Fig. G.2.2 show the DA and RT LMPs of the three PSH plants under the case of Normal load + Fixed PSH. Although PSH-1 and PSH-2 are two different plants, they are connected at the same Cpnode and share the same LMPs. From the profile of DA LMP, it can be seen that the case with N=0% leads to the highest LMP during hours of 9-12 (i.e., 1PM-4PM GMT) which are usually generating hours, while having the lowest LMPs during hours 1-3 (i.e., 5AM-7AM GMT) which are usually pumping hours. For models with N being 30%, 20%, and 10%, their LMPs at these time periods are between those of the model with N being 0% and the model without headroom/floor room. LMPs in RT deviate from those in DA but show the same pattern as described above. The difference in LMPs from DA to RT partially support the higher profits that PSH plants can achieve.

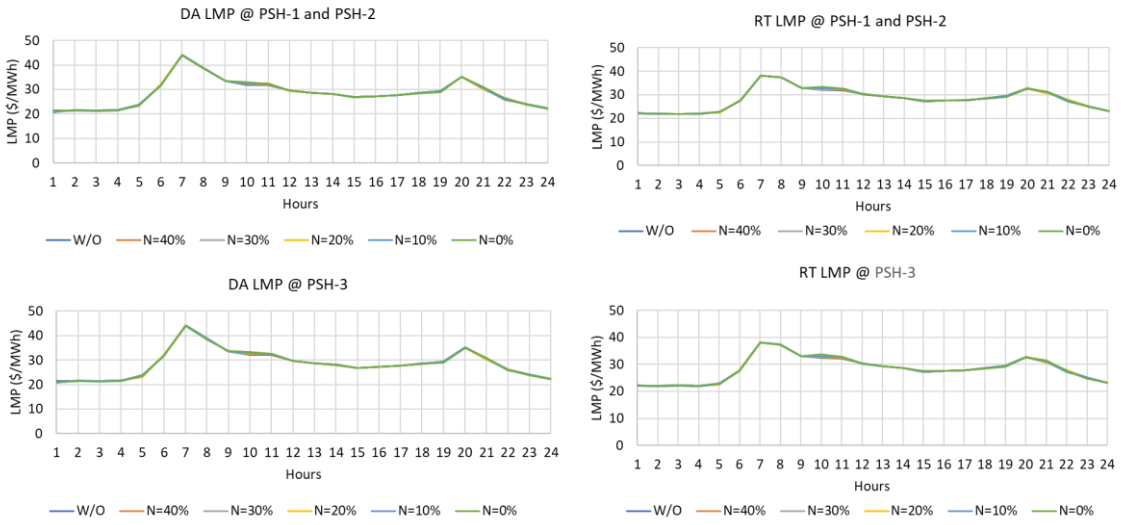

Fig. G.2.2 DA and RT LMPs of the three PSH plants for a sample day in spring 2019.

RT SOC curves of the three PSHs under the case of Normal load + Fixed PSH are respectively shown in Figs. G.2.3-G.2.5. Their DA SOC curves are also given in those figures. In Fig. G.2.3, with N going from high to low, PSH-1 in DA becomes more inactive, which agrees to the predicted impacts of headroom and floor room. This can also be observed on the other PSH plants as in Fig. G.2.4 and Fig. G.2.5, especially during hours approaching the end of the time horizon. SOC curves are arranged following the decreasing order of N. Particularly, from Fig. G.2.3, PSH-1with the case of N=0% is extremely inactive and almost does not pump at the beginning hours compared

to other models. This is because pumping can also contribute to $h_{s,t}^{LB}$, with the term of $p_t \cdot I_{s,t}^{P-O}$ under some extreme scenarios with $I_{s,t}^{P-O}$=1. In the case of PSH-1, the terminal SOC is set as a low value which forces $h_{s,t}^{LB}$ to be small; otherwise, infeasibility could occur. With the models of N being other than 0%, at least some extreme scenarios could be relaxed which allows pumping at the beginning hours. We can also see that RT SOC curves are very close to the DA ones, this is because: (i) the DA and RT load profiles are close and (ii) recommitment and decommitment in RT are not allowed which limits the change of PSH plants in RT. These two factors also contribute to the reduced profit compared to the benchmark model.

By contrast, as shown in Fig. G.2.6, RT SOC curves of the three PSH plants under the case of High load + Committable PSH are different from that of DA. One observation can be made here is that all curves with different N become very close to each other. This is because by allowing recommitment and decommitment, both dispatch and commitment of PSH plants will be adjusted in RT so that the system can achieve a lower objective. In RT, N no longer extensively affects the model of PSH plants, thus the optimal solution of PSH plants, even if unit commitments and dispatches of units other than PSH plants could still be different with different N. In summary, in the case of High load + Committable PSH, the extra wind fluctuation added into the RT load profile aggravates the deviation between DA and RT load profiles and requires more flexibility, while allowing recommitment and decommitment can fully release the reserved flexibility of PSHs. This enables a higher profit of PSH plants in the proposed models than the benchmark model.

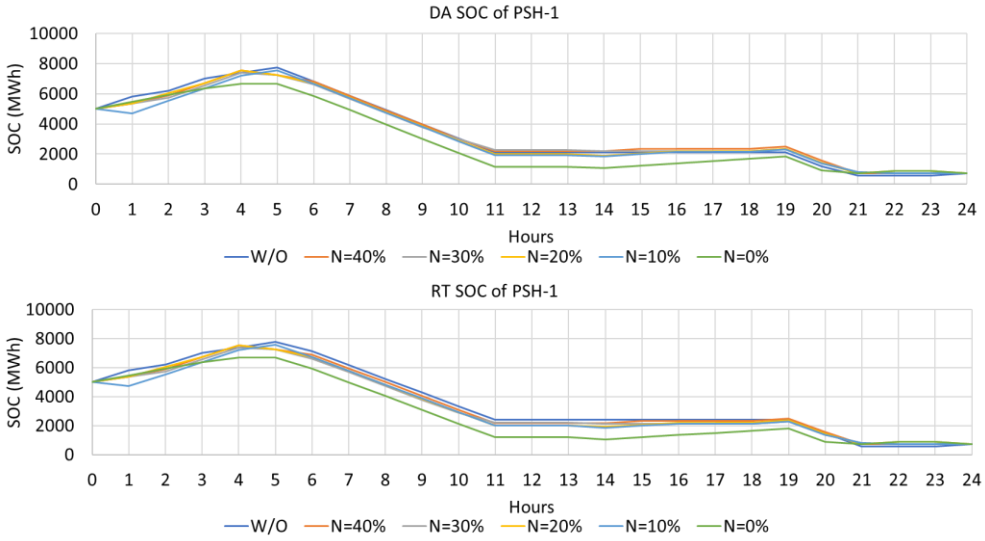

Fig. G.2.3 SOC of PSH-1 for a sample day in spring 2019.

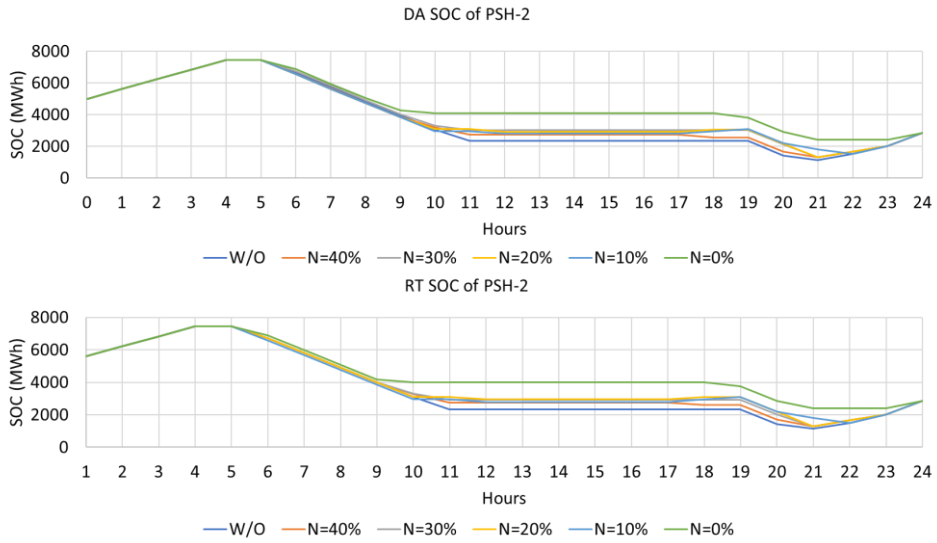

Fig. G.2.4 SOC of PSH-2 for a sample day in spring 2019.

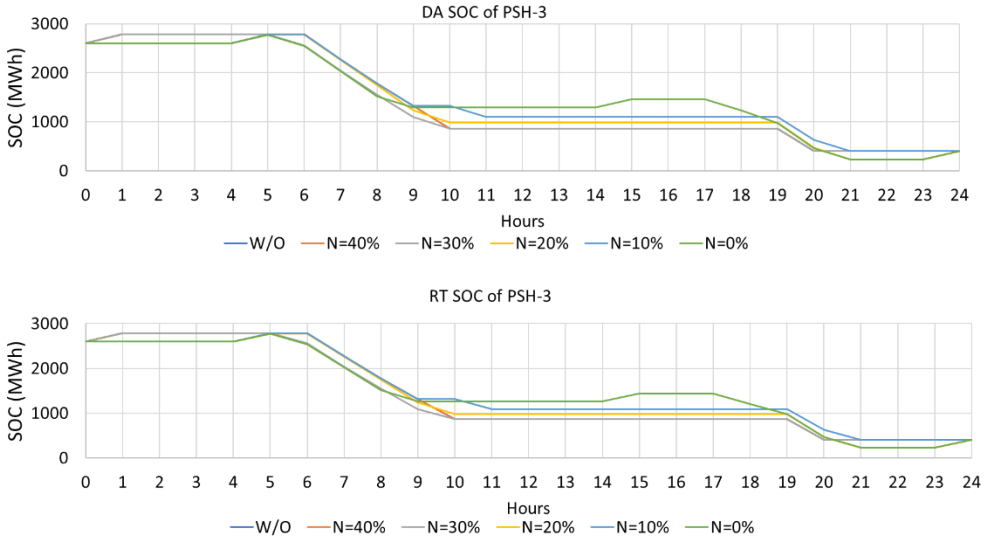

Fig. G.2.5 SOC of PSH-3 for a sample day in spring 2019.

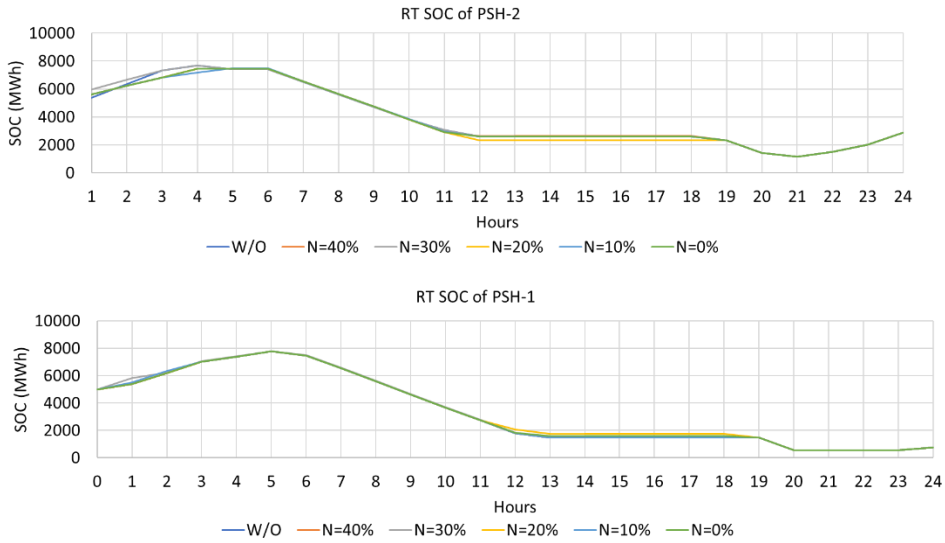

Fig. G.2.6 RT SOC of PSH-2 and PSH-1 in High load + Committable PSH for a sample day in spring 2019.

RT Result with 15min SCED

We further show the result with 15-min SCED under the case of Normal load + Fixed PSH and High load + Committable PSH. Generally, the similar observation as the hourly SCED can be made.

Table. G.2.8 DA+RT revenue with Normal load + Fixed PSH with 15-min SCED ($).

N	PSH-1	PSH-2	PSH-3	Total
w/o	**154,447**	**96,749**	**67,273**	**318,471**
40%	150,765	96,955	67,530	315,252
30%	150,201	96,662	67,512	314,376
20%	149,292	95,307	66,587	311,186
10%	149,627	94,388	66,535	310,551
0%	148,144	93,845	63,753	305,743

Table. G.2.9 DA+RT revenue with High load + Committable PSH with 15-min SCED ($).

N	PSH-1	PSH-2	PSH-3	Total
w/o	**156,049**	**94,438**	**67,356**	**317,844**
40%	156,425	96,042	68,188	320,656
30%	156,989	96,239	68,955	322,184
20%	156,984	97,893	68,894	323,772
10%	155,625	97,527	69,280	322,433
0%	156,973	97,330	68,710	323,014

Fig. G.2.7 compares RT LMPs from the 15-min SCED with DA LMPs and that from hourly SCED. It can be seen that DA LMP and RT LMP profiles are close except for some peak hours. RT LMPs from 15-min SCED and hourly SCED are rather close, and the former is smoother that

the latter because of the smoother load profile. In addition, SOC curves from 15-min SCED and hourly SCED are also very close, as shown in Fig. G.2.8 and Fig. G.2.9. As a conclusion, with the tested cases, 15-min SCED and hourly SCED do not show significant differences worth taking note of.

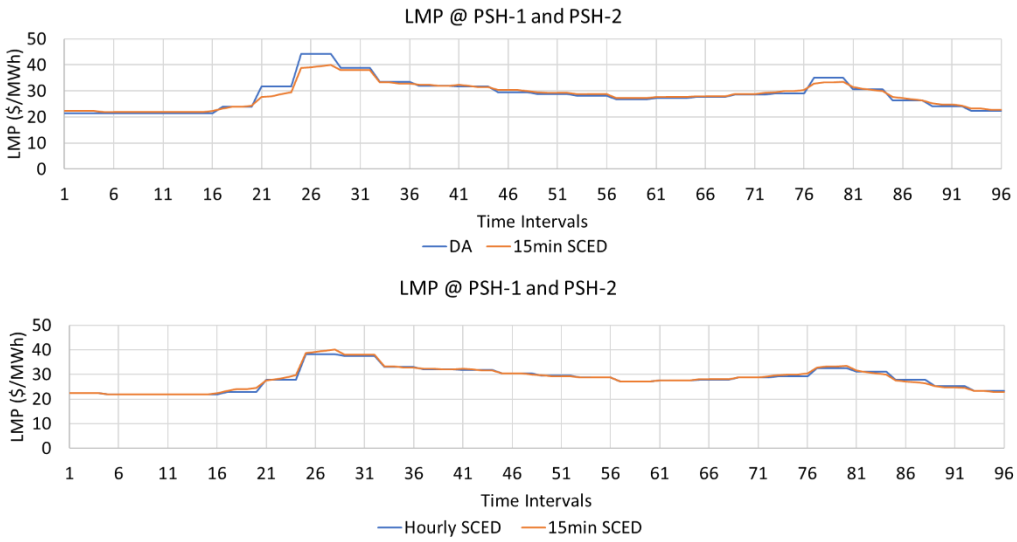

Fig. G.2.7 RT LMP comparison of PSH-1 and PSH-2 with 15-min SCED for a sample day in spring 2019.

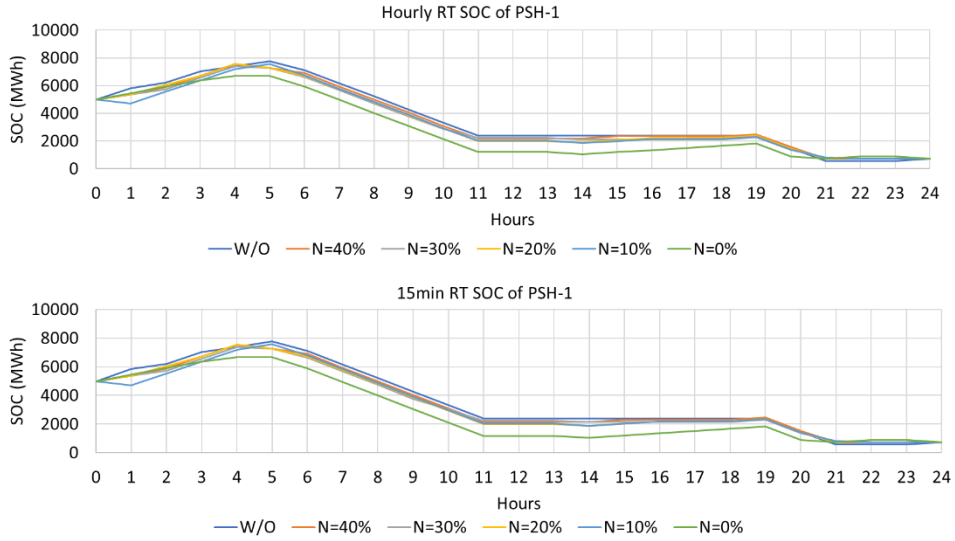

Fig. G.2.8 SOC comparison of PSH-1 with 15-min SCED for a sample day in spring 2019.

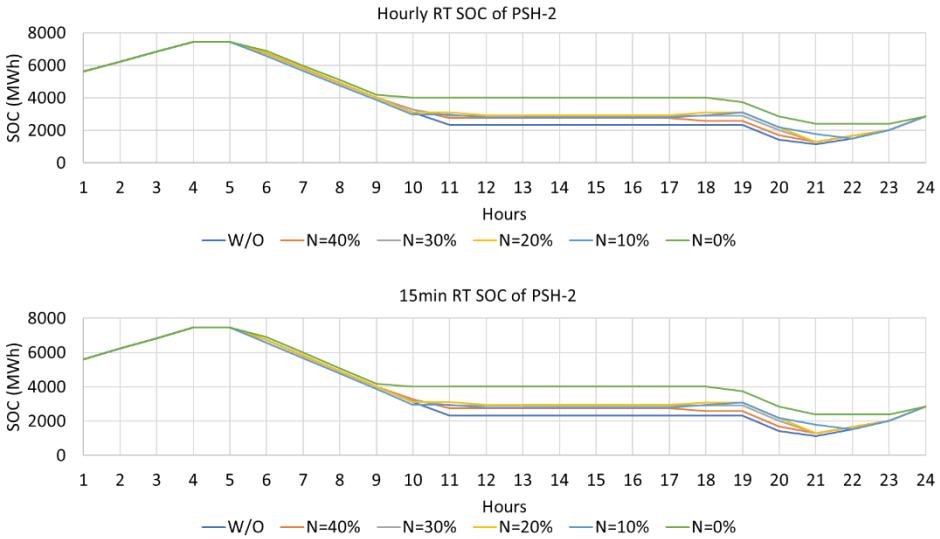

Fig. G.2.9 SOC comparison of PSH-2 with 15-min SCED for a sample day in spring 2019.

IV.G.3 ADP-based approach for evaluating the value of water outside a finite time horizon

In this section, we discuss an ADP-based approach to generate price-SOC curves which could be used in FRAC and LAC models while considering the value of water outside the finite time horizon. Specifically, we formulate an optimization model for PSHs in maximizing its arbitrage profit in the electricity market. We simulate the energy storage operation as a Markov decision process (MDP) and generate the reward function/value function, which reflects the profit from real-time LMPs and generating/pumping actions. We also derive an ADP algorithm to maximize the cumulative reward.

Dynamic programming/reinforcement learning is a general sequential model to take actions/ decisions and gain the maximum reward for the whole-time horizon. This model can benefit the exploitation and exploration. In our study, the optimal strategy will balance the profits based on the decision to generate and pump now and the opportunity profit based on the water stored for the future. Here we start from the context of classical dynamic programming in our PSH model.

State Space:
The whole model is a dynamic system that evolves in periods $t = 1, 2, \cdots, T, T+1$ and its evolution is influenced by actions[7]. At each time t, the system is characterized by state variables. The state space can also be named as the set of environment or agent states. Since the PSH can be considered as a particular case of the storage problem, we define the state space as $S_t = (R_t, W_t) \in \mathcal{S}$, where R_t is the terminal SOC at time $t-1$ and W_t is the forecasted real-time price LMP_t of time t, $\forall t = 1, \dots, T$. This means our state has two elements: The first one is the stored amount of water R_t, and the second is the market price W_t. We can treat R_t as an endogenous variable, which comes from the system itself (i.e., PSH). Variable W_t is the exogenous variable, which comes from the outside of this system.

[7] This section adopts hourly real-time price forecasts from section IV.E of the study, and therefore *t* takes the value of 1 to 24 with one-hour time step.

Action/Decision Space:
At each time t, we decide on some actions (decisions) x_t, and these actions must be chosen from a finite set $\mathcal{X}_t(S_t)$. Here the action is to decide the amount of energy change, i.e., the amount we generate or pump. We know that the action/decision at time t depends on the current system state, i.e., the terminal SOC at time $t-1$ and the price at current time t. In other words, we choose the decision based the varying of the current SOC and the current market price. We denote our action variable as $x_t = (p_t, g_t) \in \mathcal{X}_t(R_t, W_t)$, where p_t/g_t is the pump/gen amount at time t, $\forall t = 1, \dots, T$.

Transition function:
The transition function at time t is to describe the probability of transferring from one state at time t to another state at time $t+1$ under a given action. This process can be considered as a Markov decision process. Let us denote $S_{t+1} = f_t(x_t, S_t)$, where the $S_t = (R_t, W_t)$ is the current state at time t, $S_{t+1} = (R_{t+1}, W_{t+1})$ is the state at time $t+1$, and x_t is the action taken at time t. From time t to $t+1$, R_{t+1} is equals to the terminal SOC at time t, i.e., $R_{t+1} = R_t - g_t/\eta^g + p_t * \eta^p$, which η^p/η^g is the efficiency of pumping/generation. Also, we have $W_{t+1} = W_t + \widehat{W_t}$, where $\widehat{W_t}$ is the deviation of the market price from time t to time $t+1$.

Reward function:
The reward function is also referred to as cost function, which means the reward/cost based on the current action. Here we denote $C_t(x_t, S_t) = W_t(g_t - p_t)$, $\forall t = 1, \dots, T$. It means that after we decide the amount of energy generation/pumping based on the price W_t, we have the profit $W_t(g_t - p_t)$. If we consider this system for a whole day, the total reward is represented by $G_1 = \sum_{t=1}^{24} c_t = \sum_{t=1}^{24} W_t(g_t - p_t)$.
Therefore, we can have the following optimization problem as our goal:

$$\max_{x_1 \in \mathcal{X}_1} [C_1(S_1, x_1) + \mathbb{E}[\max_{x_2 \in \mathcal{X}_2} C_2(S_2, x_2) + \cdots + \mathbb{E}[\max_{x_T \in \mathcal{X}_T} C_T(S_T, x_T)]]] \quad \text{(G.3.1)}$$

Bellman equation/Value function:
The essential notion in dynamic programming is the value function $V_t(x_t)$. The value function is defined as the expected return starting with state $S_t = S_0$, and successively following a policy π.

$$V_t(S_t) = \max_{x_t} \{C_t(S_t, x_t) + \mathbb{E}[V_{t+1}(S_{t+1}^*)]\} \quad \text{(G.3.2)}$$

It is the maximum profit of operating the system in periods $t = 1, \dots, T$, under the condition that it starts from state x_t at time t. By definition, $V_{T+1}(x_{T+1}) = 0$. The value function describes how good is to be in a specific state if we consider taking one series of policies.

Approximate Dynamic Programming
Based on the Bellman equation we have, we can have a linear approximate to our reward from the future, which is shown as follows:

$$V_t(S_t) = \max_{x_t, y_{r,t}} \mathbb{E}\{C_t(S_t, x_t) + V_{t+1}(S_{t+1}^* | W_t)\} = \mathbb{E}\left[\max_{x_t, y_{r,t}} \left[C_t(S_t, x_t) + \sum_{r=1}^{R} v_{r,t} y_{r,t}\right]\right] \quad \text{(G.3.3)}$$

while $\max_{x_t, y_{r,t}} \left[C_t(S_t, x_t) + \sum_{r=1}^{R} v_{r,t} y_{r,t}\right]$ equals to the following optimization problem:

$$\max_{p_t, g_t, y_t} W_t(g_t - p_t) + \sum_{r=1}^{R} v_{r,t} y_{r,t}$$
$$0 \le g_t \le \overline{G}$$
$$0 \le p_t \le \overline{P}$$
$$e_{t-1} - \frac{g_t}{\eta^g} + p_t * \eta^p = e_t$$
$$e_t = \sum_{r=1}^{R} y_{r,t}$$
$$\underline{E} \le e_t \le \overline{E}$$
$$-(T - t_0)\overline{P}\eta^p \le e_t - E_T \le (T - t_0)\,\overline{G}/\eta^g \qquad \text{(G.3.4)}$$

This optimization problem aims to maximize the PSH profit by generating when prices are high and pumping at low prices. The first and the second constraints limit the range of pumping and generation; The third constraint describes the water storage change from time $t-1$ to time t, with respect to the generation/pumping decisions g_t and p_t at stage t; The fourth constraint is the energy at the end of time t by our linear approximation, which leverages how much to generate/pump in the current time and what SOC level to be held for the future; The fifth constraint describes the energy storage limit; The last constraint is the terminal boundary constraint, making g sure we have a feasible result by the end of the scheduling day.

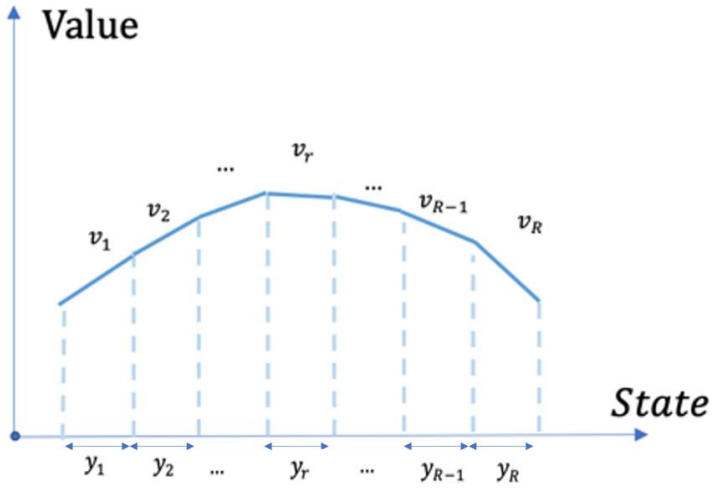

Fig. G.3.1 SOC-Value curve trained by ADP.

Here we illustrate the linear approximation curve. Fig. G.3.1 shows the linear approximation $V = \sum_{r=1}^{R} v_r y_r$ which maps the state space to the value function space. In this linear approximation, we consider v_r as the slope of the curve and y_r as the segment values for $r = 1, \dots R$. Based on the curve parameters, the linear approximation builds the relationship between the $SOC = y$ and the profit V under this water storage. For example, if we take the segment points as $y_r = [0,100,200], r = 1,2,3$, and the corresponding curve slopes as $v_r = [2,1,-3]$, for a given value of current SOC $y = 150$, we can get the value function for this SOC as $V = 2 * 100 + 1 * 50 = 250$.

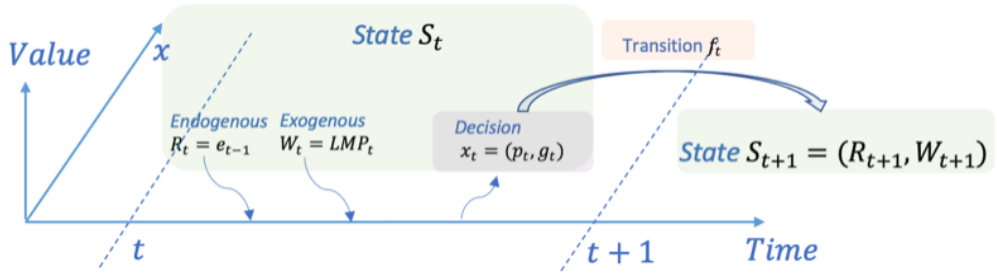

Fig. G.3.2 Transition process for ADP.

Fig. G.3.2 further illustrates how this sequential model works, primarily focusing on time t to time $t+1$. We build the x-axis for the state space, the T-axis for time, and the V-axis for the return of the value function. For each period t, the amount R_t as water storage from the last time period and the price for time t are inputs. After the algorithm run for this iteration, the optimal decision $x_t = \{g_t, p_t\}$ can be used to calculate $R_{t+1} = R_t - g_t/\eta^g + p_t * \eta^p$ as input for the next period $t+1$.

SPAR Algorithm

We choose the separable, projective approximation routine (SPAR) Algorithm to support us calculating the parameters of the curves [G.1]. This method turns the previous model from the dynamic programming problem into a machine learning problem. We use multiple scenarios of historical market prices to train our model so that we can have a fitted curve. The detail of the algorithm is as follows:

Initialize the model:

1) Set up the initial segment ending point values S_t for $t = 0, .., T-1$. We evenly divide the entire SOC range $[\underline{E}, \overline{E}]$ into 100 segments, and take these segment ending points to initialize each set of S_t.
2) Initialize slopes v_t^0 for $t = 0, .., T-1$. These values shall be monotone increasing to ensure the convexity.

For $n = 1, \ldots, N$(N is the total number of scenarios)

1) Observe the information from historical data $W_0^n, \ldots, W_T^n$
2) For $t = 0, .., T-1$
   - Step1: Find the optimal solution x_t^n and state S_t^n
   - Step2: Update slope curve/value function for time t :
     - Achieve the current slope curve $\hat{v}_{t+1}^n(\mathrm{r})$ for $r = 1, .., R$
     - Construct the new slope curve by
       - $z_t^n(r) = (1-\alpha)\bar{v}_t^{n-1}(\mathrm{r}) + \alpha\hat{v}_{t+1}^n(\mathrm{r})$
     - Observe two slopes/points $\hat{v}_{t+1}^n(S_t^{x,n})$ and $\hat{v}_{t+1}^n(S_t^{x,n} + \rho)$
     - Update the slopes by concave principle with two points $\bar{v}_t^n(\mathrm{r}) = \Pi_C(z_t^n)$

Fig. G.3.3 Pseudo codes for the SPAR algorithm.

From the algorithm, in each iteration/scenario, the first step is to find the optimal solution of the optimization model with the given curve v_t and the given historical data w_t at time t. The second step is to update our value function- state curve, which represents the relation between the water storage and the value function (i.e., as shown in Fig. G.3.4). The key for this step is to update the

current curve based on the future profits calculated out of this iteration. At the same time, we shall keep the curve's concavity to ensure convergence. Figure G.3.4 illustrates the iterative updates of the curve slopes. We can consider the blue as an old curve, and we have the orange curve as the new one under the update steps in Fig. G.3.3.

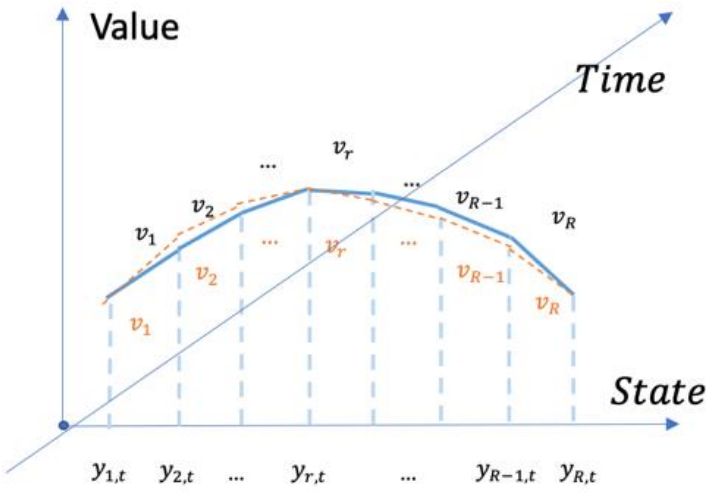

Fig. G.3.4 The iteration of SOC-Value Curve trained by ADP.

Numerical result for one-hour look-ahead PSH profit

In this section, we show the numerical result of one-hour-ahead PSH profit. We choose four different days' DA prices and forecast prices, one in March 2019 and three in April 2019 (which are referred to as D1, D2, D3, and D4 in this tudy). The day-ahead and 50 scenarios forecast prices are used to train in the ADP algorithm. Then we apply the trained SOC-price curve to help predict the one-hour look-ahead PSH profit based on the RT price.

All the numerical results are compared with the result of the rolling model, the day head, and real-time's optimization results.

The first numerical result is based on the D1 data set. This training data set contains the day ahead price and the 50 scenarios real forecast price only on D1. Table G.3.1 shows the final profit results of the four days using the trained curve of D1. It shows that the ADP algorithm gives the profit of $14,385.20 on D1, which is better than the rolling and DA models. The ADP model also shows better performance on D2 and D4, but gives less profit than the rolling model on D3.

Table G.3.1 Profit Comparison based on the trained curve of March 07th, 2009.

Prediction	D1	D2	D3	D4
ADP	$14,385.20	$14,530.62	$5,109.75	$13,872.76
RT	$17,017.01	$16,270.65	$8,294.46	$18,734.72
Rolling	$11,334.57	$10,666.31	$6,784.00	$12,863.84
DA	$10,976.77	$9,026.81	$6,743.30	$10,198.84

The second numerical result is based on the D2 data set. This training data set contains the day ahead price and the 50 scenarios real forecast price only on D2. Table G.3.2 shows the final profit results of the four days using the trained curve of D2. We can see from the table that the ADP algorithm gives a profit of $14,630.49 on D2, which is better than the rolling and DA models. The ADP model still shows better performance on D1 but gives slightly lower profits on D3 and D4. When the information of the training day and the testing days are similar, it can provide good performance; Otherwise, less profit might be expected.

Table G3.2 Profit Comparison based on the trained curve of April 01st, 2009.

Prediction	D1	D2	D3	D4
ADP	$15,261.03	$14,630.49	$6,395.11	$12,754.24
RT	$17,017.01	$16,270.65	$8,294.46	$18,734.72
Rolling	$11,334.57	$10,666.31	$6,784.00	$12,863.84
DA	$10,976.77	$9,026.81	$6,743.30	$10,198.84

The third numerical result is based on the D3 data set. This training data set contains the day ahead price and the 50 scenarios real forecast price on D3. Table G.3.3 shows the final profit results of the four days using the trained curve of D3.We can see the ADP algorithm gives the profit $7,640.57 on D3, which is higher than the rolling model. When we have the data set of the same day on D3, this gives a better result in the ADP method.

Table G.3.3 Profit Comparison based on the trained curve of April 15th, 2009.

Prediction	D1	D2	D3	D4
ADP	$15,129.48	$13,877.79	$7,640.57	$788.15
RT	$17,017.01	$16,270.65	$8,294.46	$18,734.72
Rolling	$11,334.57	$10,666.31	$6,784.00	$12,863.84
DA	$10,976.77	$9,026.81	$6,743.30	$10,198.84

The fourth numerical results are based on the D4 data set. This training data set contains the day ahead price and the 50 scenarios real forecast price on D4. Table G.3.4 shows the final profit results of the four days using the trained curve of D4. The trained data set from D4 only gives us almost the same result on DA but less than the profit of the rolling model. This shows the data set only contains one day may not be sufficient for certain cases and a larger data set might be needed.

Table G.3.4 Profit Comparison based on the trained curve of April 22nd, 2009.

Prediction	D1	D2	D3	D4
ADP	$15,143.50	$15,490.90	$6,714.35	$10,162.90
RT	$17,017.01	$16,270.65	$8,294.46	$18,734.72
Rolling	$11,334.57	$10,666.31	$6,784.00	$12,863.84

DA	$10,976.77	$9,026.81	$6,743.30	$10,198.84

The last numerical result is based on the data set including all four days, i.e., this training data set contains the day ahead price and the 50 scenarios real forecast price on D1-D4. Table G.3.5 shows the final profit results of the four days using the trained curve from all four-day data. When we combine the scenarios of all four days, the result becomes more robust (i.e., consistent performance over multiple testing days). We can have a better result on all these four days than the DA model. Also, we have a better performance than the rolling model on D1, D2, and D3. This shows when the training set has more data, the ADP model becomes more robust and accurate.

Table G.3.5 Profit Comparison based on the trained curve based on all four days

Prediction	D1	D2	D3	D4
ADP	$15,661.79	$13,197.94	$6,827.14	$12,403.79
RT	$17,017.01	$16,270.65	$8,294.46	$18,734.72
Rolling	$11,334.57	$10,666.31	$6,784.00	$12,863.84
DA	$10,976.77	$9,026.81	$6,743.30	$10,198.84

From previous numerical studies, we can see that the same-day data set significantly impacts the ADP result. On D2 and D3, with the same day data set, it gives a better result than the model without the same day data set. We can also learn that other days' data set can robust the result. On D4, the training models without the same-day data set have a good prediction (Table G.3.1, Table G.3.2, Table G.3.4), while a significant decrease is observed in Table G.3.3. When we have the four dates' data set in Table G.3.5, a good result has been preserved. For instance, for March 07th, 2009, the outcomes in Tables G.3.1-G.3.4 show robust performance, nevertheless the outcome based on all four days in Table G.3.5 has the best performance. In conclusion, the same-day data set firmly impacts the performance, and the more extensive data set could lead to a more robust result. Since most calculation burdens are moved to the training stage and the online calculation with the trained SOC-price curve is rather light, this approach could be applied to solve FRAC and LAC models while considering the uncertain value of water outside the finite time horizon.

References

[G.1] An optimal approximate dynamic programming algorithm for the economic dispatch problem with grid-level storage, Juliana M. Nascimento and Warren B. Powell, IEEE Transactions on Automatic Control, 2013

IV.H. Accomplishments Toward Deliverable 9.1

Deliverable 9.1: A detailed report on long-term value of enhanced PSH model through planning analyses.

Accomplishments Summary: (1) The team developed a stochastic optimization approach for economic planning studies. In detail, A linear program based approximated model is first used to approximate the nonconvex unit commitment model to accelerate the solution of stochastic

production cost simulation models. Test results using a MISO planning model show acceptable accuracy and significant solution time improvement from our proposed approach. (2) We also further explored a stochastic transmission expansion planning method in a test case, with the same approximation strategy together with a decomposition framework. (3) Long-term production cost simulation was performed on MISO planning cases and results showed enhanced PSH optimization can reduce load cost and in some cases increase CO_2 emission.

IV.H.1 Explore stochastic unit commitment for planning

Accelerating stochastic production cost simulation

Conventionally, deterministic unit commitment (UC) models have been considered in economic planning. With the increasing penetration of intermittent resources, deterministic approaches might cause conservative unit commitment solutions to meet system security requirements. Stochastic optimization is a promising alternative to hedge against uncertainties. However, incorporating stochastic unit commitment for planning will bring significant computational challenges. Furthermore, the time-coupled nature of pumped storage hydro facilities, which is reflected in state-of-charge evaluation and status switching logic modeling, complicates the system operation simulations. However, as a critical enabler in the pathway to a low-carbon sustainable future, to accurately reflect the features of storage and efficiently solve the resulting stochastic production cost simulation models are urgently needed.

In the current industry practice, typically a large number of production cost simulations run for a combination of scenarios and candidate planning schemes. However, only limited combinations can be enumerated given a long computational time for production cost simulations. With accelerations in solution strategies, we developed a stochastic production cost simulation method for economic planning with detailed UC constraints, as shown in (H.1.1). $\mathbf{y}_s$ represents unit commitment and economic dispatch decision variables in scenario s. $\mathbf{b}_s$ contains cost coefficients for production cost simulation. p_s is the probability for scenario s. $\Omega_s^{\mathrm{UC}}(\mathbf{x})$ is the feasible region of UC constraints given planning decisions $\mathbf{x}$. An illustrative figure for our modeling framework is shown in Fig. H.1.1.

$$\begin{aligned} &\min \textstyle\sum_{s\in S} \mathrm{p}_s \cdot \left(\mathbf{b}_s{}^{\top} \mathbf{y}_s\right) \\ &\text{s.t.} \quad \mathbf{y}_s \in \Omega_s^{\mathrm{UC}}(\mathbf{x}) \end{aligned} \tag{H.1.1}$$

To address the computational complexity of stochastic transmission expansion planning problem with UC model, solution techniques based on unit commitment approximation will be evaluated. High-quality convex approximations for the underlying unit commitment models are expected to preserve the flexibility quantification quality, meanwhile simplify the nonconvex mixed-integer formulation. Mathematically, we use $\mathbf{y}_s \in \tilde{\Omega}_s^{\mathrm{UC}}(\mathbf{x})$ to approximate the UC constraints in (H.1.1), where $\tilde{\Omega}_s^{\mathrm{UC}}(\mathbf{x})$ is a polyhedron approximation of $\Omega_s^{\mathrm{UC}}(\mathbf{x})$.

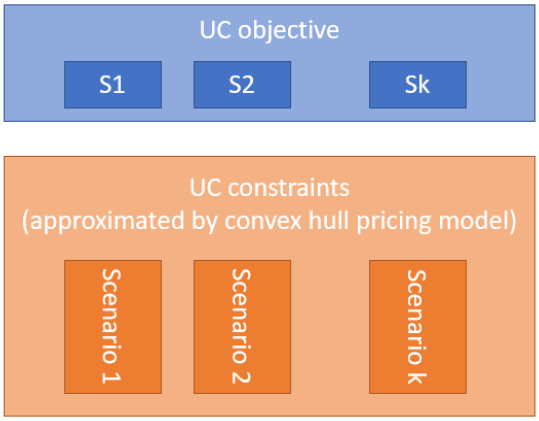

Fig. H.1.1. modeling framework for stochastic production cost simulations

As shown in (H.1.2), the generators are modeled using a tight formulation in [H.1, H.2], which considers a two-time-period convex hull of a UC model. Note the variables in (H.1.2) are continous.

$$
\begin{aligned}
&\gamma_{g,s,t} \geq \alpha_g^k p_{g,s,t} + \beta_g^k x_{g,s,t} \quad \forall k = 1,\ldots,K, \forall g \in \mathcal{G}, \forall s \in \mathcal{S}, \forall t \in \mathcal{T} \\
&u_{g,s,t} \geq x_{g,s,t} - x_{g,s,t-1} \quad \forall g \in \mathcal{G}, \forall s \in \mathcal{S}, \forall t \in \mathcal{T} \\
&x_{g,s,t-1} + u_{g,s,t} \leq 1 \quad \forall g \in \mathcal{G}, \forall s \in \mathcal{S}, \forall t \in \mathcal{T} \\
&u_{g,s,t} \leq x_{g,s,t} \quad \forall g \in \mathcal{G}, \forall s \in \mathcal{S}, \forall t \in \mathcal{T} \\
&\sum_{i=t-UT_g+1}^{t} x_{g,s,t} \leq u_{g,s,t} \quad \forall g \in \mathcal{G}, \forall s \in \mathcal{S}, \forall t \in \mathcal{T} \\
&\sum_{i=t-DT_g+1}^{t} x_{g,s,i} \leq 1 - u_{g,s,t-DT_g} \quad \forall g \in \mathcal{G}, \forall s \in \mathcal{S}, \forall t \in \mathcal{T} \\
&x_{g,s,t} \underline{p}_g \leq p_{g,s,t} \leq x_{g,s,t} \overline{p}_g \quad \forall g \in \mathcal{G}, \forall s \in \mathcal{S}, \forall t \in \mathcal{T} \\
&p_{g,s,t-1} \leq \overline{v}_g x_{g,s,t-1} + \left(\overline{p}_g - \overline{v}_g\right)\left(x_{g,s,t} - u_{g,s,t}\right) \quad \forall g \in \mathcal{G}, \forall s \in \mathcal{S}, \forall t \in \mathcal{T} \\
&p_{g,s,t} \leq \overline{p}_g x_{g,t} - \left(\overline{p}_g - \overline{v}_g\right) u_{g,t} \quad \forall g \in \mathcal{G}, \forall s \in \mathcal{S}, \forall t \in \mathcal{T} \\
&p_{g,s,t} - p_{g,t-1} \leq v_g x_{g,s,t-1} + \overline{v}_g \left(1 - x_{g,s,t-1}\right) \quad \forall g \in \mathcal{G}, \forall s \in \mathcal{S}, \forall t \in \mathcal{T} \\
&p_{g,s,t} - p_{g,s,t-1} \leq \left(\underline{p}_g + v_g\right) x_{g,s,t} - \underline{p}_g x_{g,s,t-1} - \left(\underline{p}_g + v_g - \overline{v}_g\right) u_{g,s,t} \quad \forall g \in \mathcal{G}, \forall s \in \mathcal{S}, \forall t \in \mathcal{T} \\
&p_{g,s,t-1} - p_{g,s,t} \leq \overline{v}_g x_{g,s,t-1} - \left(\overline{v}_g - v_g\right) x_{g,s,t} - \left(\underline{p}_g + v_g - \overline{v}_g\right) u_{g,s,t} \quad \forall g \in \mathcal{G}, \forall s \in \mathcal{S}, \forall t \in \mathcal{T} \\
&0 \leq x_{g,s,t}, u_{g,s,t} \leq 1 \quad \forall g \in \mathcal{G}, \forall s \in \mathcal{S}, \forall t \in \mathcal{T}
\end{aligned}
\tag{H.1.2}
$$

where, $x_{g,s,t}$ and $u_{g,s,t}$ are commitment and start-up variables for unit g in scenario s and time t. $\gamma_{g,s,t}$ is the cost for unit g, which is piecewise approximated by $\alpha_g^k p_{g,s,t} + \beta_g^k x_{g,s,t}$ with K pieces.

$\overline{p}_g$, $\underline{p}_g$, v_g , $\overline{v}_g$ are capacity, minimum stable level, ramp rate, and start-up/shut-down ramp rate, respectively. UT_g and DT_g are minimum online and offline time periods, respectively.

It should be point out that for the formulation in (H.1.2) is a genral formulation for generator modeling. We did some simplification on (H.1.2) in detailed inplemnetation to reduce the number of variables and constraints. For example, some hydro genrators with zeros start-up cost, zeros minimun stable levels, and very quick ramp rates, we can model them with simple economic dispatch models like $0 \le p_{g,s,t} \le \overline{p}_g, \forall g \in \mathcal{G}, \forall s \in \mathcal{S}, \forall t \in \mathcal{T}$.

Pumped storage hydro stations are modeled in (H.1.3). The SOC formulation that we use here is a tight formulation developed in previous tasks of this project [H.3].

$$
\begin{aligned}
&\underline{P}_h^{\mathrm{g}} \cdot x_{h,s,t}^{\mathrm{g}} \le p_{h,s,t}^{\mathrm{g}} \le \overline{P}_h^{\mathrm{g}} \cdot x_{h,s,t}^{\mathrm{g}} \quad \forall h \in \mathcal{H}, \forall s \in \mathcal{S}, \forall t \in \mathcal{T} \\
&\underline{P}_h^{\mathrm{p}} \cdot x_{h,s,t}^{\mathrm{p}} \le p_{h,s,t}^{\mathrm{p}} \le \overline{P}_h^{\mathrm{p}} \cdot x_{h,s,l}^{\mathrm{p}} \quad \forall h \in \mathcal{H}, \forall s \in \mathcal{S}, \forall t \in \mathcal{T} \\
&x_{h,s,t}^{\mathrm{g}} + u_{h,s,t}^{\mathrm{p}} \le 1 \quad \forall h \in \mathcal{H}, \forall s \in \mathcal{S}, \forall t \in \mathcal{T} \\
&e_{h,s,t} = e_{h,s,t-1} - \frac{1}{\eta^{\mathrm{g}}} p_{h,s,t}^{\mathrm{g}} \cdot \Delta t + \eta^{\mathrm{p}} p_{h,s,t}^{\mathrm{p}} \cdot \Delta t \quad \forall h \in \mathcal{H}, \forall s \in \mathcal{S}, \forall t \in \mathcal{T} \\
&\underline{E}_h + \eta^{\mathrm{p}} p_{h,s,t}^{\mathrm{p}} \cdot \Delta t \le e_{h,s,t} \le \overline{E}_h - \frac{1}{\eta^{\mathrm{g}}} p_{h,s,t}^{\mathrm{g}} \cdot \Delta t \quad \forall h \in \mathcal{H}, \forall s \in \mathcal{S}, \forall t \in \mathcal{T} \\
&0 \le x_{h,s,t}^{\mathrm{g}}, x_{h,s,t}^{\mathrm{p}} \le 1 \quad \forall h \in \mathcal{H}, \forall s \in \mathcal{S}, \forall t \in \mathcal{T}
\end{aligned}
\tag{H.1.3}
$$

where, $x_{h,s,t}^{\mathrm{g}}$ and $x_{h,s,t}^{\mathrm{p}}$ are status variables for generating and pumping statuses of PSH station h in scenario s and time t. $\overline{P}_h^{\mathrm{g}}$ and $\overline{P}_h^{\mathrm{p}}$ are generating and pumping capacities, respectively. $\underline{P}_h^{\mathrm{g}}$ and $\underline{P}_h^{\mathrm{p}}$ are minimum stable levels for generating and pumping modes, respectively. $e_{h,s,t}$ is SOC of PSH upper reservoir of station h in scenario s and time t. $\overline{E}_h$ and $\underline{E}_h$ are upper and lower bounds for reservoir of station h, respectively.

Given the constraints in (H.1.2) and (H.1.3) are linear, they form set $\tilde{\Omega}_s^{\mathrm{UC}}(\mathbf{x})$. The objective function is the sum of investment and operation cost, as shown in (H.1.4). Note PSH units are assumed to be operated by ISOs, thus their bidding and offering curves are not modeled in the objective function.

$$
\sum_{\forall s \in \mathcal{S}} \sum_{\forall t \in \mathcal{T}} \sum_{g \in \mathcal{G}} \left(\gamma_{g,s,t} + CST_g u_{g,s,t} \right) \tag{H.1.4}
$$

where, CST_g is the start-up cost for generator g.

A MISO planning model is used to evaluate the performance of approximation quality and solution time of our proposed stochastic production cost simulation approach. We notice the problem is naturally decoupled for each scenario. Thus, production cost simulations are run separately for each scenario first; the expected cost is then evaluated with (H.1.4). The tested system contains all the generators in the eastern interconnection. We run a simulation with 5

stochastic scenarios for 7 days in a transmission unconstrainted case. All the optimization problems are solved by using Gurobi 8.0.1. MILP gap is set as 0.5%.

The overall performance is summarized in Table H.1.1. As indicated, the expected cost values from MILP unit commitment model (denote as "MILP UC" in tables and figures hereafter) and LP relaxation model (denote as "LP approximation" in tables and figures hereafter) are very close. The two expected objective values have only a small difference of 0.35% in percentage. In terms of the solution time, the LP relaxation model can result in a significant time reduction of 71.6%. In detail, a performance comparison for each scenario is summarized in Table H.1.2. As indicated, the expected cost values from MILP unit commitment model and LP relaxation approximation model are also very close. We also see significant time reductions in all the scenarios.

Table H.1.1. Overall objective value and solution time comparison

	Objective Value ($10^{8})			CPU time (sec)		
	MILP UC	LP approx.	Difference in Percentage	MILP UC	LP approx.	Time Reduction in Percentage
Stochastic production cost simulation	8.935	8.904	0.35%	17174.1 (or 4.771 hours)	4873.8 (or 1.354 hours)	71.6%

Table H.1.2. Objective value and solution time comparison for each scenario

Scenario	Objective Value ($10^{8})			CPU time (sec)		
	MILP UC	LP approx.	Difference in Percentage	MILP UC	LP approx.	Time Reduction in Percentage
Base case scenario	8.923	8.892	0.35%	3092.4	961.5	68.9%
Case 1 scenario	11.721	11.687	0.29%	2855.9	731.1	74.4%
Case 2 scenario	10.306	10.271	0.34%	3344.5	711.4	78.7%
Case 3 scenario	6.267	6.241	0.43%	4170.9	1480.0	64.5%
Case 4 scenario	7.574	7.545	0.38%	3710.4	989.9	73.3%

In Fig. H.1.2 and Fig. H.1.3, detailed generation levels for all types of generators are shown for MILP unit commitment model and LP relaxation approximation model, respectively. As indicated, for each type, the patterns of total generation levels in two models are also very close. SOC levels of all PSH stations for MILP unit commitment model and LP relaxation approximation

model are shown in Fig. H.1.4 and Fig. H.1.5, respectively. For each PSH station, the patterns of SOC levels in two models are also similar. Taking one of the PSH station as an example, as shown in Fig. H.1.6, its SOC levels in two models generally have a similar pattern. Thus, we conclude the two models have similar performance in terms of the schedule pattern of PSH and other generators.

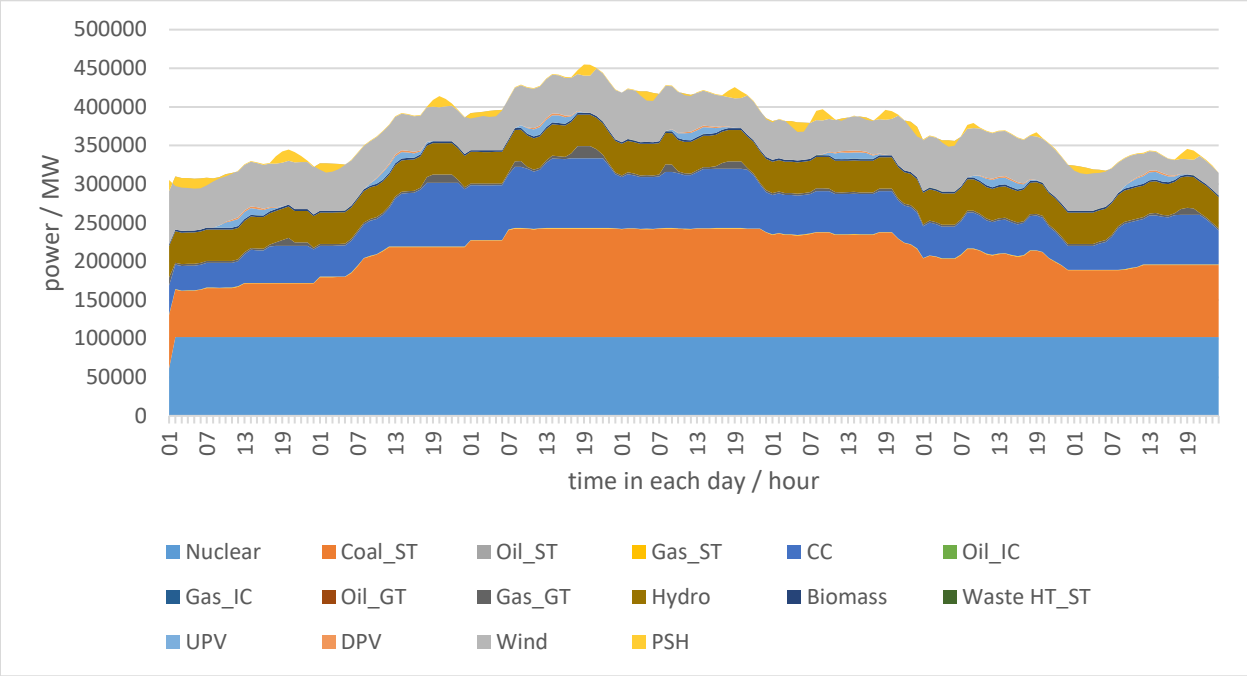

Fig. H.1.2. Generation levels for all types of generators in a week (MILP UC model)

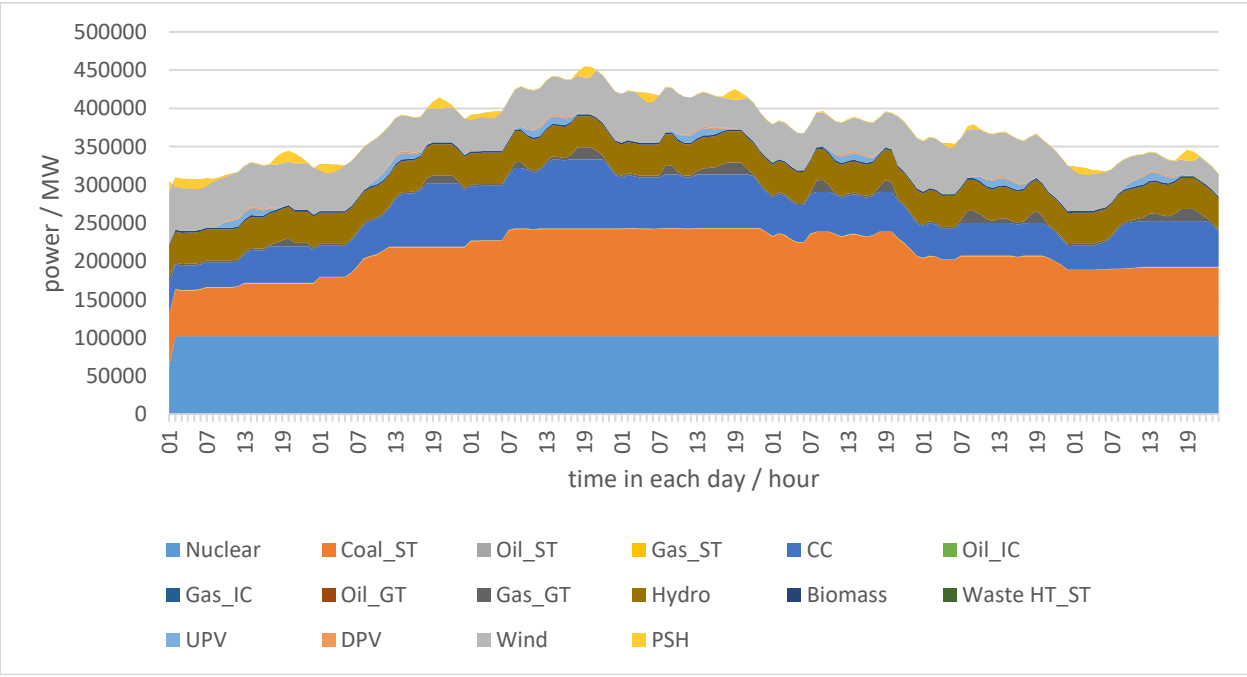

Fig. H.1.3. Generation levels for all types of generators in a week (LP approximation model)

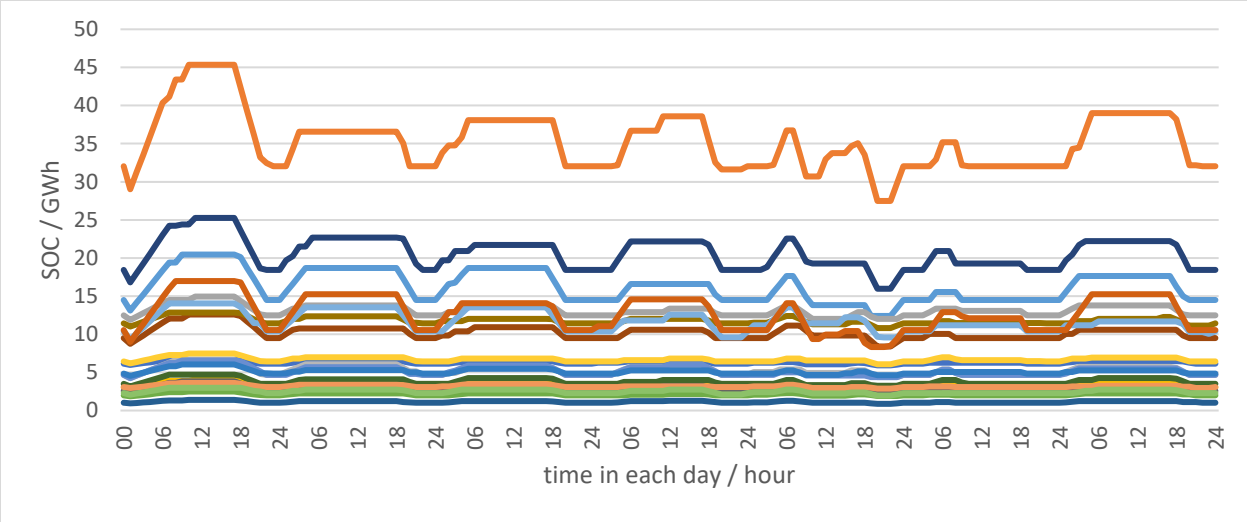

Fig. H.1.4. SOC levels of all PSH stations in a week (MILP UC model)

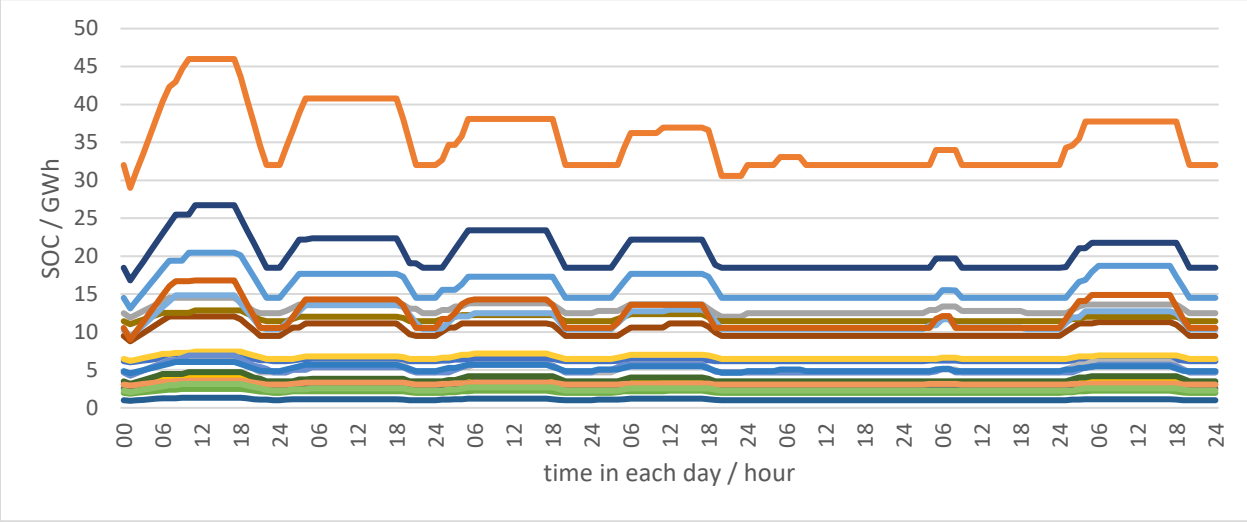

Fig. H.1.5. SOC levels of all PSH stations in a week (LP approximation model)

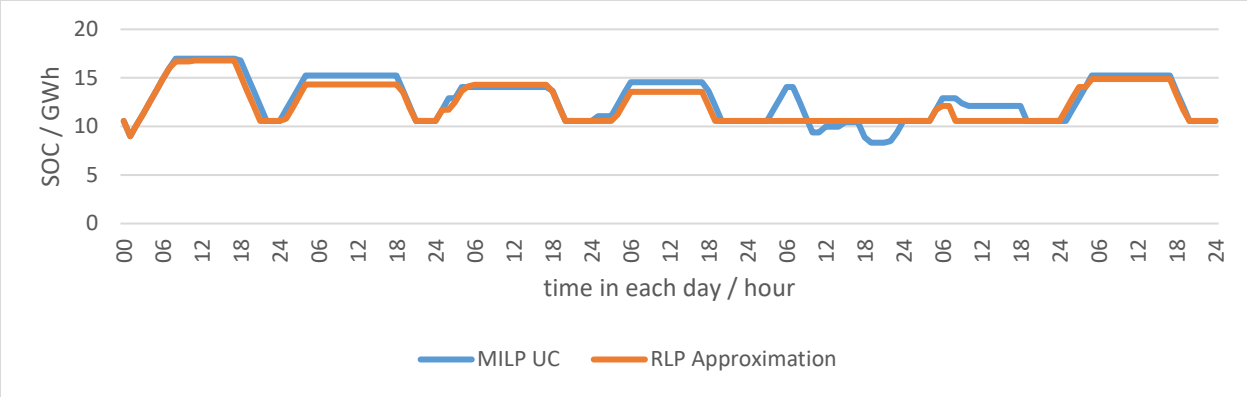

Fig. H.1.6. SOC level of one PSH station in a week (MILP UC model versus relaxed LP approximation model)

Thus, from the proposed method, we can obtain a solution with a small difference of 0.35% in comparison to the MILP unit commitment model, as well as a similar schedule pattern. However, the proposed model can enable a significant time reduction of 71.6% in this test case. Note our test is based on a transmission unconstrained case, which may mathmaticaly reduce the gap between MILP and its LP relaxation. Further studies on transmission constrained cases can be investigated in the future.

Further exploration work on embedding UC constraints in stochastic transmission expansion planning

In economic planning, unit commitment (UC) modeling can accurately reflect the system operational flexibility and quantify long-term economic performances. Given the volatility of renewable energy and thus increased time couplings in the modeling, the need to consider UC-based production cost simulation in transmission expansion planning formulation is growing. It is worth mention that the existence of pumped storage hydro unit and the expectation of increasing storage penetration in the future are also important driving forces for the inclusion of production cost simulation in transmission expansion planning.

As described, although it is appealing to consider both UC model and stochastic optimization approach in transmission expansion planning, this would bring great computational challenges for large-scale practical power systems. In the literature, two-stage or multi-stage stochastic [H.4] or robust [H.5] transmission expansion planning problems have been widely investigated. However, economic dispatch models are usually used in the system operation stage under representative day settings [H.4, H.5], to achieve tractable solutions at the expense of optimality.

We consider a stochastic transmission expansion planning approach considering UC model, as shown in (H.1.5). $\mathbf{x}$ and $\mathbf{y}_s$ represents planning decision variables and unit commitment/economic dispatch decision variables in scenario s, respectively. $\mathbf{a}$ and $\mathbf{b}_s$ are cost coefficients for planning and operation, respectively. p_s is the probability for scenario s. Ω^{PLAN} is feasible region for planning decisions constructed by planning constraints. $\Omega_s^{\mathrm{UC}}(\mathbf{x})$ is the feasible region of UC constraints given planning decisions. An illustrative figure for our modeling framework is shown in Fig. H.1.7.

$$\begin{aligned} &\min \mathbf{a}^{\top}\mathbf{x} + \sum_{s\in S}\left(\mathrm{p}_s \cdot \mathbf{b}_s^{\top}\mathbf{y}_s\right) \\ &\text{s.t.} \quad \mathbf{x} \in \Omega^{\mathrm{PLAN}}, \mathbf{y}_s \in \Omega_s^{\mathrm{UC}}(\mathbf{x}) \end{aligned} \tag{H.1.5}$$

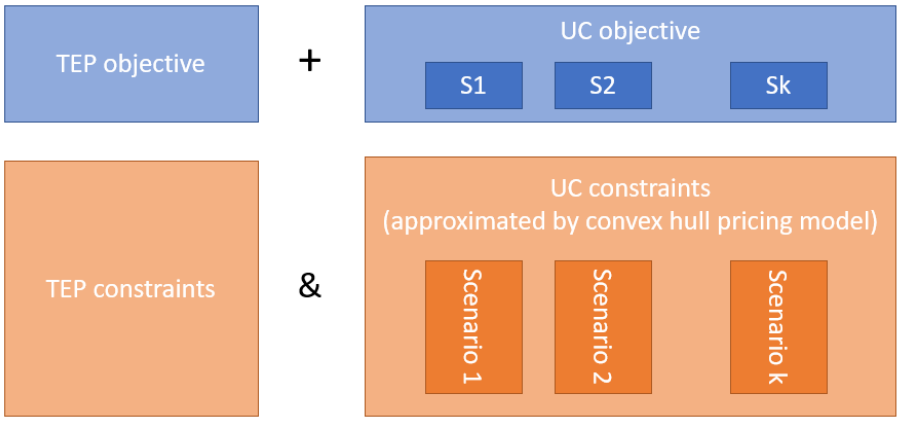

Fig. H.1.7. Modeling framework for stochastic transmission expansion planning with UC constraints

In detail, the planning constraints is (H.1.6), which corresponds to Ω^{PLAN}.

$$\begin{aligned} &z_{i1} \le z_{i1} \quad \forall i1 < i2 \in \mathcal{L}^n \text{ and } i1,\ i2 \text{ have the same parameter} \\ &z_i \in \{0,1\} \quad \forall i \in \mathcal{L}^n \end{aligned} \tag{H.1.6}$$

where, z_i is the binary decision variable for transmission line i, i.e., line i is planned to build if $z_i = 1$. $\mathcal{L}^n$ is the set of candidate lines.

The system balance and transmission constraints are shown in (H.1.7). Candidate lines are modeled with a disjunctive formulation.

$$\begin{aligned} &\sum_{i\,|\,i=(m,b)\in\mathcal{L}\bigcup\mathcal{L}^n} f_{i,s,t} - \sum_{i\,|\,i=(b,n)\in\mathcal{L}\bigcup\mathcal{L}^n} f_{i,s,t} + \sum_{g\in\mathcal{G}_b} p_{g,s,t} = \sum_{d\in\mathcal{D}_b} p_{d,s,t} \quad \forall b\in\mathcal{B}, \forall s\in\mathcal{S}, \forall t\in\mathcal{T} \\ &f_{i,s,t} = \frac{\theta_{m,s,t} - \theta_{n,s,t}}{x_i} \quad \forall i=(m,n)\in\mathcal{L}, \forall s\in\mathcal{S}, \forall t\in\mathcal{T} \\ &-F_i \le f_{i,s,t} \le F_i \quad \forall i\in\mathcal{L}, \forall s\in\mathcal{S}, \forall t\in\mathcal{T} \\ &\left| f_{i,s,t} - \frac{\theta_{m,s,t} - \theta_{n,s,t}}{x_i} \right| \le M\cdot(1-z_i) \quad \forall i=(m,n)\in\mathcal{L}^n, \forall s\in\mathcal{S}, \forall t\in\mathcal{T} \\ &-F_i \cdot z_i \le f_{i,s,t} \le F_i \cdot z_i \quad \forall i\in\mathcal{L}^n, \forall s\in\mathcal{S}, \forall t\in\mathcal{T} \end{aligned} \tag{H.1.7}$$

where, $f_{i,s,t}$ is the flow in line i in scenario s and time t. $p_{g,s,t}$ and $p_{d,s,t}$ are power from unit g and to load d, respectively. $\theta_{b,s,t}$ is the phase angle of bus b. x_i and F_i are line admittance and power

rating for line i. $\mathcal{L}$ and $\mathcal{L}^n$ are sets of existing and candidate lines, respectively. $\mathcal{G}$ and $\mathcal{D}$ are set of generators and loads, respectively. $\mathcal{S}$ is the set of scenarios. $\mathcal{T}$ is the set of time periods.

To address the computational complexity, we again use $\mathbf{y}_s \in \tilde{\Omega}_s^{\mathrm{UC}}(\mathbf{x})$ to approximate the UC constraints in (H.1.5), where $\tilde{\Omega}_s^{\mathrm{UC}}(\mathbf{x})$ is a polyhedron approximation of $\Omega_s^{\mathrm{UC}}(\mathbf{x})$. In detail, we use (H.1.2) and (H.1.3) to approximate $\tilde{\Omega}_s^{\mathrm{UC}}(\mathbf{x})$.

The objective function is the sum of investment and operation cost, as shown in (H.1.8).

$$\sum_{i\in\mathcal{L}^n} CINV_i z_i + \sum_{\forall s\in\mathcal{S}} \sum_{\forall t\in\mathcal{T}} \sum_{g\in\mathcal{G}} \left(\gamma_{g,s,t} + CST_g u_{g,s,t}\right) \tag{H.1.8}$$

where, $CINV_i$ is the investment cost for line i, CST_g is the start-up cost for generator g.

For this exploration work, we performed a preliminary test to assess the feasibility of the convex approximation approach for underlying unit commitment models. Garver's 6 bus system, which is a classical test system for transmission expansion planning studies is used in our test. We employ a linear program (LP) relaxation of a tight unit commitment formulation to solve a deterministic transmission expansion planning problem (noted as 'LP approximation' in Table H.1.3). As a reference for comparison, binary UC variables are kept for in another transmission expansion planning run (noted as 'MILP UC' in Table H.1.3). Given including annual UC model is computational unmanageable, this test incorporates one-day operation constraints for model accuracy validation purposes. As indicated in Table H.1.3, the investment costs from the two models are exactly the same, meanwhile the operation costs are very close, so as the total costs. This result verifies that approximating unit commitment models in the operation stage of transmission expansion planning is a promising approach worth further investigation.

Table H.1.3. Accuracy of LP approximation for UC model

model	investment (10^3 \$)	operation (10^3 \$)	total (10^3 \$)
LP approximation	500.0	312.3	812.3
MILP UC	500.0	316.7	816.7

Already considering both UC characteristics and stochastic optimization approach in transmission expansion planning, massive scenarios, large practical system size and long study time horizon would make the decision making more computationally challenging in practice. Mathematical decomposition approaches can be leveraged to reduce computational burden together with advanced high-performance computing techniques. A well-designed decomposition framework can enable the parallel computing capability of high-performance computers in subproblem solution process to significantly reduce the total solution time.

The optimization problem structure among scenarios can be utilized to facilitate the design of the decomposition framework. In our proposed stochastic transmission expansion planning model, given fixed expansion decisions, the production cost simulation models for different scenarios are naturally decoupled, as shown in Fig. H.1.8. To achieve scenario-based decomposition, techniques

such as Benders decomposition will be explored to coordinate the master problem for transmission expansion planning in (H.1.9) and production cost simulation subproblems $\mathbf{y}_s \in \tilde{\Omega}_s^{\mathrm{UC}}(\hat{\mathbf{x}}^k)$. In (H.1.9), $\phi_s \geq \mathbf{c}_{s,k}{}^{\top}\mathbf{x} + \mathrm{d}_{s,k}$ is Benders cut from subproblem in scenario s in iteration k.

$$\begin{aligned} &\min \mathbf{a}^{\top}\mathbf{x} + \sum_{s\in S}(\mathrm{p}_s \cdot \phi_s) \\ &\text{s.t.} \quad \mathbf{x} \in \Omega^{\mathrm{PLAN}}, \phi_s \geq \mathbf{c}_{s,k}{}^{\top}\mathbf{x} + \mathrm{d}_{s,k} \ \forall s,k \end{aligned} \tag{H.1.9}$$

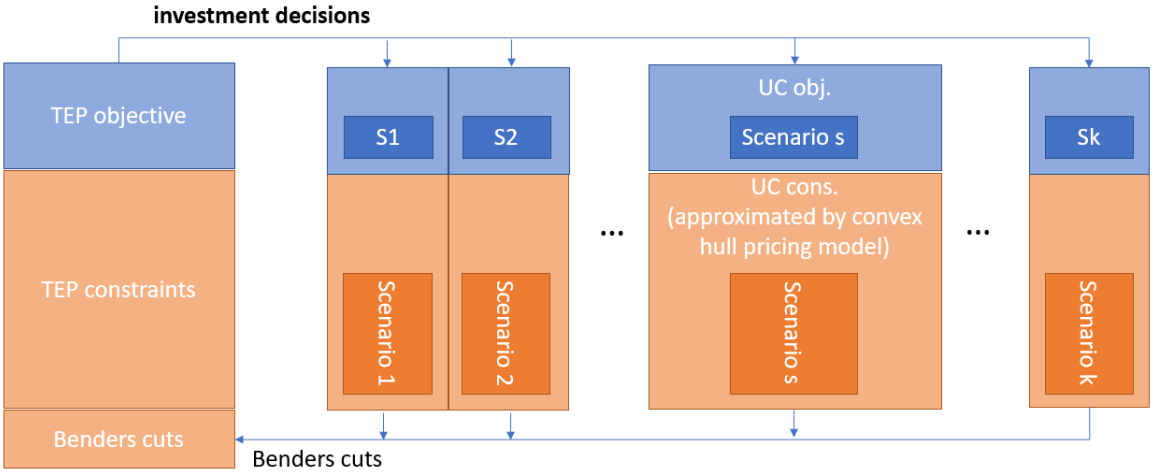

Fig. H.1.8. Illustration for scenario decomposition

We also test stochastic transmission expansion planning with full annual chronological UC constraints in Garver's 6 bus system. The feasibility of using scenario decomposition to speed up is assessed. We use Benders decomposition to decouple the scenarios. In this preliminary test, the subproblems are solved sequentially. As indicated in Table H.1.4, the solution time significantly is reduced by using scenario decomposition even without parallel accelerations. Further speed-up can be expected with fine-grained decomposition and parallel computing techniques.

Table H.1.4. Speed up with scenario decomposition

Number of scenarios	Method	Objective value (10^6 \$)	Time (sec)
5	w/o scenario decomposition	-	>1200
	w/ scenario decomposition	104.43	501.3

IV.H.2 Long-term impact of enhanced PSH model through planning analyses

In order to evaluate the long-term impact of enhanced PSH modeling, numerical studies were performed using MISO planning cases. For each study, two PSH modeling were developed: Current Practice model and Proposed Practice model. Current Practice model is designed to reflect the current market rules, where pumping and generating hours are specified by PSH owners. For study purpose, a generic rule was employed for all PSH units in the study footprint, where generating hours are 7am-21pm, and pumping hours are 22pm-6am. Proposed Practice model is designed to capture the enhanced PSH model, where pumping and generating schedule is optimized by ISO.

Impact on Load Cost

A MISO planning case (referred to as MISO Planning Case 1) was used to evaluate the impact of enhanced PSH modeling on load cost. In this planning case, the generation of most of the US Eastern Interconnection and a simplified zonal transmission system were included. The case was built for year 2024, and therefore a whole year (8784-hour) production cost simulation was performed for year 2024 using PLEXOS for each of the two models, where 24-hour SCUC and hourly SCED are simulated in a chronological fashion. MIP solver was used in solving SCUC. A daily recycling pattern was modeled in this study.

Fig. H.2.1 shows the load cost change in percentage between Current Practice model and Proposed Practice model. The annual load cost comparison is shown in Table H.2.1. It can be seen that, generally speaking, the Proposed Practice model can result in a reduction in monthly load cost. On annual basis, the load cost can be reduced by 1.42%. The reduction in load cost is intuitive as the Proposed Practice model allows more flexibility in choosing the time of pumping and generating in comparison to the predetermined pumping/generating times. Specifically, in the Proposed Practice model, PSH units pump more and generate more due to increased flexibility. The increased pumping will increase LMP at some locations and therefore increase load cost during pumping hours. The increased cost reflects the cost of additional generation, typically from inexpensive generation during the pumping hours. On the other hand, the pumped energy is stored in the upper reservoir and is used to generate electricity in other times to displace more expensive generation. The increased PSH generation during generating hours decreases LMP at some locations and subsequently reduces load cost. The reduced load cost during generating hours is generally considerably larger than the increased load cost during pumping hours, resulting in a net reduction of load cost.

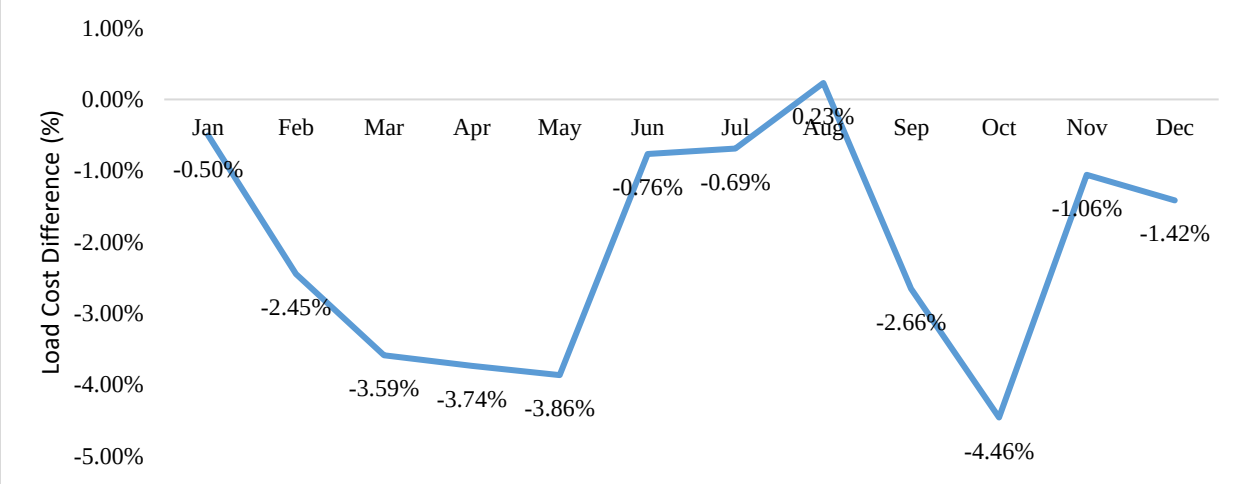

Fig. H.2.1: Monthly load cost difference between Current Practice and Proposed Practice. The Proposed Practice model can generally bring load cost reduction across the year.

Table H.2.1: The Total Annual Load Cost Comparison Between Current Practice and Proposed Practice

Study Case and Study Period	Total System Load Cost in Year 2024 ($)		Difference of Total System Load Cost (%)
	Current Practice Model	Proposed Practice Model	
MISO Planning Case 1 01/01/2024-12/31/2024	453,361,269,181	446,945,866,587	-1.42%

The simulation results further show the increase pumping power in the Proposed Practice model is provided from inexpensive generation including wind, hydro and nuclear units. The increased PSH generated power replaces more expensive generation including those from Coal-ST, and Gas-GT, and combined cycle units. In addition, the increased pumping in Proposed Practice helps reduce energy curtailment. This is because, for this specific MISO planning case, load is low during the pumping periods in the Current Practice model and therefore wind and hydro generation gets curtailed due to transmission congestion. In the Proposed Practice model, the increased pumping during the pumping periods effectively increase the load, and takes power from those generating units and therefore leads to less curtailment. The strong correlation between increased pumping and reduced curtailment (from Current Practice model to Proposed Practice model) can be seen from Fig. H.2.2, which shows the hourly data of increased pumping and reduced curtailment for May 2024.

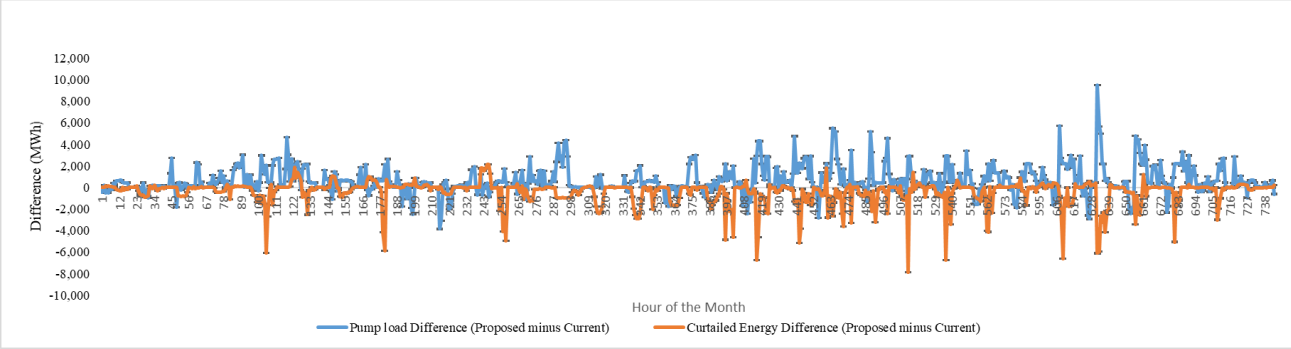

Fig. H.2.2: Increased pumping and reduced curtailment between Current Practice and Proposed Practice in May 2024. A strong correlation between increased pumping and reduced curtailment is observed.

Impact on CO_2 emission

Another MISO planning case (referred to as MISO Planning Case 2) was used to evaluate the impact of enhanced PSH modeling on CO_2 emission due to the available emission rates in the case. In this planning case, the generation of most of the US Eastern Interconnection and a full transmission system were included. The case was built for year 2017, and therefore a whole year (8760-hour) production cost simulation was performed for year 2017 using PLEXOS, where 24-hour SCUC and hourly SCED are simulated in a chronological fashion. No recycling pattern was specifically modeled in this study. The simulation was performed for each of the two models (Current Practice model and Proposed Practice model) respectively. It should be noted that, due to the prolonged simulation time, transmission constraints are ignored in this study to speed up the simulation.

Table H.2.2 compares the simulated annual CO_2 emission in 2017 for the two models. It shows the Proposed Practice results in higher CO_2 emission, or 0.07% increase in annual CO_2 emission in comparison to the Current Practice. It may appear surprising at first glance but not counterintuitive given the SCUC/SCED is based on economics and security of the system, not CO_2 emission. Further investigation reveals the CO_2 emission in MISO Planning Case 2 increases due to two major reasons: 1) in the Proposed Practice, the increased flexibility allows for increased utilization of PSHUs for economics. That leads to more pumping and generating from the PSHUs. Due to 75%-80% cycle efficiency of PSHUs, the increased pumping is higher than the increase generation from PSHUs, which effectively increased the total demand. The increased demand in turn needs to be served by increased generation from other generating sources, which result in increased CO_2 emission; 2) in the Proposed Practice, more expensive yet lower emission rate generation is replaced by generation from PSHUs, while less expensive and higher emission rate generation serves the pumping load from PSHUs. It causes a net increase of CO_2 emission despite the net decrease in cost.

The second point is further illustrated using data in Table H.2.3 and Table H.2.4. Table H.2.3 shows the pumped storage hydro generation increases significantly (by about 25%) in the Proposed Practice. Pumping load is not directly shown in this generation table, yet implied by the total increased generation. The difference between the total increased generation and increased PSH generation represents the total increased generation from all other generation sources. Among those, CC and ST Coal provides most of the increased generation, which mostly happen when

PSHUs pump. ST Gas and ST Oil has most of the decreased generation, which mostly happen when PSHUs generate. In consequence, the CO_2 emission increased for CC and ST Coal, and decreased for ST Gas and ST Oil, as seen in Table H.2.4. It should be noted that, although ST Coal generation increased in slightly less amount than the decrease in ST Gas generation, the increased CO_2 emission from ST Coal is considerably larger than the decreased CO_2 emission from ST Gas, which is due to the emission rate difference between generation categories.

Table H.2.2: The Total CO_2 Emission Comparison Between Current Practice and Proposed Practice

Study Case and Study Period	Total CO_2 emission in Year 2017 (lb)		Difference of Total CO_2 emission (%)
	Current Practice	Proposed Practice	
MISO Planning Case 2 01/01/2017-12/31/2017	2,394,514,615,461	2,396,280,506,607	0.07%

Table H.2.3: The Total Generation Comparison Between Current Practice and Proposed Practice

Generation Category	Total Generation in Year 2017 (MWh)		Generation Difference (MWh)
	Current Practice	Proposed Practice	
CC	848,927,420	849,932,130	1,004,710
Conventional Hydro	116,905,340	116,904,330	(1,010)
CT Gas	91,629,201	91,946,878	317,677
CT Oil	-	-	-
CT Other	623	363	(260)
CT Renewable	-	-	-
External Transaction	(3,180,264)	(3,180,264)	-
Fuel Cell	182,243	184,097	1,854
Geothermal	330,686	330,686	-
IC Gas	1,686,312	1,783,455	97,143
IC Oil	47,560	51,971	4,411
IC Renewable	868,750	881,128	12,378
IGCC	8,636,717	8,750,485	113,768
Industrial Loads	(15,268,680)	(15,268,680)	-
Interruptible Loads	-	-	-
Nuclear	631,777,810	631,777,810	-
Pumped Storage Hydro	19,220,090	24,029,821	4,809,731
Qualifying Facilities	16,558,612	16,558,612	-
ST Coal	687,597,850	688,023,150	425,300
ST Gas	53,105,837	52,654,518	(451,319)
ST Oil	2,117,801	2,114,578	(3,223)
ST Other	1,599,051	1,626,927	27,876
ST Renewable	17,956,441	18,010,383	53,942
Existing Solar PV	3,745,556	3,745,556	-
Existing Wind	157,572,450	157,572,450	-

Total	**2,642,017,406**	**2,648,430,384**	**6,412,978**

Table H.2.4: The Total CO_2 Emission Comparison Between Current Practice and Proposed Practice By Generation Category

Generation Category	Total CO_2 emission in Year 2017 (lb)		CO_2 emission Difference (lb)
	Current Practice	Proposed Practice	
CC	736,365,872,816	737,264,258,650	898,385,834
CT Gas	114,170,422,002	114,503,836,084	333,414,082
CT Oil	-	-	-
CT Other	336,326	263,990	(72,336)
CT Renewable	-	-	-
IC Gas	1,176,638,303	1,220,404,576	43,766,273
IC Oil	73,125,645	80,909,172	7,783,527
IC Renewable	955,459,768	966,781,955	11,322,187
IGCC	11,111,941,451	11,217,388,009	105,446,558
Qualifying Facilities	17,198,079,795	17,198,079,795	-
ST Coal	1,412,251,741,813	1,413,044,652,727	792,910,914
ST Gas	65,379,854,959	64,839,521,300	(540,333,659)
ST Oil	2,672,029,020	2,667,959,691	(4,069,329)
ST Other	3,420,997,828	3,507,670,400	86,672,572
ST Renewable	29,738,115,735	29,768,780,258	30,664,523
Total	**2,394,514,615,461**	**2,396,280,506,607**	**1,765,891,146**

Sensitivity Analysis

It should be pointed that the above observations and conclusions are based on simulations of MISO Planning Case 2. When assumptions in the planning case change, the results may change and demonstrate a different pattern. For example, when renewable penetration level is set to very high (for example at 50%), when PSHUs pump, the required energy may require committing more nuclear generators (which has no CO_2 emission). Due to the long minimum-up time of nuclear generators, the newly committed nuclear generators will stay on for a few days, causing other generation sources such as CC and ST Coal to ramp down, which effectively reduces CO_2 emission. In this case, the total CO_2 emission may reduce in Proposed Practice. A one-week results of the aforementioned dispatch pattern is illustrated in Fig. H.2.3.

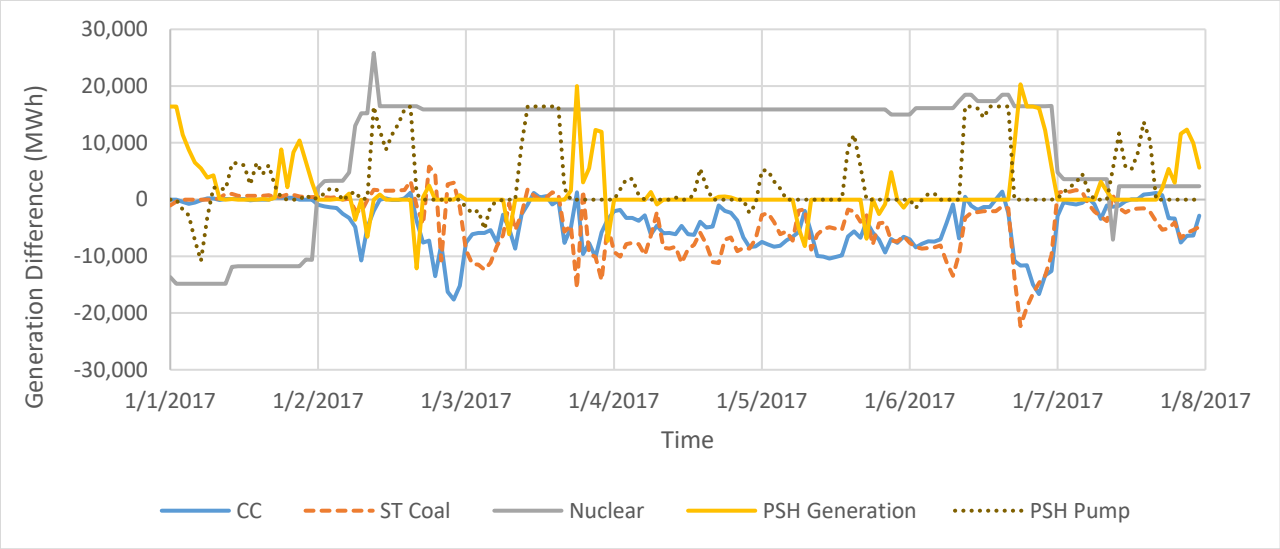

Fig. H.2.3. The generation difference by generation category between Current Practice and Proposed Practice in MISO Planning Case 2 with 50% renewable penetration for simulation period of January 1, 2017 through January 7, 2017

References:

[H.1] Pan, K. and Guan, Y. (2016). A polyhedral study of the integrated minimum-up/-down time and ramping polytope. working paper. Available online: https://arxiv.org/abs/1604.02184

[H.2] Hua, B., Baldick, R. and Wang, J. (2016). Representing operational flexibility in generation expansion planning through convex relaxation of unit commitment. *IEEE Transactions on Power Systems*, 33(2), 2272-2281.

[H.3] Baldick, Ross, Yonghong Chen, and Bing Huang (2021). Optimization formulations for storage devices. working paper. Available online: http://www. optimization-online.org/DB_FILE/2021/07/8502. pdf

[H.4]Bagheri, A., Wang, J. and Zhao, C (2016). Data-driven stochastic transmission expansion planning. *IEEE Transactions on Power Systems* 32(5), 3461-3470.

[H.5] Wang, S., Geng, G. and Jiang, Q (2019). Robust co-planning of energy storage and transmission line with mixed integer recourse. *IEEE Transactions on Power Systems* 34(6), 4728-4738.

V. Key Personnel

The research team consists primarily of the following personnel.

- Missouri University of Science and Technology: Rui Bo (PI), Siyuan Wang, Haotian Chen, Jian Liu
- MISO: Yonghong Chen (Co-PI), Bing Huang, Arezou Ghesmati
- Stevens Institute of Technology: Lei Wu (Co-PI), Yang Lin, Yafei Yang, Yikui Liu
- Ross Baldick Educational and Consulting Services: Ross Baldick (Co-PI)

Industry partners participating in this project include:

- DTE Electric: Nicholas A Griffin
- Consumers Energy: Kevin J. Van Oirschot
- Ameren Missouri: Mike Fiala

VI. Project Output

A. Published Papers

Related to Task 1:

B. Huang, Y. Chen, R. Baldick, "A Configuration Based Pumped Storage Hydro Model in MISO Day-Ahead Market", *IEEE Transactions on Power Systems*, accepted.

Related to Task 2 and Task 5:

J. Liu, R. Bo, S. Wang, H. Chen, "Optimal Scheduling for Profit Maximization of Energy Storage Merchants Considering Market Impact Based on Dynamic Programming", accepted, *Computers & Industrial Engineering*, 2021

R. Das, R. Bo, W. Rehman, H. Chen, D. Wunsch, "Cross-Market Price Difference Forecast Using Deep Learning for Electricity Markets", *2020 IEEE PES Innovative Smart Grid Technologies Europe (ISGT-Europe)*, Hague, Netherlands.

R. Das, R. Bo, W. Rehman, H. Chen, D. Wunsch, "Forecasting Nodal Price Difference between Day-ahead and Real-time Electricity Markets using Long-Short Term Memory and Sequence-to-Sequence Networks", accepted, *IEEE Access*, 2021.

Related to Task 3 and Task 6:

S. Wang, J. Liu, H. Chen, R. Bo, Y. Chen, "Modeling State Transition and Head-Dependent Efficiency Curve for Pumped Storage Hydro in Look-Ahead Dispatch", *IEEE Transactions on Power Systems*, accepted.

Related to Task 4:

Z. Tang, Y. Liu, L. Wu, J. Liu, and H. Gao, "Reserve Model of Energy Storage in Day-ahead Joint Energy and Reserve Markets: A Stochastic UC Solution," *IEEE Transactions on Smart Grid*, vol. 12, no. 1, pp. 372-382, 2021.

Y. Liu, L. Wu, Y. Yang, Y. Chen, R. Baldick, and R. Bo, "Secured Reserve Scheduling of Pumped-Storage Hydropower Plants in ISO Day-ahead Market," *IEEE Transactions on Power Systems*, accepted, 2021.

Y. Liu, Z. Tang, and L. Wu, "On Secured Spinning Reserve Deployment of Energy-Limited Resources Against Contingencies", *IEEE Transactions on Power Systems*, accepted, 2021.

Related to Task 9:

S. Wang, R. Bo, "Joint Planning of Electricity Transmission and Hydrogen Transportation Networks", *IEEE Transactions on Industry Applications*, accepted.

B. Under Review and Under Submission Papers

Related to Task 1:

R. Baldick, Y. Chen, and B. Huang, "Optimization formulations for storage devices," submitted to *Operations Research*, 2021.

J. Liu, R. Bo, et al, "Implication of Market Impact and Price Forecast Accuracy on Energy Arbitrage for Electricity Merchants with Storage and Renewable Power Plant", *Manufacturing & Service Operations Management*, in submission.

Related to Task 2 and 5:

A.Ghesmati, B.Huang, Y.Chen, R. Baldick. "Scheduling Pumped Storage Hydro in a Realtime Market with Probabilistic Price Forecast", *IEEE Transactions Power System*, in submission.

B.Huang, A.Ghesmati, Y.Chen, R. Baldick. "Pumped Storage Hydro Modeling and Simulation in a Look-ahead Commitment using Price Forecast", *IEEE Transactions Power System*, in submission.

Related to Task 3 and 6:

S. Wang, R. Bo, "Approximate Input-Output Curve for Pumped Storage Hydro: A Disjunctive Convex Hull Model", *IEEE Transactions on Power Systems*, under review.

C. Technical Presentations

R. Baldick, Y. Chen, and B. Huang, "Optimization formulations for storage devices," Presented at The 4th Georgia Tech Workshop on Energy Systems and Optimization, Atlanta, GA, December 10-11, 2020.

Y. Chen, et al, "Developing Optimization Algorithms and Computational Techniques for Future Resource Integration", panel presentation at 2021 IEEE PES General Meeting.

B. Huang, A. Ghesmati, Y. Chen, R. Baldick, R. Bo, "Modeling and Optimizing Pumped Storage in a Multi-stage Large Scale Electricity Market under Portfolio Evolution", presentation at 2021 FERC Technical Conference on Increasing Market and Planning Efficiency through Improved Software.

B. Huang, A. Ghesmati, Y. Chen, R. Baldick, "Pumped Storage Optimization in Day-ahead and Real-time Market under Uncertainty", presentation at 2021 INFORMS Annual Meeting.

VII. Conclusions

The project developed a prototype enhanced pumped storage hydro (PSH) model for incorporation into the multi-stage market clearing process with proper consideration of the unique characteristics of PSH. In the market clearing process, energy products and ancillary service products (including capacity-based regulating reserve and energy-based reserve) in energy and ancillary service market are co-optimized. The enhanced PSH model in the multi-stage market clearing process can facilitate a deeper participation of PSH resources in organized electricity markets.

Through the investigation of three research areas (as mentioned in the Executive Summary), the project delivered the below specific outcomes:

- A prototype deterministic day-ahead (DA) SCUC model with PSH optimization has been developed and implemented using HIPPO. It meets MISO's solution quality and

performance requirement. Studies on actual MISO system showed 0.04%-0.67% reduction in system total cost and up to 97% increase in PSH profit. The benefits are expected to be significantly higher with higher penetration of PSH and renewable generation.

- A "tighter" formulation of the state-of-charge constraints with binary variables has been proposed and implemented to improve the computational performance of the proposed deterministic day-ahead (DA) SCUC model. Statistical data based on repeated tests using MISO cases show that the tightened constraints typically have approximately neutral or positive impact (e.g., up to 34% reduction in studied cases) on the computational time.
- An energy reserve (or MWh reserve) concept has been proposed to deal with the SOC deviation in real-time. Head room and floor room are derived using statistical models. Both the rolling based stochastic approach and the approximate dynamic programming (ADP) approach have been employed to evaluate the value of water of PSHs outside a finite time horizon. Studies show that both approaches can lead to a better utilization of available water with higher profits for PSHs in RT markets, than exactly staying with the DA solutions. In addition, no approach consistently outperforms the other, and their performances depend on the quality of RT price forecasts as well as similarities between price patterns in RT and those used for ADP training.
- A rolling window simulation platform has been developed in HIPPO, which closely mimics the LAC of MISO. It is a valuable tool for investigation of the intra-day clearing process.
- An ARIMAX-based deterministic price forecast and a scenario generation-based stochastic price forecast have been developed to predict RT prices. The price forecasts can be used in the developed deterministic and stochastic PSHU models respectively to guide intra-day dispatch. Studies using MISO data show the developed ARIMAX model can capture the trend, the peaks and the turning points of the actual RT-LMP significantly better than the Facebook Prophet model.
- A risk-averse formulation has been developed to address the concern of profit loss in the RT market. Studies demonstrate the effect of the risk management formulation in reducing system total cost and avoiding negative profits for the PSHU.
- A planning model with improved realistic characteristics of PSH and the incorporation of market optimization enhancement has been developed. Studies using actual PSH plant parameters and MISO planning models reveal the SOC error from inaccurate PSH input-output curve modeling will accumulate quickly in chronological production cost simulation, and consequently requires periodical adjustment of SOC or the adoption of proposed improved input-output curve modeling.
- A novel disjunctive convex hull model for input-output curve approximation has been developed to improve the computational performance, and studies show an order of magnitude speedup over the common piece-wise linear approximation methods.
- Studies using MISO planning models show using DA storage shadow price as an indicator for future value of water can exploit the flexibility of PSH in RT and reduce RT system total cost (with a monthly average of 0.22% reduction in studied cases).
- A linear program based approximated model is used to approximate the nonconvex unit commitment model to accelerate the solution of stochastic production cost simulation models. Studies using a MISO planning model show the proposed method can produce acceptable accuracy in results (with 0.35% difference in system total cost) and significant solution time improvement (with 71.6% reduction in solution time).

Appendix for Section IV.A.1

Deterministic PSH model in SCUC

Nomenclature:

Sets and indices:

$t \in \mathcal{T}$	set of time intervals;
$g \in \mathcal{G}_{psh}$	set of PSHUs;
$g \in \mathcal{G}_{psh,r}$	set of PSHUs that share the same reservoir r;
$g \in \mathcal{G}$	set of the rest of the generating units in a system;
$m \in \mathcal{M}_g$	set of configurations, $\mathcal{M}_g = [alloff, gen, pump]$;
$n \in \mathcal{M}_g^{F,m}$	set of configurations that configuration m can feasibly transit to;
$r \in \mathcal{R}$	set of reservoirs.

Data [units]:

D_t	system net load at period t [$/MW];
$\underline{Q}_g^{gen}$	minimum generation power of PSHU g [MW];
$\overline{Q}_g^{gen}$	maximum generation power of PSHU g [MW];
$\underline{Q}_g^{pump}$	minimum pumping power of PSHU g [MW];
$\overline{Q}_g^{pump}$	maximum pumping power of PSHU g [MW];
η_g^{gen}	generating efficiency of the PSHU g [NA];
η_g^{pump}	pumping efficiency of the PSHU g [NA];
$E_{r,0}$	initial energy level of the reservoir r [MWh];
$E_{r,\lvert\mathcal{T}\rvert}$	final energy level of the reservoir r [MWh];
$\overline{E}_r$	maximum energy level of the reservoir r [MWh];
$\underline{E}_r$	minimum energy level of the reservoir r [MWh];
$C_{g,t}^{pump}$	the bid price of pump load at unit g during time interval t [$/MW].

Variables [units]:

$e_{r,t}$	energy stored in the reservoir r at time t [MWh];
$u_{g,t}^m$	binary variable, commitment variable of unit g configuration m during time interval t [NA];
$ur_{r,t}^m$	continuous variable, if $ur_{r,t}^m = 1$, it represents the status of reservoir r in mode $m \in \{gen, pump\}$, at time interval t [NA];
$v_{g,t}^{m,n}$	binary variable, transition variable between configuration m and configuration n of PSHU g during time interval t [NA];
$q_{g,t}^{gen}$	continuous variable, amount of generation at a PSHU g during time interval t [MW];
$q_{g,t}^{pump}$	continuous variable, amount of pumping load at a PSHU g during time interval t [MW];
$q_{g,t}$	continuous variable, amount of generation at unit g during time interval t [MW].

Auxiliary Variables [units]:

$f_{g,t}^{gen}$ continuous variable, energy opportunity cost of gen configuration offered at PSHU g during time interval t [$ /hr];

$C(q_{g,t})$ cost function of generating unit g [$ /hr].

Objective Function: The objective of the unit commitment problem is to minimize the system operating costs. Under MISO current practice, the costs related to a PSHU are the offered production costs of the generating mode minus the virtual bid prices for the pumping mode. However, assuming that the operating cost of PSH is close to zero due to negligible O&M cost, the bid and offer from a PSHU are eliminated in the proposed model. That is, in the proposed model the true opportunity cost of generating and pumping in a PSHU is already reflected in the cost of other generation plants. That is, the objective is as shown in (A.1.1), representing the piece-wise linear production costs of the rest of generators in the system:

$$\min_{q,u,v,e} \sum_{g\in\mathcal{G}} \sum_{t\in\mathcal{T}} C(q_{g,t}) \tag{A.1.1}$$

System Energy Balance Constraints: The generation has to be balanced with net load in the system at all times. In (A.1.2), during each interval *t*, the total generation in the system including the generation from PSHUs on the left should be balanced with the sum of the net load and the pumping load from the PSHUs on the right.

$$\sum_{g\in\mathcal{G}} q_{g,t} + \sum_{g\in\mathcal{G}_{psh}} q_{g,t}^{gen} = D_t + \sum_{g\in\mathcal{G}_{psh}} q_{g,t}^{pump}, \ \forall t \in \mathcal{T}. \tag{A.1.2}$$

State and Transition Logic Constraints: Constraints (A.1.3) guarantee that the unit commitment variables of each mode in a PSHU described in Fig. A.1.1 are mutually exclusive. The variables representing the modes are shown in Fig. A.1.1.

$$\sum_{m\in\mathcal{M}_g} u_{g,t}^{m} = 1, \quad \forall g \in \mathcal{G}_{psh}, \forall t \in \mathcal{T}. \tag{A.1.3}$$

The transition between two modes *m*, *n* in a PSHU *g* at time *t* is defined as a binary variable $v_{g,t}^{m,n}$. These transition variables are shown in Fig. A.1.1 near to the double-headed arrows.

Notice that the start-up and shut-down of a mode are modeled as the transition between the mode and the *alloff* mode.

$$u_{g,t}^{m} - u_{g,t-1}^{m} = \sum_{n\in\mathcal{M}_g^{F,m}} v_{g,t}^{n,m} - \sum_{n\in\mathcal{M}_g^{F,m}} v_{g,t}^{m,n}, \quad \forall g \in \mathcal{G}_{psh}, \forall m \in \mathcal{M}, \forall t \in \mathcal{T}. \tag{A.1.4}$$

In addition to the mutual exclusivity constraints on the commitment variable of each configuration, there should be at most one feasible transition at any time.

$$\sum_{m\in\mathcal{M}_g} \sum_{n\in\mathcal{M}_g^{F,m}} v_{g,t}^{m,n} \le 1, \quad \forall g \in \mathcal{G}_{psh}, \forall t \in \mathcal{T}. \tag{A.1.5}$$

Box constraints: The amount of pumping load during interval t from the PSHU is constrained by the capacity of the pump unit in (A.1.6). The pump output of a PSHU will be forced to zero by (A.1.6) when $u_{g,t}^{pump} = 0$ indicating the unit is not in a pumping mode. Symmetrically, the amount

of generation during interval t from the PSHU is constrained by the capacity of the generation unit shown in (A.1.7). The generation output of a PSHU will be forced to zero by (A.1.7) when $u_{g,t}^{gen}$ = 0 indicating the unit is not in a generating mode.

$$u_{g,t}^{pump}\underline{Q}_{g}^{pump} \leq q_{g,t}^{pump} \leq u_{g,t}^{pump}\overline{Q}_{g}^{pump}, \quad \forall r \in \mathcal{R}, \forall g \in \mathcal{G}_{psh,r}, \ \forall t \in \mathcal{T}. \tag{A.1.6}$$

$$u_{g,t}^{gen}\underline{Q}_{g}^{gen} \leq q_{g,t}^{gen} \leq u_{g,t}^{gen}\overline{Q}_{g}^{gen}, \forall r \in \mathcal{R}, \forall g \in \mathcal{G}_{psh,r}, \ \forall t \in \mathcal{T}. \tag{A.1.7}$$

Storage Energy Balance and State of Charge (SOC) Constraints: The energy stored in the PSH system is linked at each consecutive time interval as shown in (A.1.8). Notice that there can be more than one PSHU sharing a reservoir in the model. Parameters η_g^{gen} and η_g^{pump} are the efficiencies of generating and pumping indicating energy loss in both modes. The energy stored in the reservoir at the beginning and end of the day is given by (A.1.9) and (A.1.10), respectively. The upper and lower bounds of the SOC are provided by (A.1.11).

$$e_{r,t+1} = e_{r,t} + \sum_{g \in \mathcal{G}_{psh,r}} \eta_g^{pump} q_{g,t}^{pump} - \sum_{g \in \mathcal{G}_{psh,r}} \frac{q_{g,t}^{gen}}{\eta_g^{gen}}, \quad \forall r \in \mathcal{R}, \quad \forall t \in [0, |\mathcal{T}| - 1]. \tag{A.1.8}$$

$$e_{r,0} = E_{r,0}, \quad \forall r \in \mathcal{R}. \tag{A.1.9}$$

$$e_{r,|\mathcal{T}|} = E_{r,|\mathcal{T}|}, \quad \forall r \in \mathcal{R}. \tag{A.1.10}$$

$$\underline{E_r} \leq e_{r,t} \leq \overline{E_r}, \quad \forall r \in \mathcal{R}, \quad \forall t \in \mathcal{T}. \tag{A.1.11}$$

The start up and shut down time, transition time, minimum up/down time and security constraints are not listed here. They can be easily accommodated in the proposed configuration based model.

Practical Operational Limits: To demonstrate the adaptability of the proposed configuration based PSH model to industry practice, two additional constraints are presented to reflect some of the physical limits the PSHUs have in their daily operations.

$$\sum_{g \in \mathcal{G}_{psh,r}} \sum_{n \in \mathcal{M}_g^{F,pump}} v_{g,t}^{n,pump} \leq N, \quad \forall r \in \mathcal{R}, \forall t \in \mathcal{T}. \tag{A.1.12}$$

At some PSH plants, due to the physical limits in the start up procedure of pump units, only a limited number of pump units can be brought online in a given time period. In constraints (A.1.12), $\mathcal{M}_g^{F,pump}$ is the set of modes for which unit *g* can feasibly transit to a *pump* mode, bearing in mind that $v_{g,t}^{n,pump}$ is the transition variable of unit *g* from mode *n* to the *pump* mode. Therefore, without introducing new variables, constraints (A.1.12) precisely capture the operational feature that no more than *N* units sharing reservoir *r* can transit from any mode to a pumping mode in time interval *t*.

For the PSH plant with large reservoirs, there are typically multiple PSH units installed in the plant and they are jointly operated with the reservoirs. It is usually not economical and physically

not feasible for the plant to have one unit pumping and another generating at the same time. To incorporate this feature for a PSH plant with multiple units, constraints (A.1.13) and (A.1.14) are introduced.

$$ur_{r,t}^{pump} + ur_{r,t}^{gen} \leq 1, \quad \forall r \in \mathcal{R}, \forall t \in \mathcal{T}. \tag{A.1.13}$$

$$u_{g,t}^{m} \leq ur_{r,t}^{m}, \quad \forall r \in \mathcal{R}, \forall g \in \mathcal{G}_{psh,r}, \; \forall m \in \{gen, pump\}, \forall t \in \mathcal{T}. \tag{A.1.14}$$

A pair of variables $ur_{r,t}^{pump}, ur_{r,t}^{gen}$ are introduced for a reservoir or a PSH plant *r* to represent the status of the plant as pumping or generating at time interval *t*. Therefore, constraints (A.1.13) are the mutual exclusivity constraints at the plant level with (A.1.14) constraining $u_{g,t}^{m}$ which is the commitment variable of PSHU *g* in mode *m* at time interval *t*. Constraint (A.1.14) indicates if any unit *g* of the plant *r* is in *pump* mode then the plant status will be in *pump* mode indicated by $ur_{r,t}^{pump}$ = 1. The same for the *gen* mode. Notice that since $u_{g,t}^{m}$ is binary, $ur_{r,t}^{m}$ can be continuous and bounded by (A.1.13) and (A.1.14).

Combining (A.1.13) and (A.1.14), if any unit in a reservoir is generating at a time interval, all the other units sharing the same reservoir would not pump at the same time interval and vice versa.

With the configuration based model, constraint (A.1.13) and (A.1.14) can be easily adapted to reflect different PSH constraints such as ternary PSH.

Appendix for Section IV.B.1

HIPPO LAC Simulation Validation Results

The DA problem with the entire horizon is solved before the LAC rolling window starts. The DA solutions are used to fix the variables after the LAC window in the LAC simulations. The constraints linking LAC and DA intervals are kept for benchmarking results purpose in this test. In this simulation validation, the system conditions in LAC rolling window simulations including demand and generator inputs remain the same as they are in DA. Therefore, we expect that the solutions from LAC rolling windows would repeat the DA solutions, except where there was primal degeneracy in the model or because of non-zero MIP relative gaps in the either or both of the DA and LAC solutions.

Two PSH units are included in the current study namely PSHU1 and PSHU2. Although the Ludington reservoir is physically shared by PSHU1 and PSHU2, based on the reservoir capacity split agreement, it is modeled as two separate reservoirs and one for each of the PSHUs. The PSH dispatch results for each of the plants in the LAC rolling windows and its DA solution are shown in Figs B.1.2 and B.1.3. The generation and pump of the PSH units are illustrated as positive and negative values, respectively, using the vertical axis on the left of the figures. The LAC solutions and DA solutions are perfectly overlapped showing that the unit dispatch results from the LAC rolling windows repeat the DA solutions.

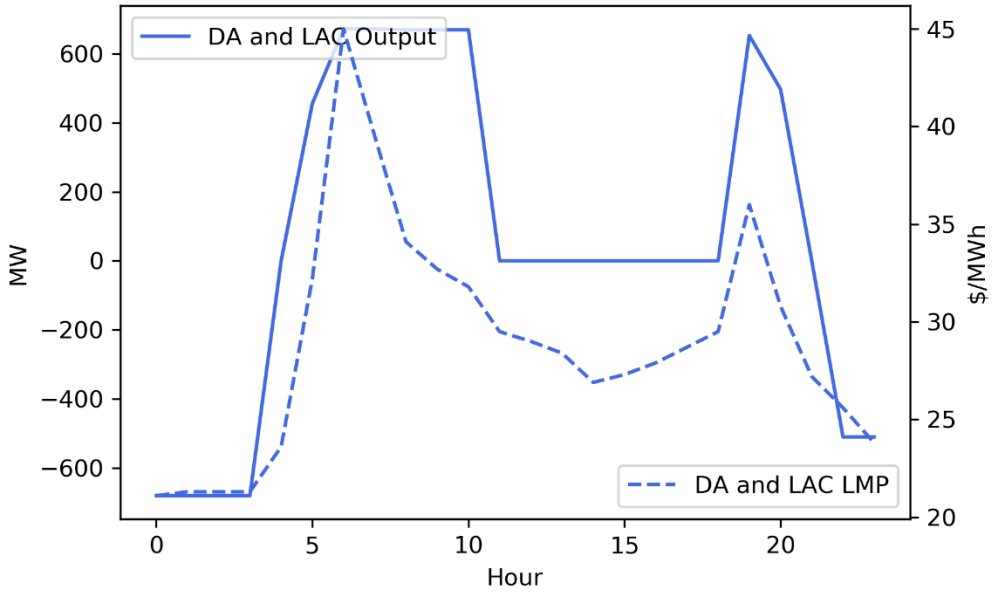

Fig. B.1.2. LAC Rolling Window Simulation Validation Results PSHU 1

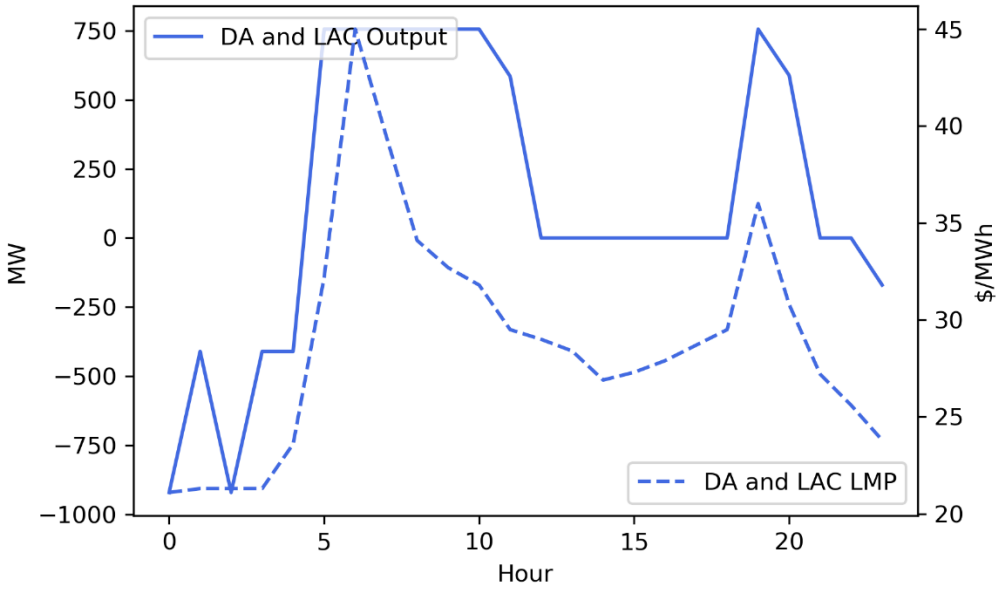

Fig. B.1.3. LAC Rolling Window Simulation Validation Results PSHU 2

Appendix for Section IV.E.3

Quantile Regression:

Quantile regression (QR) as a method of non-parametric forecast method is an extension of linear regression that is used when the conditions for linear regression are not met (i.e., linearity, homoscedasticity, independence, or normality). The two main assumptions in using QR methods read as follows:

- No pre-assumption on distribution of data is considered.
- Distribution of data varies over time.

Assuming that residuals are normally distributed, regular linear regression estimates the conditional mean of the response variable, conditioned on the exogenous variable, using the following model:

$$y_i = \beta_0 + \beta_1 x_{i1} + \beta_2 x_{i2} + \cdots + \beta_p x_{ip}, \quad i = 1,2, \dots, n \quad \text{(E. 3. 1)}$$

with Mean-Square-Error as a "loss function" to measure the performance of fitted model,

$$MSE = \frac{1}{n} \sum_{i=1}^{n} \left(y_i - (\beta_0 + \beta_1 x_{i1} + \beta_2 x_{i2} + \cdots + \beta_p x_{ip})\right)^2, \quad \text{(E. 3. 2)}.$$

In quantile regression, unlike regular linear regression, for any quantile $0 < \alpha < 1$, we estimate the conditional *median* of the target across different values of the features.

$$Q_\alpha\, y_i = \beta_0(\alpha) + \beta_1(\alpha) x_{i1} + \beta_2(\alpha) x_{i2} + \cdots + \beta_p(\alpha) x_{ip}, \quad i = 1,2, \dots, n \quad \text{(E. 3. 3)}$$

Median-Absolute-Deviation is used as the loss function in QR , where median is calculated for for each α of interest, and the loss function is defined as:

$$MAD = \frac{1}{n} \sum_{i=1}^{n} \rho_\alpha \left(Q_\alpha\, y_i - (\beta_0(\alpha) + \beta_1(\alpha) x_{i1} + \beta_2(\alpha) x_{i2} + \cdots + \beta_p(\alpha) x_{ip})\right) \quad \text{(E. 3.4)}$$

Where $\rho_\alpha(\epsilon) = \alpha \max(\epsilon, 0) + (1 - \alpha)\max(0, -\epsilon)$. Here $\rho_\alpha(\epsilon)$ gives weights to the error depending on the given quantile, and the sign of error. This implies if the error is positive then $\rho_\alpha(\epsilon)$ multiples the error by α, and if error is negative multiples the error by (1-α). For example, for α=0.2 , the median of 20th quantile, means in equation (E.3.4) we want 80% of errors to be positive and 20% of errors to be negative.

Non-Parametric Probabilistic Forecast:

The following is a summary of the methodology we used to reconstruct the conditional distributions (PDF and CDF) for the time series values at any given time in look-ahead window:

- Get the dataset for which we wanted to do the forecasting for look-ahead hours.
- Fit Quantile-Regression (QR) curves through the predicted data in look-ahead time window.

To reconstruct the conditional distributions (PDF and CDF) for the time series values at any given time, we can use quantiles as a result of fitting the Quantile-Regression (QR) which for each time ahead t+k and each quantile $\mathbf{0} \leq \boldsymbol{\alpha_1} < \boldsymbol{\alpha_2} < \ \dots < \boldsymbol{\alpha_i} < \ \dots < \boldsymbol{\alpha_m} < \mathbf{1}$ is shown with $\hat{\boldsymbol{q}}_{\boldsymbol{t+k}}^{(\boldsymbol{\alpha_i})}$.

Here we do not assume any shape for the target distription namely LMP, thus a non-parametric forecast of **Cumulative Distribution Function** $\widehat{\boldsymbol{CDF}}$ of the variable of interest at any given time can be produced by gathering a set of m quantile forecasts. For any target time, t+k, in look ahead horizon, Probability Density Function (PDF) can be derived by taking derivative of the corresponding CDF.

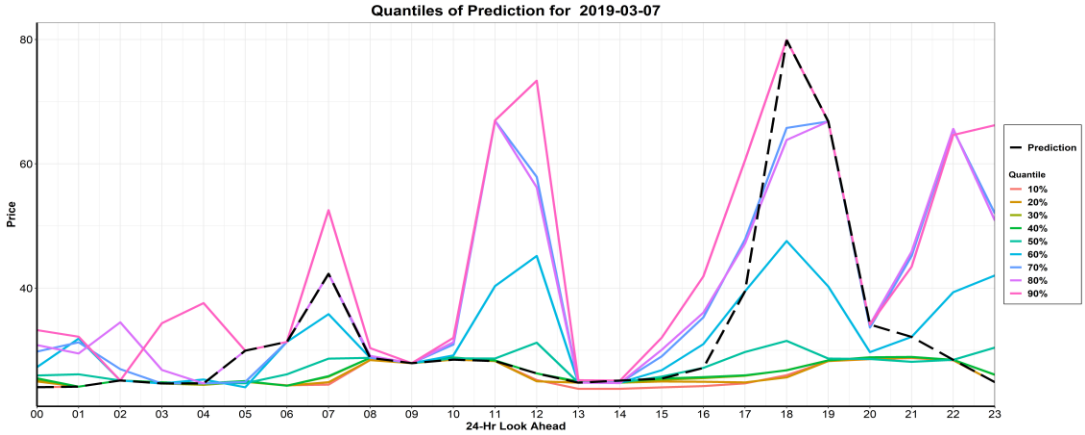

Fig. E.3.1. quantile regressions for 10%, 20%, ..., 90% quantiles associated with predicted RT-LMP.

Assumptions to describe the relation between our random variable, the quantiles, the probability density function (PDF), and its associated cumulative distribution function (CDF):

- $\boldsymbol{p_{t+k}}$: random variable; $\boldsymbol{f_{t+k}}$: PDF; $\boldsymbol{F_{t+k}}$: CDF
- $\boldsymbol{q^{\alpha}_{t+k}} = \boldsymbol{F^{-1}_{t+k}}(\boldsymbol{\alpha})$ quantile with proportion $\alpha \in [\mathbf{0}, \mathbf{1}]$ or $P(\boldsymbol{P_{t+k}} < \boldsymbol{x}) = \alpha$.

For our application, we produce a set of quantile regression for the given point forecast obtained from our statistical predictive model, namely ARIMAX method.

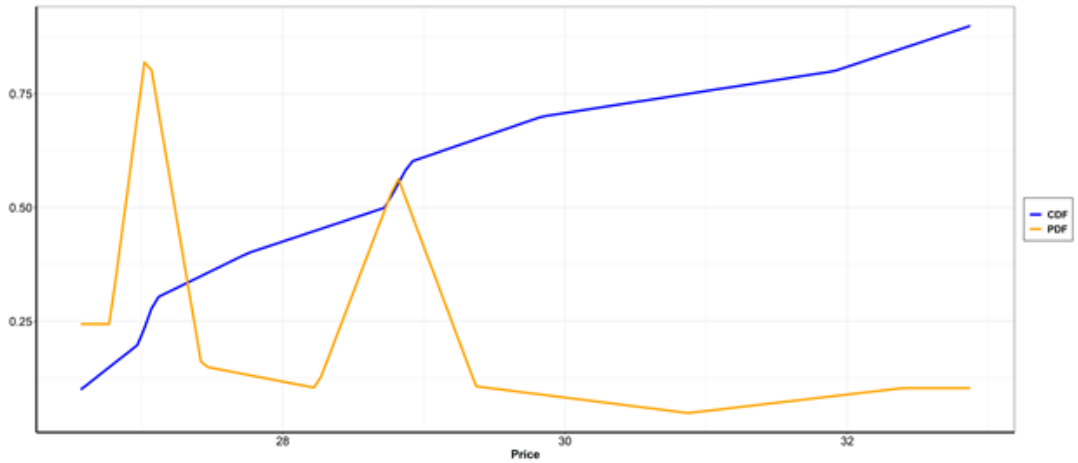

Fig. E.3.2. CDF and PDF for one selected hour in look-ahead window.

Scenario Generation:

In General, the probabilistic forecasts do not reflect the interdependence structure of forecast errors during look-ahead time, so these methods do not inform about prediction errors. This interdependence structure of errors is very important for many time dependent decision-making problems. In the context of PSHU optimization, if LMPs are high in a particular interval, this might

suggest additional PSHU generation or decreased pumping, with the SOC restored during later intervals; however, if LMPs are correlated over time, then there is a risk that increased generation in a high priced interval will necessitate increased pumping in another interval with high prices, resulting in a net increase in costs.

In order to fulfill this requirement and reflect the prediction errors, we follow the method of statistical scenario generation for wind production adapted from [E.1]. The method has some generic value, since the results of any type of forecasting methodology can be used as input.

1) Creating the Gaussian multivariate random variables:

The random variable $\boldsymbol{Y_k}$ whose realization Y_k^t at time t is defined by $Y_k^t = \hat{F}_{t+k}(p_{t+k}),\ \forall t$; is uniformly distributed on the unit interval U[0,1].

A fundamental property of a reliable probabilistic prediction is that the prediction errors can be made Gaussian by applying a suitable transformation using the Probit function, known as the quantile function for standard normal distribution. Therefore, we can Transform Uniform distribution to Normal distribution; using the Probit function

$$X_k^{(t)} = \Phi^{-1}(Y_k^t),\ \forall t.$$

2) Creating Covariance Matrix:

The random variable $X_k \sim \aleph(0,1)$. The transformed random vector $X = (X_1, X_2, \dots, X_K)^T \sim \aleph(\mu_0, \Sigma)$ μ_0 being a vector of zeros, and K is the max forecast horizon. e.g. 24-hour.

The sample covariance Matrix is formulated as: $\Sigma_t = \frac{1}{t-1} \sum_{j=1}^{t} X^j\ X^{j^T}$.

Due to non-stationary characteristics of price, long term variations in the interdependence structure of prediction errors are tracked by recursively estimating this covariance matrix.

$$\sum_t = \boldsymbol{\lambda}\left(\frac{t-2}{t-1}\right)\Sigma_{t-1} + \left(1 + \boldsymbol{\lambda}\left(\frac{1}{t-1} - 1\right)\right) X^t X^{(t)^T},\ \lambda \in [0,1).$$

The covariance matrix is initialized by setting all its off-diagonal elements to 0 and its diagonal elements to 1. The parameter $\boldsymbol{\lambda}$ is a "forgetting factor" that adjusts how quickly new information, in the form of $X^t X^{(t)^T}$, are incorporated into the estimate $\sum_t$.

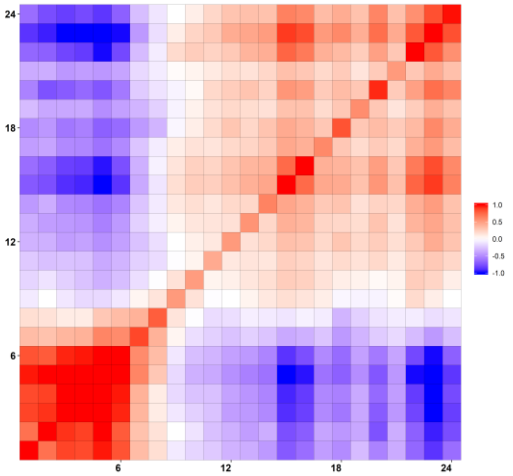

Fig. E.3.3. *Covariance matrix of the multivariate normal random variable- March 7th,2019*

In **Error! Reference source not found.** E.3.3, the horizontal and vertical axes range over the window of prediction, *k*=24 hours. Each pixel gives the covariance between two forecast horizons, and hence variance values for each forecast horizon on the diagonal.

Now that the covariance matrix containing the whole information on variance and covariance of the transformed variable $X = (X_1, X_2, \dots, X_K)^T$ is calculated. The following are steps to create statistical scenarios associated with forecasted RT-LMP.

3) Generating Statistical Scenarios [E.1]:

1. In order to have S-realizations [8] of the random variable $X = (X_1, X_2, \dots, X_{24})^T \sim \aleph(\mu_0, \Sigma_{t-24})$, we use a multivariate Gaussian random number generator with zero mean, and covariance matrix, Σ_{t-24}. The i^{th} scenario of S-realizations is denoted as X^i.

2. For each horizon $k \in \{1,2, \dots, 24\}$, S-realizations Y_k^i of the uniform variable Y_k are obtained by applying the inverse probit function Φ to each component of X^i as $Y_k^i = \Phi(X_k^i)$, $\forall\, i = \{1,2, \dots S\},\ k = \{1,2, \dots,24\}$.

3. For each look-ahead time $k \in \{1,2, \dots, 24\}$, the scenarios of RT price, result from the application of the inverse cdf $\hat{F}_{t+k|t}^{-1}$ to the S realizations Y_k^i of the uniform variable Y_k: $\hat{p}_{t+k|t}^i = \hat{F}_{t+k|t}^{-1}(Y_k^i)$, $\forall\, i,\ k$.

Appendix for Section IV.E.4

Up-sampling and Interpolating the RT-LMP Point Forecast Results for intra-hour 15-min Intervals

To produce the more granular data points, or in other words to increase the frequency of the samples, we need to derive a new data set from the existing one. In our case, we are interested in intra-hour, 15 minutes intervals, RT-LMP forecasts, which requires data points to be created at a 4-times higher rate than the forecasted RT-LMP prices. For that purpose, the first thing we do is create datapoints at higher frequency to report the RT-LMP prediction on those new data points. Once the data points are created at a more granular level, we start to use the hourly RT-LMP forecast information from the lower rate data and define an interpolation function to generate the RT-LMP forecast values for those higher rate missing data points. Given the realized RT-LMP values are in 5-minute granularity, the existing hourly RT-LMP data are derived by averaging those realized 5-minute RT-LMP data during each hour. Given the mentioned averaging constraint, we make sure that the new intra-hour RT-LMP dataset satisfies the averaging constraint as well. To interpolate those values there is a wide selection of simple and more complex interpolation functions. However, in most cases a linear interpolation is considered as a good start. In the linear interpolation, it basically draws a straight line between available data (which in this context is the forecasted hourly RT-LMP) and then interpolates and fills in values in between (which in this context is the 5-minute RT-LMP). Figure E.4.2 shows the original hourly RT-LMP Point Forecast and its associated 50 scenarios.

[8] S-realization of multivariate variable X means creating S number of scenarios to represent the potential values of X.

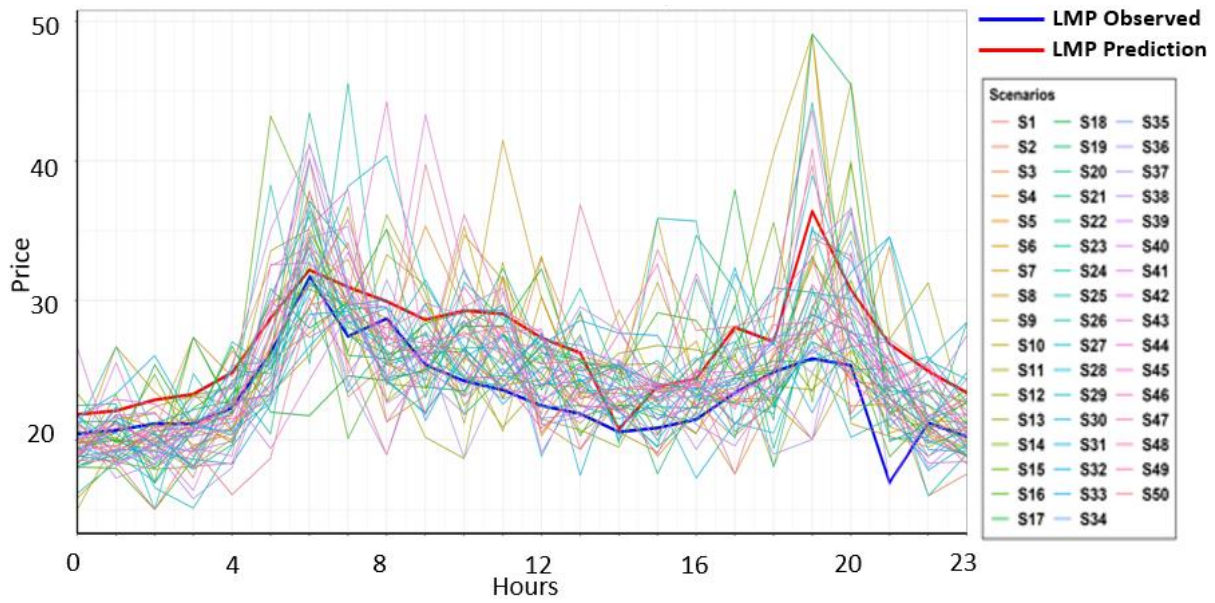

Fig. E.4.2. Observed price, point forecast price and probabilistic forecast with 50 scenarios of RT-LMP for day of April 15th, 2019. ARIMAX method is used with X being DA-LMP.

In order to do the Up-Sampling and creating high frequency data points we proceed as follows. First, we create data points for minutes in between each of consecutive hours.
Given the original hourly data points as follows:
[4/15/2019 0:00 AM, 4/15/2019 1:00 AM, 4/15/2019 2:00 AM, … , 4/15/2019 23:00]
The intra-hour data points would be as follows:
[4/15/2019 0:00, 4/15/2019 0:15, 4/15/2019 0:30 , 4/15/2019 0:45 , 4/15/2019 1:00, 4/15/2019 1:15, 4/15/2019 1:30 , 4/15/2019 1:45, 4/15/2019 2:00, …, 4/15/2019 23:00, 4/15/2019 23:15, 4/15/2019 23:30 , 4/15/2019 23:45]
Now that we could derive the higher frequency dataset. We use linear interpolation on the forecasted hourly RT-LMP to get the velues for these 15-minute intra-hour intervals, considering the average constraint as described above.

Appendix for Section IV.E.5

ARIMAX formulation to model multi-days ahead LMP single point forecasting:

$$[y_{d=1}, y_{d=2}, y_{d=3},\ y_{d=4}, y_{d=5}, y_{d=6}, y_{d=7}] = \sum_{i=1}^{p} \varphi_i \, \boldsymbol{y_{t-i}} + \sum_{j=1}^{q} \theta_j \, \epsilon_{t-j} + \sum_{m=1}^{3} \beta_m \, x_{m,t=[d=1,2,3,4,5,6,7]} + \epsilon_t, \quad \epsilon \sim N(0, \sigma^2)$$

The target value is forecasting the day ahead LMP for the next 7-days. The potential candidates to include into the model for the exogenous varibles are x_m={GasPrice, Load, Wind-Solar, Online Margin, Net Schedule Interchange (NSI)}, and the level of granularity is hourly for each day.

Figure E.5.2 shows the deterministic point forecast as a result of applying ARIMAX methodology. As observed from the figure, the red line demonstrates the ARIMAX forecasted result versus the blue line which shows the realized LMP, for the week of October 15, 2019 for the nodes where the studied PSHU are connected to.

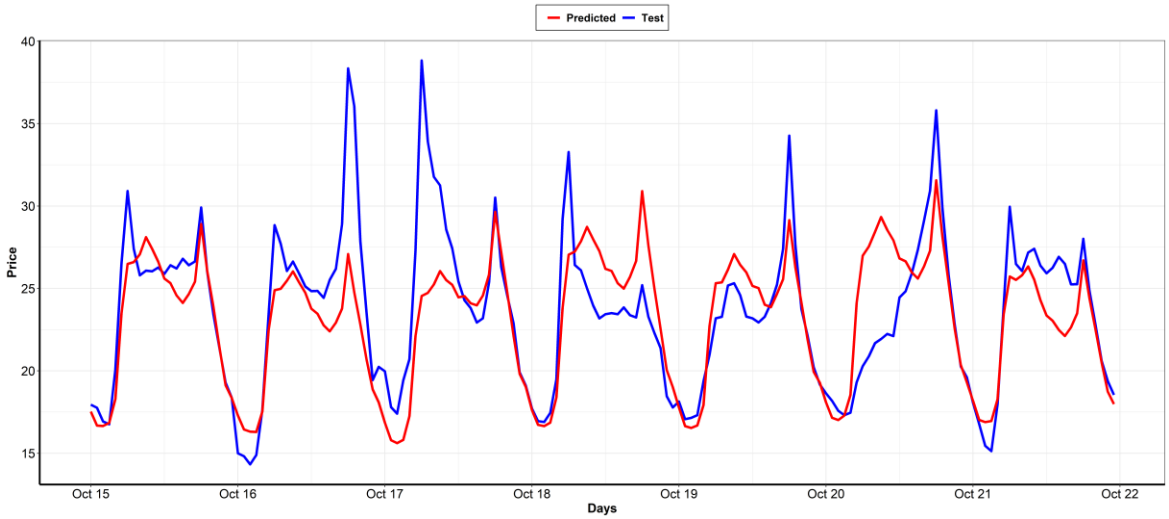

Fig. E.5.2. LMP point forecast along with the actual realized LMP for the week of Oct15th, considering the past 30days for the training set for forecasting the price for 7-days ahead look ahead time horizon.

Facebook Prophet to model multi-days ahead LMP single point forecasting:

The quality of the generated statistical scenarios is directly related to the level of the accuracy of the method of deterministic point forecast. In this study we tried to run a comparison study between our statistical ARIMAX based method and another method of time-series analysis named Facebook Prophet. This method is developed by Facebook as a procedure for forecasting time series data based on an additive model where non-linear trends are fit with yearly, weekly, and daily seasonality, plus holiday effects.

Components of Facebook Prophet as an additive model:

$$Y(t)= G(t) + S(t) + H(t) + \text{Noise}$$

G(t): Growth, piecewise linear curves for modelling non-periodic changes in time series.
S(t): Seasonality, periodic changes (e.g. weekly/yearly seasonality) Seasonal effects S(t) are approximated by Fourier Series:

$$s(t) = \sum_{n=1}^{N} \left(a_n \cos\left(\frac{2\pi nt}{P}\right) + b_n \sin\left(\frac{2\pi nt}{P}\right) \right)$$

H(t): Holiday, effects of holidays (user provided) with irregular schedules.
Noise: error term accounts for any unusual changes not accommodated by the mode.

Figure E.5.3 shows the results of single point forecast applying the Facebook Prophet approach and evaluates the performance of the results by computing Root-Mean-Square-Error (RMSE).

$$\text{RMSE} = \sqrt{\frac{1}{n}\sum_{j=1}^{n}(y_j - \hat{y}_j)^2}$$

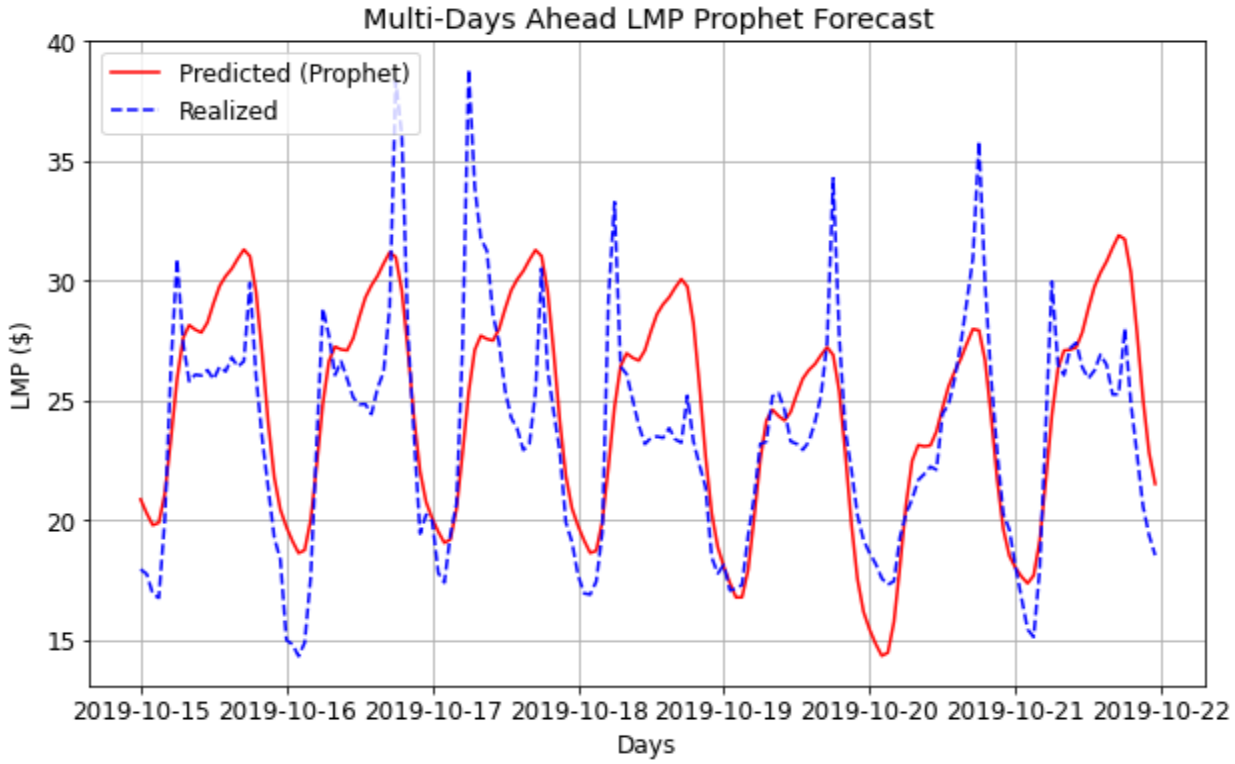

Fig. E.5.3. The forecasted LMP using prophet methodology for the week of Oct, 15th, 2019 shown in red along with the realized LMP.

Appendix for Section IV.G.1

Additional auxiliary constraints and final SOC stochastic constraints

Additional auxiliary constraints are included as follows:

$$s_{s,t}^{LB} \leq \sum_{k=1}^{t} h_{s,t}^{LB}; \quad \text{(G.1.5)}$$

$$s_{s,t}^{UB} \leq \sum_{k=1}^{t} h_{s,t}^{UB}; \quad \text{(G.1.6)}$$

$$0 \leq s_{s,t}^{LB} \leq M \cdot y_s; \quad \text{(G.1.7)}$$

$$0 \leq s_{s,t}^{UB} \leq M \cdot y_s; \quad \text{(G.1.8)}$$

$$\sum_s y_s \leq N \cdot \Lambda \quad \text{(G.1.9)}$$

It can be seen that the SOC limitation constraint (G.1.4) is not formulated as a hard constraint, because slack variable $s_{s,t}^{LB}$ and $s_{s,t}^{UB}$ are introduced. $s_{s,t}^{LB}$ and $s_{s,t}^{UB}$ are limited by the total amount of added headroom and floor room as in (G.1.5) and (G.1.6), which means the physical limits of PSH plants will be always respected. Constraints (G.1.7) and (G.1.8) are auxiliary constraints that enable slack variables or turn them OFF. y_s is a binary indicator, describing if the SOC limitation is violated in scenario s. The total violation $\sum_s y_s$ is required to be no larger than a certain threshold, for example, 95% of the total number of scenarios. This is enforced by (G.1.9), where Λ is the total number of scenarios and N is the percentage. In summary, violations are allowed in some extreme scenarios, but the majority shall be satisfied. The violation is actually caused by the insufficiency of enforcing headroom and floor room, while the physical limits are always satisfied under all scenarios, which is guaranteed by limiting the range of slack variables.

The above constraints are formulated based on the assumption that a PSH has only one unit, namely the reservoir of the PSH plant has a one-to-one mapping with the unit. In fact, a PSH could have multiple units, and these units share the same reservoir. We extend the above formulation to consider this, and the final SOC stochastic constraints are summarized as follows:

$$SOC^{LB} + \sum_{k=1}^{t} h_{s,t}^{LB} - s_{s,t}^{LB} \le soc_t \le SOC^{UB} - \sum_{k=1}^{t} h_{s,t}^{UB} + s_{s,t}^{UB};$$

$$s_{s,t}^{LB} \le \sum_{k=1}^{t} h_{s,t}^{LB};$$

$$s_{s,t}^{UB} \le \sum_{k=1}^{t} h_{s,t}^{UB};$$

$$0 \le s_{s,t}^{LB} \le M \cdot y_s;$$

$$0 \le s_{s,t}^{UB} \le M \cdot y_s;$$

$$\sum_s y_s \le N \cdot \Lambda;$$

$$h_{s,t}^{UB} = R_{s,t}^{G,DN}(g_t - G^{LB} \cdot u_t^G) + R_{s,t}^{P,UP}(P^{UB} \cdot u_t^P - p_t) + P^{UB} \cdot I_{s,t}^{O-P}\left(1 - u_t^G - u_t^p\right) + g_t \cdot I_{s,t}^{G-O};$$

$$h_{s,t}^{LB} = R_{s,t}^{G,UP}(G^{UB} \cdot u_t^G - g_t) + R_{s,t}^{P,DN}(p_t - P^{LB} \cdot u_t^P) + G^{UB} \cdot I_{s,t}^{O-G}\left(1 - u_t^G - u_t^p\right) + p_t \cdot I_{s,t}^{P-O};$$

$$u_t^G \ge u_{i,t}^G; \quad \text{(G.1.10)}$$

$$u_t^P \ge u_{i,t}^P; \quad \text{(G.1.11)}$$

$$u_t^G \le \sum_i u_{i,t}^G; \quad \text{(G.1.12)}$$

$$u_t^P \le \sum_i u_{i,t}^P; \quad \text{(G.1.13)}$$

$$g_t = \sum_i g_{i,t}; \quad \text{(G.1.14)}$$

$$p_t = \sum_i p_{i,t}; \quad \text{(G.1.15)}$$

where $g_{i,t}$, $p_{i,t}$, $u_{i,t}^G$, and $u_{i,t}^P$ are the counterparts of g_t, p_t, u_t^G, and u_t^P but defined on the individual unit level for unit *i*. The stochastic SOC constraints are imposed on the plant level, which contains multiple units. To this end, auxiliary variables and aggregations constraints are defined and imposed to aggregate the units onto the plant level. This is done by constraints (G.1.10)-(G.1.15). The plant is indicated as ON (pumping or generationg) if any of its units is ON. The output of a PSH plant is equal to the output summationg of all units contained by it.